THE STUDY OF PARATHYROID HORMONE ACTION AND SIGNALING PATHWAYS IN THE REGULATION OF ION TRANSPORT IN CACO-2 MONOLAYER USING ALTERNATING CURRENT AND DIRECT CURRENT ELECTROPHYSIOLOGICAL TECHNIQUES

SUPARERK LAOHAPITAKWORN

A THESIS SUBMITTED IN PARTIAL FULFILLMENT OF THE REQUIREMENTS FOR THE DEGREE OF DOCTOR OF PHILOSOPHY (MOLECULAR MEDICINE) FACULTY OF GRADUATE STUDIES MAHIDOL UNIVERSITY 2011

Thesis
entitled

THE STUDY OF PARATHYROID HORMONE ACTION AND SIGNALING PATHWAYS IN THE REGULATION OF ION TRANSPORT IN CACO-2 MONOLAYER USING ALTERNATING CURRENT AND DIRECT CURRENT ELECTROPHYSIOLOGICAL TECHNIQUES

……
Mr. Suparerk Laohapitakworn
Candidate

……
Assoc. Prof. Narattaphol Charoenphandhu, M.D., Ph.D.
Major advisor

……
Prof. Nateetip Krishnamra, Ph.D.
Co-advisor

……
Assoc. Prof. Sutthasinee Poonyachoti, D.V.M., Ph.D.
Co-advisor

……
Prof. Banchong Mahaisavariya, M.D., Dip Thai Board of Orthopedics
Dean
Faculty of Graduate Studies
Mahidol University

……...…
Assoc. Prof. Sukumal Chongthammakun, Ph.D.
Program Director
Doctor of Philosophy Program in Molecular Medicine
Faculty of Science
Mahidol University

Thesis
entitled

THE STUDY OF PARATHYROID HORMONE ACTION AND SIGNALING PATHWAYS IN THE REGULATION OF ION TRANSPORT IN CACO-2 MONOLAYER USING ALTERNATING CURRENT AND DIRECT CURRENT ELECTROPHYSIOLOGICAL TECHNIQUES

was submitted to the Faculty of Graduate Studies, Mahidol University
for the degree of Doctor of Philosophy (Molecular Medicine)
on
February 23, 2011

……
Mr. Suparerk Laohapitakworn
Candidate

……
Assoc. Prof. Chatsri Deachapunya, Ph.D.
Chair

……
Assoc. Prof. Narattaphol Charoenphandhu, M.D., Ph.D.
Member

……
Assoc. Prof. Sutthasinee Poonyachoti, D.V.M., Ph.D.
Member

……
Prof. Nateetip Krishnamra, Ph.D.
Member

……
Prof. Banchong Mahaisavariya, M.D., Dip Thai Board of Orthopedics
Dean
Faculty of Graduate Studies
Mahidol University

……
Prof. Skorn Mongkolsuk, Ph.D.
Dean
Faculty of Science
Mahidol University

ACKNOWLEDGEMENTS

I would like to express my sincere gratitude and appreciation to my major advisor, Assoc. Prof. Narattaphol Charoenphandhu, for his excellent guidance, supervision, ideas for improvement, and critical reading of the thesis.

My deepest appreciation is also expressed to Prof. Nateetip Krishnamra for her helpful suggestion, kindness, and encouragement throughout my study. Grateful acknowledgement is also given to my co-advisor, Assoc. Prof. Suthasinee Poonyachoti, as well as my thesis-examining committee, Assoc. Prof. Chatsri Deachapunya, for their valuable suggestion, criticism, and correction of my thesis.

I would like to thank the Institute of Nutrition, Mahidol University, Bangkok, Thailand for kindly providing Caco-2 cells. My cordial gratitude is expressed to Asst. Prof. Narin Nattavut from the Department of Physics, Faculty of Science, Mahidol University and Mr. Chadin Kulsing for their excellent discussion regarding impedance analysis. I am grateful to the faculty engineers, Mr. Supreecha Jaroonsuck and Mr. Somkid Khanmune for their help in Ussing chamber maintenance. I would like to acknowledge Miss Jirawan Thongbunchoo and Mr. Warut Tulalamba for their helpful technical assistance concerning cell culture and molecular techniques. In addition, I would like to thank all the members of the Consortium for Calcium and Bone Research (COCAB) for their kind support and friendship.

I wish to extend my appreciation to the Medical Scholars Program, Mahidol University, for my research funding and scholarship, and the research grants from the Thailand Research Fund (to Assoc. Prof. Narattaphol Charoenphandhu and Prof. Nateetip Krishnamra).

Finally, I am deeply indebted to my parents for their support, encouragement, care, and love. I dedicate this thesis to my parents and all of my teachers.

Suparerk Laohapitakworn

THE STUDY OF PARATHYROID HORMONE ACTION AND SIGNALING PATHWAYS IN THE REGULATION OF ION TRANSPORT IN CACO-2 MONOLAYER USING ALTERNATING CURRENT AND DIRECT CURRENT ELECTROPHYSIOLOGICAL TECHNIQUES

SUPARERK LAOHAPITAKWORN 4702094 SCMM/D

Ph.D. (MOLECULAR MEDICINE)

THESIS ADVISORY COMMITTEE: NARATTAPHOL CHAROENPHANDHU, M.D., Ph.D., NATEETIP KRISHNAMRA, Ph.D., SUTTHASINEE POONYACHOTI, D.V.M., Ph.D.

ABSTRACT

The electrical circuit of epithelial cells, formed by the plasma membranes and tight junctions, could be explained by combinations of capacitors and resistors. However, a direct current (DC)-based technique could not determine each of the electrical components in this circuit. In the present study, alternating current (AC)-based impedance spectroscopy was applied to analyze the capacitive and resistive properties of intestinal epithelial cell line Caco-2. The results showed that Caco-2 monolayer exhibited apical (C_a) and basolateral (C_b) capacitance of 28.98 ± 0.69 and 12.36 ± 0.23 $\mu F/cm^2$, respectively, and apical (R_a) and basolateral (R_b) resistance of 2141.30 ± 222.50 and 993.96 ± 60.96 $\Omega \cdot cm^2$, respectively. Impedance analysis successfully determined the forskolin-induced reduction in the plasma membrane resistance. This technique was then applied to study the biological responses of Caco-2 cells to parathyroid hormone (PTH), the direct action of which in the intestine has not been known. PTH reduced both apical and basolateral membrane resistance but had no effect on membrane capacitance, indicating that PTH activated transporters in the plasma membrane and not transporter-rich vesicle fusion. The mechanism and signaling pathways of PTH were further examined by the DC-based Ussing chamber technique. PTH significantly increased short-circuit currents (I_{sc}) in a dose-dependent manner. HCO_3^- depletion abolished the PTH action, while Cl^- depletion had no effect, suggesting that PTH induced apical HCO_3^- secretion in Caco-2 cells. By using various inhibitors, it was found that HCO_3^- came from the uptake via the basolateral electrogenic Na^+/HCO_3^- cotransporter-1 (NBCe1) and from intracellular production catalyzed by carbonic anhydrase. HCO_3^- was later secreted through the apical cystic fibrosis transmembrane conductance regulator (CFTR). Apical Na^+/H^+ exchanger (NHE)-3 and basolateral NHE1 might help extrude excess H^+ produced by carbonic anhydrase. This ion regulatory action of PTH was exerted through the protein kinase A (PKA)- and phosphoinositide-3-kinase (PI3K)-dependent pathways. In conclusion, impedance analysis could be used to determine the plasma membrane capacitance and resistance of epithelial cells and help predict responses of cells to PTH. PTH induced HCO_3^- secretion in Caco-2 cells through CFTR.

KEY WORDS: ANION SECRETION/CYSTIC FIBROTIC TRANSMEMBRANE CONDUCTANCE REGULATOR (CFTR)/ELECTROGENIC Na^+/HCO_3^- COTRANSPORTER-1(NBCe1)/PARATHYROID HORMONE

112 pages

การศึกษาผลของฮอร์โมนพาราไทรอยด์และการส่งสัญญาณเพื่อควบคุมการขนส่งไอออนในแผ่นเซลล์เพาะเลี้ยงชนิดคาโคทูโดยใช้เทคนิคทางสรีรวิทยาไฟฟ้ากระแสสลับและกระแสตรง

THE STUDY OF PARATHYROID HORMONE ACTION AND SIGNALING PATHWAYS IN THE REGULATION OF ION TRANSPORT IN CACO-2 MONOLAYER USING ALTERNATING CURRENT AND DIRECT CURRENT ELECTROPHYSIOLOGICAL TECHNIQUES

ศุภฤกษ์ เลาหพิทักษ์วร 4702094 SCMM/D

ปร.ด. (เวชศาสตร์ระดับโมเลกุล)

คณะกรรมการที่ปรึกษาวิทยานิพนธ์: นรัตถพล เจริญพันธุ์, พ.บ., ปร.ด., นทีทิพย์ กฤษณามระ, ปร.ด., สุทธาสินี ปุญญโชติ, สพ.บ., Ph.D.

บทคัดย่อ

วงจรไฟฟ้าซึ่งเกิดจากเยื่อหุ้มเซลล์และไทจังชั่นของเซลล์เยื่อบุประกอบไปด้วยตัวเก็บประจุและตัวต้านทาน อย่างไรก็ตามการใช้ไฟฟ้ากระแสตรงไม่สามารถวัดค่าตัวเก็บประจุและตัวต้านทานเหล่านี้ได้ ในการศึกษาครั้งนี้ได้ใช้การวัดคุณสมบัติความต้านทานไฟฟ้าซึ่งใช้อุปกรณ์ปล่อยไฟฟ้ากระแสสลับเพื่อหาค่าตัวเก็บประจุและตัวต้านทานของวงจรไฟฟ้าทั้งนี้ได้ทำการทดลองในเซลล์เพาะเลี้ยงจากของลำไส้ชนิดคาโคทู ผลการทดลองพบว่าเซลล์เพาะเลี้ยงคาโคทูมีค่าตัวเก็บประจุที่เยื่อหุ้มเซลล์ด้านเอปิเคิ้ลและด้านเบโซแลทเทอรัล คือ 28.98 ± 0.69 และ 12.36 ± 0.23 ไมโครฟารัดต่อตารางเซนติเมตร ตามลำดับ ค่าตัวต้านทานที่เยื่อหุ้มเซลล์ด้านเอปิเคิ้ลและด้านเบโซแลทเทอรัล คือ 2141.30 ± 222.50 และ 993.96 ± 60.96 โอห์มตารางเซนติเมตร ตามลำดับ การวัดคุณสมบัติความต้านทานไฟฟ้าตรวจพบการลดลงของความต้านทานที่เยื่อหุ้มเซลล์หลังการกระตุ้นด้วยฟอร์สโคลินได้ จากนั้นได้ประยุกต์เทคนิคดังกล่าวเพื่อศึกษาการตอบสนองของเซลล์เพาะเลี้ยงคาโคทูต่อฮอร์โมนพาราไทรอยด์ ฮอร์โมนพาราไทรอยด์ลดความต้านทานทั้งด้านเอปิเคิ้ลและด้านเบโซแลทเทอรัลของเยื่อหุ้มเซลล์ แต่ไม่มีผลต่อค่าตัวเก็บประจุของเยื่อหุ้มเซลล์ซึ่งแสดงให้เห็นว่า ฮอร์โมนพาราไทรอยด์กระตุ้นการทำงานของโปรตีนขนส่ง แต่ไม่มีผลต่อการเชื่อมถุงเก็บโปรตีนขนส่งกับเยื่อหุ้มเซลล์ จากการศึกษาโดยใช้อุซซิ่งแชมเบอร์พบว่า ฮอร์โมนพาราไทรอยด์เพิ่มกระแสไฟฟ้าของเซลล์ตามความเข้มข้นของฮอร์โมนที่เพิ่มขึ้น การลดไบคาร์บอเนตในสารละลายสามารถลดผลของฮอร์โมนพาราไทรอยด์ได้ ขณะที่การลดคลอไรด์ไม่มีผลต่อการทำงานของฮอร์โมน จึงกล่าวได้ว่าฮอร์โมนพาราไทรอยด์กระตุ้นการหลั่งไบคาร์บอเนตในเซลล์เพาะเลี้ยงคาโคทู จากการใช้ตัวยับยั้งหลายชนิดพบว่าไบคาร์บอเนตเข้าสู่เซลล์ทางด้านเบโซแลทเทอรัลโดยอาศัยโปรตีนขนส่งเอ็นบีซีอี-1 และอาจสร้างไบคาร์บอเนตเองจากภายในเซลล์โดยอาศัยคาร์บอนิคแอนไฮเดรส ไบคาร์บอเนตออกจากเซลล์ผ่านทางซีเอฟทีอาร์ที่อยู่ด้านเอปิเคิ้ลของเซลล์ เอ็นเอชอี-3 ที่อยู่ด้านบน และเอ็นเอชอี-1 ที่อยู่ด้านเบโซแลทเทอรัลของเซลล์ อาจมีส่วนในการขับไฮโดรเจนไอออนซึ่งผลิตจากคาร์บอนิคแอนไฮเดรส ฮอร์โมนพาราไทรอยด์ทำงานผ่านทางเอ็นไซม์ไคเนสเอและฟอสโฟอิโนสิไทด์-3-ไคเนส กล่าวโดยสรุปคือการวัดคุณสมบัติทางไฟฟ้าของเซลล์โดยอาศัยเทคนิคไฟฟ้ากระแสสลับสามารถวัดค่าตัวเก็บประจุและตัวต้านทานของเยื่อหุ้มเซลล์และใช้พยากรณ์ผลของฮอร์โมนพาราไทรอยด์ได้ และยังพบว่าฮอร์โมนนี้กระตุ้นการขับไบคาร์บอเนตในเซลล์ลำไส้ผ่านทางโปรตีนซีเอฟทีอาร์

112 หน้า

CONTENTS

LIST OF TABLES

LIST OF FIGURES

LIST OF FIGURES (cont.)

LIST OF ABBREVIATIONS

$1,25(OH)_2D_3$	1,25-dihydroxyvitamin D_3
1–34 PTH	parathyroid hormone fragment 1–34
13–34 PTH	parathyroid hormone fragment 13–34
% v/v	percent volume per volume
°C	degree Celsius
θ	phase difference between the current and voltage
µA	microampere
$\mu A/cm^2$	microampere per square centimeter
$\mu F/cm^2$	microfarad per square centimeter
µg/L	microgram per liter
µg/mL	microgram per milliliter
µL	microliter
µmol/L	micromole per liter
$\Omega \cdot cm^2$	ohm square centimeter
a	surface area of the Caco-2 monolayer
A/cm^2	ampere per square centimeter
AC	alternating current
Ag/AgCl	silver/silver chloride
AM	acetoxymethyl
ANOVA	analysis of variance
Arg	arginine
ATP	adenosine-5′-triphosphate
BAPTA-AM	1,2-bis(o-aminophenoxy)ethane-N,N,N′,N′-tetraacetic acid tetra(acetoxymethyl) ester
bp	base pair
C_a	capacitance of the apical membrane
Ca^{2+}	calcium ion

LIST OF ABBREVIATIONS (cont.)

CaCC	calcium-activated chloride channel
$CaCl_2$	calcium chloride
cAMP	cyclic adenosine monophosphate
CaR	calcium-sensing receptor
C_b	capacitance of the basolateral membrane
cDNA	complimentary deoxyribonucleic acid
CFTR	cystic fibrosis transmembrane conductance regulator
$CFTR_{inh}$-172	thiazolidinone cystic fibrosis transmembrane conductance regulator inhibitor-172
C_H	mean radioactivity in the hot side
Cl^-	chloride ion
cm^2	square centimeter
CO_2	carbon dioxide
cpm	count per minute
cpm/h	count per minute per hour
cpm/nmol	count per minute per nanomole
C_T	total concentration of mannitol in the hot side
DAG	diacyl glycerol
DC	direct current
DIDS	4,4′-diisothiocyanatostilbene-2,2′-disulfonic acid disodium salt hydrate
DMEM	Dulbecco’s modified Eagle’s medium
DMSO	dimethyl sulfoxide
e	Euler’s number
EGF	epidermal growth factor
EIPA	5-(N-ethyl-N-isopropyl)amiloride
ENaC	epithelial sodium channel

LIST OF ABBREVIATIONS (cont.)

ERK	extracellular signal-regulated kinase
f	frequency
FBS	fetal bovine serum
GAPDH	glyceraldehydes-3-phosphate dehydrogenase
GlyH-101	glycine hydrazide GlyH-101
GPCR	G protein-coupled receptor
H^+	hydrogen ion
H_2O	water
HCl	hydrochloric acid
HCO_3^-	bicarbonate anion
HEPES	4-(2-hydroxyethyl)-1-piperazineethanesulfonic acid
HEPES-Na	4-(2-hydroxyethyl)-1-piperazineethanesulfonic acid sodium salt
HPO_4^{2-}	hydrogen phosphate ion
Hz	hertz
i	imaginary unit = $\sqrt{-1}$
IGF-I	insulin-like growth factor-I
IP_3	inositol 1,4,5-trisphosphate
I	current in the direct-current system
I_{sc}	short-circuit current
$\tilde{I}$	current in the alternating-current system
$J_{H\rightarrow C}$	hot-to-cold unidirectional flux
K^+	potassium ion
$KC_6H_{11}O_6$	potassium gluconate
KCl	potassium chloride
keV	kiloelectron volt
kg	kilogram
KH_2PO_4	potassium hydrogen phosphate

LIST OF ABBREVIATIONS (cont.)

kHz	kilohertz
MΩ·cm	megaohm centimeter
MAPK	mitogen-activated protein kinase
mCi/mol	millicurie per mole
Mg^{2+}	magnesium ion
$MgSO_4 \cdot 7H_2O$	magnesium sulfate heptahydrate
min	minute
mmol/kg	millimole per kilogram
mmol/L	millimole per liter
mol/L	mole per liter
mRNA	messenger ribonucleic acid
ms	millisecond
mV	millivolt
Na^+	sodium ion
Na^+/K^+-ATPase	sodium/potassium adenosine trisphosphatase
Na_2HPO_4	sodium hydrogen phosphate
$NaC_6H_{11}O_6$	sodium gluconate
NaCl	sodium chloride
$NaHCO_3$	sodium bicarbonate
NaP_i	sodium/phosphate cotransporter
NBCe1	electrogenic sodium/bicarbonate cotransporter-1
NCX	sodium/calcium exchanger
NEAA	nonessential amino acid
NHE1	sodium/hydrogen exchanger-1
NHE3	sodium/hydrogen exchanger-3
NKCC1	sodium/potassium/2 chloride cotransporter-1
nm	nanometer
$nmol/h/cm^2$	nanomole per hour per square centimeter

LIST OF ABBREVIATIONS (cont.)

nmol/L	nanomole per liter
NPPB	5-nitro-2-(3-phenylpropylamino)benzoic acid
O_2	oxygen gas
PBS	phosphate buffered saline
PCR	polymerase chain reaction
pg/mL	picogram per milliliter
PGE_1	prostaglandin E_1
PI3K	phosphoinositide-3-kinase
PIP_2	phosphatidylinositol 4,5-bisphosphate
PKA	protein kinase A
PKI 14–22	protein kinase inhibitor 14–22 amide
PKC	protein kinase C
PLC	phospholipase C
PTH	parathyroid hormone
PTHR	parathyroid hormone receptor
PTHR1	type 1 parathyroid hormone receptor
PTHR2	type 2 parathyroid hormone receptor
PTHrP	parathyroid hormone-related peptide
R	resistive impedance
R_a	resistance of the apical membrane
RANKL	receptor activator of nuclear factor kappa-B ligand
R_b	resistance of the basolateral membrane
RER	rough endoplasmic reticulum
$R_{H\rightarrow C}$	rate of tracer appearance in the cold side
RNA	ribonucleic acid
R_p	paracellular resistance
rRNA	ribosomal ribonucleic acid
R_s	resistance of the unstirred layer

LIST OF ABBREVIATIONS (cont.)

R_t	transepithelial resistance
SE	standard error
SER	smooth endoplasmic reticulum
S_H	specific activity of the hot side
TGF-β	transforming growth factor-beta
TIP39	tuberoinfundibular peptide-39
Tyr	tyrosine
U/mL	unit per milliliter
UV	ultraviolet
V	volt
VDR	vitamin D receptor
VDRE	vitamin D response element
VIP	vasoactive intestinal peptide
V_t	transepithelial voltage
$\tilde{V}$	voltage in the alternating current system
X	reactive impedance
Z	ratio of a voltage magnitude to a current magnitude
Z_I	imaginary part of the impedance
Zn	zinc
Z_R	real part of the impedance
$\tilde{Z}$	impedance
|Z|	magnitude of the impedance

PUBLICATION

Laohapitakworn S, Thongbunchoo J, Nakkrasae L, Krishnamra N, Charoenphandhu N. Parathyroid hormone (PTH) rapidly enhances CFTR-mediated HCO_3^- secretion in intestinal epithelium-like Caco-2 monolayer: a novel ion regulatory action of PTH. Am J Physiol Cell Physiol 2011. (Accepted, in press)

CHAPTER I
INTRODUCTION

Epithelium is composed of electrical barrier networks formed by plasma membranes and tight junctions (Powell, 1981). This elementary circuit of the epithelium is simply explained by a combination of ohmic capacitors and resistors. Conventional direct current (DC) analysis of transepithelial resistance could not sufficiently examine each capacitive and resistive component in the cell circuit. However, alternating current (AC)-based impedance analysis provides advantages over the DC-based technique because the plasma membrane responds to the frequency-dependent AC and the hidden electrical components, e.g., membrane resistance and capacitance, could be obtained experimentally (Clausen, 1989; Gordon et al., 1989). In other words, all electrical elements of the epithelial cells can be analyzed simultaneously by the impedance technique. The impedance analysis has been used to determine the electrical properties of several epithelia, such as gastric, corneal, gall bladder, and renal epithelia (Clausen et al., 1982; Clausen et al., 1986; Moser et al., 2007; Paunescu and Helman, 2001; Wills et al., 1992; Wills et al., 1993).

To demonstrate the application of the impedance measurement in the analyses of cellular capacitance and resistance in the intestinal epithelium, human colorectal adenocarcinoma cell line Caco-2, was used as a model in this study. The use of this cell line helps avoid complicated circuit modeling due to the presence of connective tissue and a muscle layers in the intact intestine as well as cellular heterogeneity of the epithelial layer. During cell culture, Caco-2 cells form a monolayer on a supporting material (i.e., Snapwell) and show similar structure and function to the absorptive cells of the small intestine (Bailey et al., 1996; Hilgers et al., 1990; Sambuy et al., 2005). This cell line has been used in many studies of electrolyte and drug transport (Grasset et al., 1985; Inoue et al., 1997; Zhu et al., 2005). Therefore, Caco-2 cells provide a suitable model for studying electrical properties of the intestinal epithelial cells by impedance analysis.

Parathyroid hormone (PTH) is known to have a fundamental role in ion transport systems, especially in the kidney (Bank et al., 1978; Bezerra et al., 2008; Bourdeau et al., 1987; Iino and Burg, 1979; Laverty et al., 2003; Quamme, 1997). However, its ion regulatory function in the intestine is poorly understood. Several lines of evidence have suggested direct actions of PTH in the intestine (Nemere and Larsson, 2002), since PTH receptor (PTHR) mRNA and protein have been found in rat small intestinal epithelium (Urena et al., 1993; Watson et al., 2000) and rat and human intestinal cell lines (Li et al., 1995). Experiments on rat enterocytes showed that PTH processed signaling transduction through cyclic adenosine monophosphate (cAMP)/protein kinase A (PKA), phospholipase C (PLC)/inositol triphosphate (IP_3)/intracellular Ca^{2+}, and diacylglycerol (DAG)/protein kinase C (PKC) pathways (Massheimer et al., 2000). In addition, Nemere demonstrated binding of PTH to its receptor in chick duodenum (Nemere, 1996), and PKA activation after PTH incubation in isolated chick enterocytes (Nemere, 1999). Since PTH uses these signaling pathways to induce Cl^- secretion in the proximal tubular cells (Laverty et al., 2003) and to induce receptor activator of nuclear factor kappa-B ligand (RANKL) production in osteoblasts (Chesnoy-Marchais and Fritsch, 1989), These same signals may be used by PTH to regulate anion secretion in the intestinal cells.

The present study emphasized the use of the impedance analysis in predicting the mechanisms of action of PTH on the membrane electrical properties of the intestinal epithelium using Caco-2 model. The PTH-induced alterations in the plasma membrane capacitance and resistance were determined and were used to anticipate the responses of cells and transporters during PTH stimulation. The transporters were identified by DC-based Ussing chamber technique with the use of various inhibitors to HCO_3^-, Cl^-, Na^+, and K^+-related transporters. This could be a novel application of impedance measurement to predict the biological responses of the cells to drug and/or chemical treatments in vitro.

Objectives

The objectives of the present study were:

1. To demonstrate the application of AC-based impedance measurement in analyses of the plasma membrane capacitance and resistance in intestinal epithelium-like Caco-2 monolayer.

2. To examine the action of PTH on the plasma membrane capacitance and resistance in Caco-2 monolayer by using AC-based impedance analysis.

3. To demonstrate changes in the DC electrical properties, i.e., transepithelial potential difference (V_t), short-circuit current (I_{sc}), and transepithelial resistance (R_t), in Caco-2 monolayer after PTH stimulation.

4. To investigate the action of PTH on ion transport as well as the responsible transporters and signaling pathways in Caco-2 monolayer by using DC-based Ussing chamber technique.

Hypotheses

Hypotheses of the present study were:

1. Impedance analysis was able to determine the plasma membrane capacitance and resistance of Caco-2 cells.

2. PTH may modify both apical and basolateral membrane resistance and capacitance in Caco-2 cells.

3. PTH action probably involved the PKA, PKC and/or PI3K signaling pathways.

CHAPTER II
LITERATURE REVIEW

2.1 Impedance analysis

2.1.1 The principle of impedance analysis

Impedance is an electrical property to impede currents that flow through a particular material. This characteristic is described by a current-voltage relationship in the alternating current (AC) system. Unlike resistance, the impedance does not only explain the relative amplitudes of the current and voltage, but it also illustrates the phase difference between these 2 parameters.

The impedance is a complex quantity composed of real and imaginary terms which can be generally demonstrated in a polar form. This form shows the magnitude and phase features of the impedance.

$$\tilde{Z} = Ze^{i\theta} \quad (1)$$

where $\tilde{Z}$ is the impedance ($\Omega \cdot cm^2$)

Z is the ratio of the voltage magnitude to the current magnitude ($\Omega \cdot cm^2$)

e is the Euler's number

i is the imaginary unit = $\sqrt{-1}$

θ is the phase difference between the current and voltage

The Euler's formula is

$$e^{i\theta} = \cos\theta + i\sin\theta \quad (2)$$

When $e^{i\theta}$ from equation 2 is substituted in equation 1, the equation 1 can be written as

$$\tilde{Z} = Z\cos\theta + iZ\sin\theta \quad (3)$$

The term $Z\cos\theta$ is the real part of the impedance, while the imaginary part is the term $Z\sin\theta$. Since the impedance of a pure resistor-containing circuit shows no phase difference between the current and voltage, **the resistor only contributes to the real part of the impedance**. This real part is thus called the **resistive impedance**. On the other hand, **capacitors and inductors which influence the phase difference contribute to the imaginary part of the impedance.** This part is thus referred as the **reactive impedance**. Thus, the impedance can be written as

$$\tilde{Z} = R + iX \quad (4)$$

where R is the resistive impedance ($\Omega \cdot cm^2$)
X is the reactive impedance ($\Omega \cdot cm^2$)

Using an impedance analyzer, the impedance of a material can be measured based on Ohm's law,

$$\tilde{V} = \tilde{I}\tilde{Z} \quad (5)$$

where $\tilde{V}$ is the voltage (V)
$\tilde{I}$ is the current (A/cm^2)

When a sinusoidal AC current is applied to a material, a resulting voltage including amplitudes and phase differences can be detected. Vice versa, the impedance analyzer can generate the sinusoidal voltage, and observe the current change instead. Both current and voltage are used to calculate the impedance. The impedance derived from Ohm's equation characterizes overall real and imaginary components of the impedance at a specific frequency of the applied signal.

A. Nyquist plot

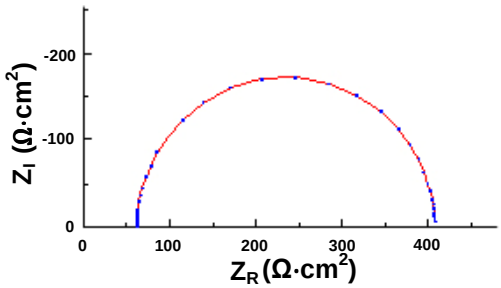

B. Bode magnitude plot

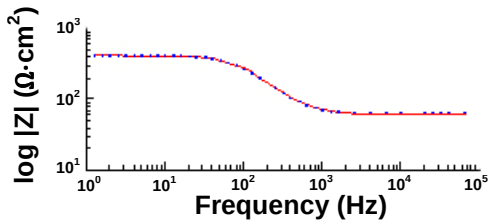

C. Bode phase plot

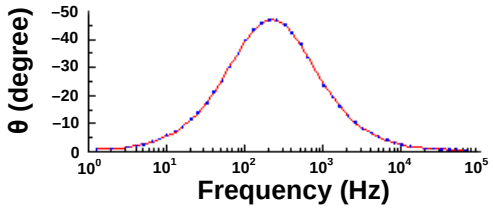

Figure 2.1 Three types of plots for impedance data. **A.** Nyquist plot. Z_R and Z_I refer to real and imaginary parts of the impedance, respectively. **B.** Bode magnitude plot. Log |Z| refers to log of the magnitude of the impedance. **C.** Bode phase plot. θ refers to the phase difference between the current and voltage.

Impedance analysis interprets the impedance values which are measured from various frequencies of the applied signal. Data is typically presented by Nyquist and Bode plots. The Nyquist plot shows the real (Z_R) and imaginary (Z_I) parts in the abscissa and ordinate respectively (Figure 2.1A). On the other hand, the Bode plot is composed of 2 graphs; one with the frequency versus the log of the magnitude of the impedance (log |Z|), and the other with the frequency versus the phase difference (θ; Figure 2.1B and 2.1C).

The Nyquist and Bode plots define the material's electrical circuit system. Notably, each particular circuit yields **unique patterns** and **values** in the plots. Thus, the electrical elements and their arrangement in the circuit can be indicated by simulating an equivalent circuit. The equivalent circuit models a circuit that manifests

similar patterns and values of the Nyquist and Bode plots to the experimental circuit. So the electrical components, e.g., resistors and capacitors, and their arrangement in the circuit can actually represent the experimental circuit features.

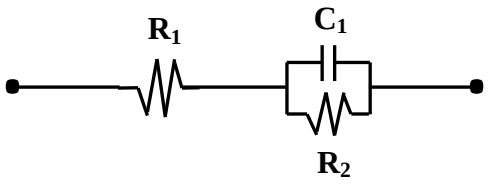

Figure 2.2 An example of an electrical circuit for demonstrating impedance analysis. The circuit is composed of a resistor (R_1) connected to a R-C combination (R_2-C_1).

For example, given an electrical circuit consisting of a resistor connected in parallel to a R-C combination as shown in Figure 2.2, the impedance of this circuit can be written as

$$\tilde{Z} = \tilde{Z}_{R1} + \tilde{Z}_{R2\text{-}C1} \tag{6}$$

$$= \tilde{Z}_{R1} + \frac{\tilde{Z}_{R2} \cdot \tilde{Z}_{C1}}{\tilde{Z}_{R2} + \tilde{Z}_{C1}} \tag{7}$$

where
- $\tilde{Z}$ is the total impedance of the circuit ($\Omega \cdot cm^2$)
- $\tilde{Z}_{R1}$ is the impedance of R_1 ($\Omega \cdot cm^2$)
- $\tilde{Z}_{R2\text{-}C1}$ is the impedance of the R_2-C_1 combination ($\Omega \cdot cm^2$)
- $\tilde{Z}_{R2}$ is the impedance of R_2 ($\Omega \cdot cm^2$)
- $\tilde{Z}_{C1}$ is the impedance of C_1 ($\Omega \cdot cm^2$)

Since $$\tilde{Z}_R = R \tag{8}$$

and $$\tilde{Z}_C = \frac{1}{i2\pi fC} \tag{9}$$

where $\tilde{Z}_R$ is the impedance of a resistor ($\Omega \cdot cm^2$)

R is the resistance ($\Omega \cdot cm^2$)

$\tilde{Z}_C$ is the impedance of a capacitor ($\Omega \cdot cm^2$)

f is the frequency (Hz)

C is the capacitance ($\mu F/cm^2$)

the equation 7 can be written as

$$\tilde{Z} = R_1 + \frac{R_2 \cdot 1/i2\pi fC_1}{R_2 + 1/i2\pi fC_1} \quad (10)$$

$$= \frac{R_1 + R_2 + R_1(2\pi fC_1R_2)^2}{1 + (2\pi fC_1R_2)^2} - i\frac{2\pi fC_1R_2^2}{1 + (2\pi fC_1R_2)^2} \quad (11)$$

The term $\frac{R_1 + R_2 + R_1(2\pi fC_1R_2)^2}{1 + (2\pi fC_1R_2)^2}$ represents the real part of the impedance, while the term $-\frac{2\pi fC_1R_2^2}{1 + (2\pi fC_1R_2)^2}$ represents the imaginary part of the impedance. When the current at a certain frequency is applied to the circuit, the resulting voltage can be detected and these 2 parameters can be used to calculate the real and imaginary impedance. To calculate R_1, R_2, and C_1, the currents at various frequencies are applied to the circuit, and thus the calculated real and imaginary impedance values are used to solve for R_1, R_2, and C_1. This process is usually done automatically by the impedance analysis software such as Zplot with Zview (Scribner Associates, Inc., Southern Pines, NC, USA).

2.1.2 Application of impedance measurement in analysis of the plasma membrane resistance and capacitance

Epithelium consists of electrical barrier networks formed by the two plasma membranes (apical and basolateral) and tight junctions, which can be illustrated as an electrical circuit in Figure 2.3. This circuit is simply explained by "lumped model" comprising of 4 resistors and 2 capacitors. Electrical elements of the apical and basolateral membranes consist of parallel R-C combinations. R_a and R_b are resistances of the apical and basolateral membranes, respectively. The capacitances of

the apical and basolateral membranes are symbolized by C_a and C_b, respectively. This transcellular circuit connects in parallel to a paracellular resistance (R_p). Additionally, the resistances of solution and Snapwell (a parallel scaffold, R_s) link in series to the circuit of the cell.

Clausen and coworkers (1979) showed the involvement of the lateral intercellular space resistance and included this parameter into the equivalent circuit. This circuit is known as the "distributed model" (Figure 2.4). However, this parameter is considered negligible in leaky epithelia, such as the intestine. Thus, the lumped model is adequate for determining resistive and capacitive components, as shown in the previous studies in human colonic T84 cells (Singh et al., 2002) and human bronchial epithelial cells (Kreindler et al., 2005).

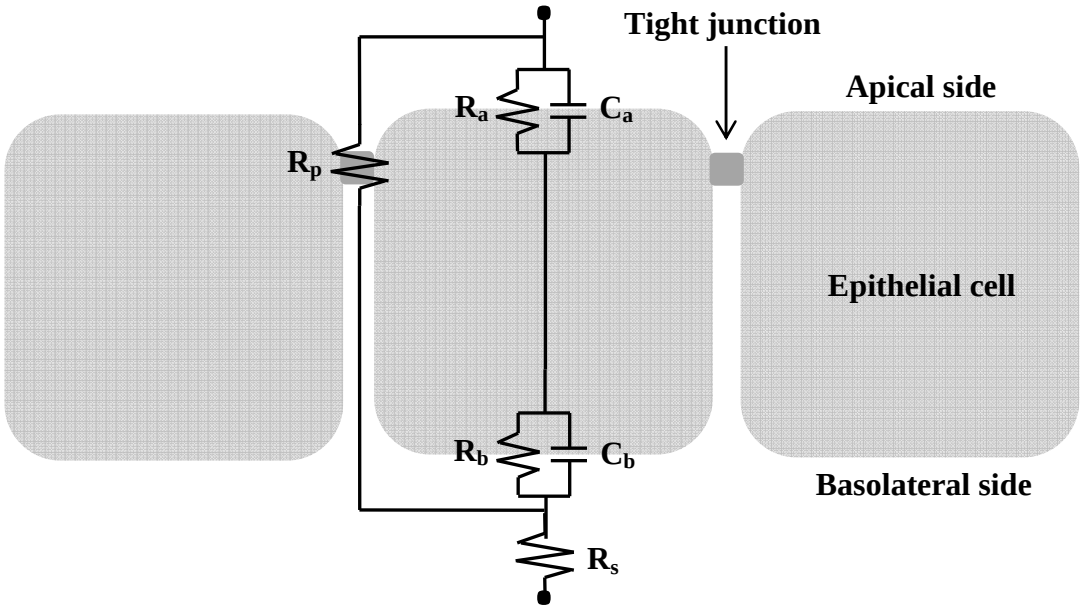

Figure 2.3 The "lumped model" representing an electrical circuit of the epithelium. The apical and basolateral membranes are composed of parallel R-C circuit. R_a and C_a are resistance and capacitance of the apical membrane. R_b and C_b are resistance and capacitance of the basolateral membrane. This transcellular circuit connects in parallel to a paracellular resistance (R_p). The resistance of the solution and Snapwell (R_s) is linked in series to the circuit of the cell.

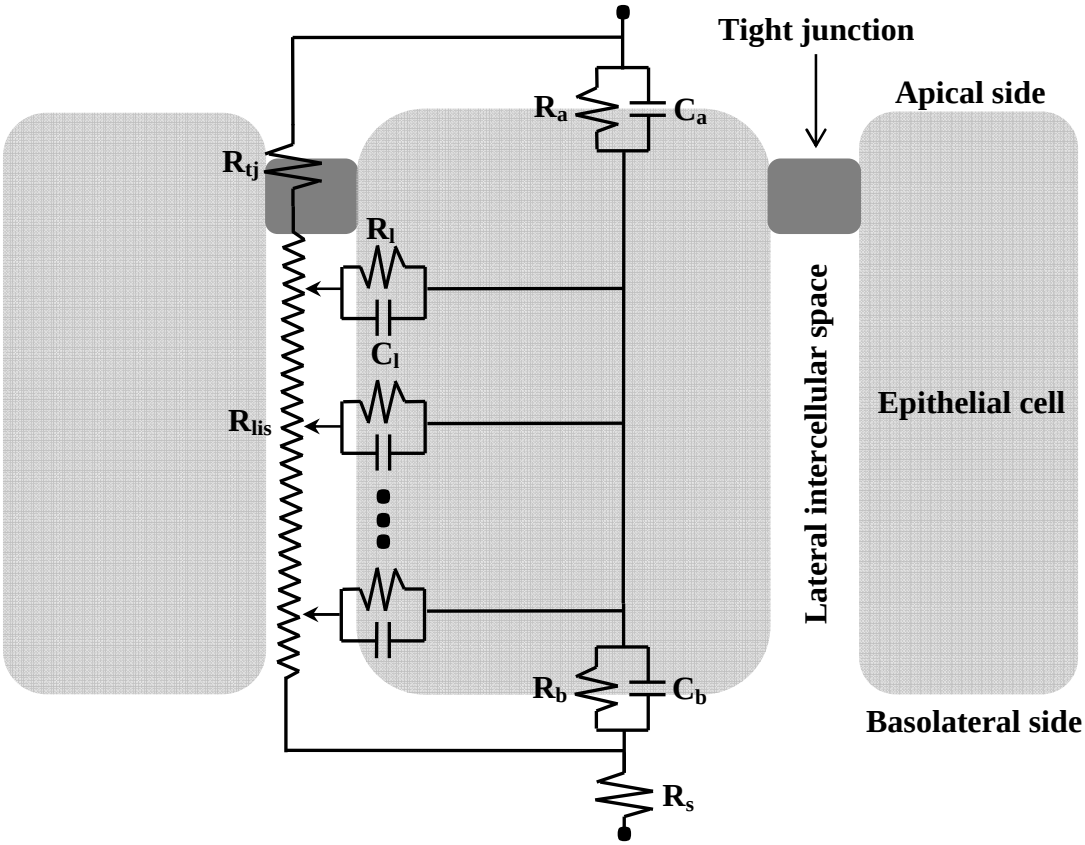

Figure 2.4 The "distributed model" representing an electrical circuit of the epithelium. The apical and basolateral membranes are composed of parallel R-C components. R_a and C_a are resistance and capacitance of the apical membrane. R_b and C_b are resistance and capacitance of the basolateral membrane. The paracellular pathway consists of 2 resistors from the tight junction (R_{tj}) and lateral intercellular space (R_{lis}). The R_{lis} acts as a "distributed resistor" which joins multiple R-C components of the lateral membrane (R_l and C_l). This transcellular circuit connects to R_{tj} and R_{lis} as depicted. The series resistance of the solution and Snapwell (R_s) is linked to the circuit of the cell.

Electrophysiological analysis of a monolayer using a DC approach provides limited information regarding the cellular capacitive and resistive components. Transepithelial resistance (R_t) calculated from the transepithelial potential difference (V_t) and short-circuit current (I_{sc}) across the monolayer mainly indicates the tightness of the tight junction and ion resistibility of the paracellular route to the overall ion transport (i.e., paracellular permeability). In other words, **the plasma membrane capacitance and resistance cannot be examined by DC method**. The AC-based impedance analysis provides an advantage over the DC-based technique since the plasma membrane properties can be obtained.

The electrical elements of the cells could be characterized by measuring the cells' impedances using AC signals with different frequencies. These values are used to simulate an equivalent circuit that shows the same impedance spectrum as the cell monolayer. The values and arrangement of the equivalent circuit can represent each electrical component of the cells. This technique is also useful for determining the single membrane and tight junction electrical elements. Ultimately, it can predict the biological responses of the cells to drug and/or chemical treatments in term of channel opening, activated transporter or recruitment of channel to the plasma membrane (see below).

2.1.3 Examples of the application of impedance measurement

Recent preliminary data showed that parathyroid hormone (PTH) could change I_{sc} and V_t in the DC method. However, changes in the electrical parameters may be due to the changes in the apical membrane, e.g., opening of apical anion channels, basolateral transporters, and/or tight junction properties. Impedance analysis can reveal which particular resistors (i.e., resistors in the apical membrane, basolateral membrane, and/or tight junction) or capacitors (i.e., capacitors in the apical and basolateral membranes) that are changed.

For instance, if the electrical components in the apical membrane are changed, we can focus our study on the channels or transporters localized in the apical membrane. Importantly, the tight junction resistance is difficult to measure using the DC-based technique since the cellular conductance may interfere with the measured parameters. However, such paracellular parameters can be simply determined in the

AC mode. Moreover, AC impedance analysis is rapid (completed within 2 min), and non-destructive (i.e., the monolayer can later be used in other experiments).

2.2 Parathyroid hormone (PTH)

PTH plays an important regulatory role in Ca^{2+} homeostasis, i.e., maintenance of serum Ca^{2+} level within the narrow physiological range. It exerts hypercalcemic effects by inducing bone resorption, renal Ca^{2+} reabsorption, and intestinal Ca^{2+} absorption (Arnaud et al., 1967). PTH is a polypeptide hormone secreted by the parathyroid glands when the plasma free Ca^{2+} is decreased (Murray et al., 2005). In addition, PTH has been found to exert its actions on Na^{+} (Azarani et al., 1995; Bezerra et al., 2008; Fan et al., 1999; Girardi et al., 2000), Cl^{-} (Laverty et al., 2003), HPO_4^{2-} (Zhang et al., 1999), HCO_3^{-} (Bank et al., 1978; Iino and Burg, 1979; McKinney and Myers, 1980a and 1980b), and Mg^{2+} (Quamme, 1997) transport. This implicates its non-calciotropic, ion regulatory function of PTH.

2.2.1 Chemistry and biology of PTH

2.2.1.1 PTH gene and structure

Human PTH gene locates on the short arm of chromosome 11 at band 11p15 (Naylor et al., 1983). PTH is originally synthesized from PTH mRNA as preproPTH containing 115 amino acids (Kemper et al., 1974; Milstein et al., 1972). Cleavage of this protein by rough endoplasmic reticulum (RER) excises 25-amino-acid pre-peptide yielding proPTH that still contains 6 extended amino acids at the N-terminus (Cohn et al., 1972; Dorner and Kemper, 1978; Kemper et al., 1972). Golgi apparatus converts proPTH to PTH with 84 amino acids (Habener et al., 1979).

Structure of native PTH (1–84) was predicted by Zull and Lev (1980). The first α-helix at the N-terminus forms a structure that incorporates N-terminal residues into a hydrophobic site. Residues 26–29 that are exposed to the surrounding environment are significant for receptor binding (Gardella et al., 1993; Rosenblatt et al., 1980). Moreover, this sequence links the next hydrophobic subdomain (34–37) to

the N-terminal hydrophobic structure. Tyrosine (Tyr) at position 43 is a terminal amino acid of the N-terminal hydrophobic region. Tyr-43 also bridges the remaining amino acids (45–84) which are poorly investigated because of the lack of biological functions. This tail sequence is plausibly important for molecular stability and secretion (Kronenberg et al., 1994; Lim et al., 1992).

Indeed, the residues 1–34 at the N-terminus of PTH retain a high receptor-binding property, and are sufficient for PTH functions (Pines, et al., 1996; Potts, et al., 1971). **Thus, commercial human PTH (1–34) was used in the present study**.

2.2.1.2 PTH synthesis and secretion

The parathyroid glands are the major source of plasma PTH. Chief cells of the parathyroid glands are responsible for PTH synthesis and release. PTH enters the circulation via fusion of PTH-containing vesicles to plasma membrane of the chief cells in response to low plasma Ca^{2+}, HPO_4^{2-} and 1,25-dihydroxyvitamin D_3 [$(1,25(OH)_2D_3)$] (Kronenberg et al., 1994).

Plasma Ca^{2+} directly controls PTH secretion through Ca^{2+}-sensing receptor (CaR) expressed on the chief cells. CaR is a member of G-protein-coupled receptor (GPCR) superfamily. Binding of the extracellular Ca^{2+} to CaR induces conformational change and subsequently conveys the signal through various pathways. Hypercalcemia inhibits PTH production and secretion as a part of negative feedback mechanism. This process is considered a 3-level regulation. Low plasma Ca^{2+} results in a fast response through CaR which rapidly stimulates PTH secretion into the circulation within seconds (Brown et al., 1999). Prolonged hypocalcemia in a period of hours decreases PTH mRNA level that consequently suppresses PTH synthesis (Chung et al., 1996; Moallem et al., 1998). Furthermore, chronic hypocalcemia induces parathyroid gland enlargement which can be detected within days or even months (Li et al., 1998; Malloy et al., 1999).

PTH prevents HPO_4^{2-} reabsorption in the kidney by promoting Na^+/HPO_4^{2-} cotransporter (NaP_i) internalization (Zhang et al., 1999). On the other hand, HPO_4^{2-} controls PTH secretion independent of blood Ca^{2+} and $1,25(OH)_2D_3$. In contrast to the regulation of PTH secretion by plasma Ca^{2+}, a high plasma HPO_4^{2-}

level increases PTH secretion, PTH mRNA expression, and parathyroid gland proliferation (Kilav et al., 1995; Naveh-Many et al., 1995; Rodriguez et al., 1996).

PTH secretion is also controlled by $1,25(OH)_2D_3$ at the transcriptional level (Russell et al., 1984; Silver et al., 1986). $1,25(OH)_2D_3$ binds to nuclear vitamin D receptor (VDR) and acts on vitamin D response element (VDRE) in the promoter of the PTH gene (Okazaki et al., 1988). This action consequently suppresses PTH gene transcription. Further effect of $1,25(OH)_2D_3$ is demonstrated by upregulation of VDR in the target cells by $1,25(OH)_2D_3$ itself (Naveh-Many et al., 1990). These mechanisms are considered as a part of the negative feedback loop resulting from PTH-induced increase in $1,25(OH)_2D_3$ production. This process prevents too much increase in the plasma Ca^{2+} levels induced by the effects of both hormones (Garabedian et al., 1972).

2.2.1.3 Serum PTH level

PTH is eliminated from the circulation mainly by liver and kidney resulting in a short half-life of a few minutes (Bringhurst et al., 1988). In the liver, PTH is taken up and degraded by Küpffer cells (Bringhurst et al., 1982). Filtrated PTH in kidney is mostly reabsorbed and proteolysed by tubular cells (Martin et al., 1979). Since the body provides an extremely high rate of PTH breakdown without mechanisms for modulation, circulating PTH is mainly determined by the rate of synthesis and release. (Kronenberg et al., 1994). Plasma PTH levels vary in the range of 10–60 pg/mL, depending on the plasma Ca^{2+} concentrations (Endres et al., 1991). Neither age nor gender has been observed to have effects on the plasma PTH levels (Haden et al., 2000).

2.2.2 PTH receptor (PTHR) and signal transduction

PTHR possesses 7 transmembrane domains with C- and N-termini at the intracellular and extracellular portions, respectively. The whole configuration of PTH-PTHR complex consists of 3 main parts: the linear PTH, the transmembrane PTHR, and binding G proteins. This classifies PTHR as a member of GPCR superfamily. Ligand binding induces conformational change of the receptor which, in turn, activates G protein and downstream signaling molecules (Chorev et al., 2001).

Activation of PTHR stimulates 2 distinct signaling pathways depending on which G protein is recruited. $G_{\alpha s}$ activates adenylyl cyclase which, in turn, induces cAMP production and subsequently activates PKA (Figure 2.5). PKA phosphorylates many proteins that later initiate PTH functions. PLC is stimulated by $G_{\alpha q}$, and converts phosphatidylinositol 4,5-bisphosphate (PIP_2) in the plasma membrane to DAG and IP_3. Cytoplasmic IP_3 binds to its receptor on the membrane of the smooth endoplasmic reticulum (SER). IP_3 receptor is a Ca^{2+} channel, the activation of which causes Ca^{2+} release into the cytoplasm. In the presence of Ca^{2+}, DAG stimulates PKC that further phosphorylates the downstream protein targets (Tovey et al., 2006). A study on activation domains of the PTH molecule reveals that the sequences which are responsible for adenylyl cyclase and PKC stimulation are the N-terminal residues and residues 28–32, respectively (Schluter, 1999).

There are 2 isoforms of PTHR, type 1 and 2 PTHR (PTHR1 and PTHR2), which differ in ligand specificity and tissue expression. PTHR1 found in bone, kidney, and intestine is activated by both PTH and PTH-related peptide (PTHrP) (Abou-Samra et al., 1992; Gensure et al., 2005; Urena et al., 1993; Watson et al., 2000). In contrast, PTHR2 is only stimulated by PTH and is exclusively expressed in the brain, where PTH synthesis is inconspicuous (Juppner, 1999; Usdin et al., 1995). Lack of PTHR2 expression in bone, kidney, and intestine suggests that this PTHR isoform does not play a physiological role in mineral regulation in these organs. Interestingly, tuberoinfundibular peptide-39 (TIP39), an endogenous ligand extracted from bovine hypothalamus, has been found to specifically activate PTHR2. Additionally, PTHR2 are strongly expressed in the hypothalamus and spinal cord, which implies a novel function of PTHR2 on the hypothalamic regulation of pituitary hormone secretion and pain sensation (Usdin et al., 1999).

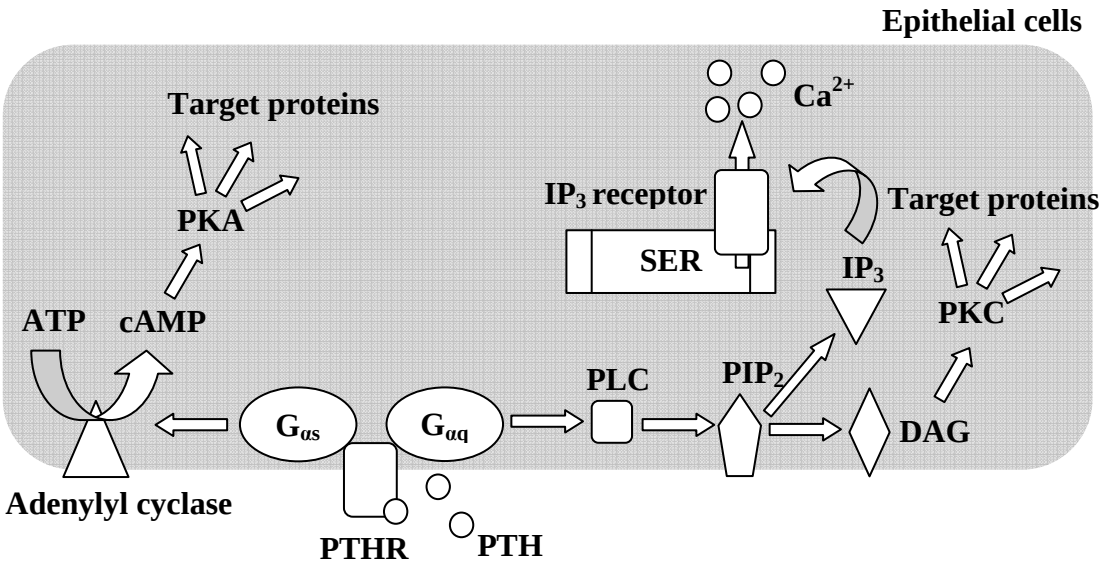

Figure 2.5 Classical PTH signaling pathways. PTH binds to PTH receptor (PTHR) and consequently activates $G_{\alpha s}$ and/or $G_{\alpha q}$. $G_{\alpha s}$ increases cyclic adenosine monophosphate (cAMP) levels and in turn activates protein kinase A (PKA). PKA, a member of the protein kinase family, phosphorylates many target proteins. On the other hand, $G_{\alpha q}$ stimulates phospholipase C (PLC) that cleaves phosphatidylinositol 4,5-bisphosphate (PIP_2) into diacyl glycerol (DAG) and inositol 1,4,5-trisphosphate (IP_3). DAG activates protein kinase C (PKC), which can phosphorylate various target proteins. IP_3 binds to its receptor, which acts as a Ca^{2+} channel, in the smooth endoplasmic reticulum (SER) membrane, and subsequently raises the intracellular Ca^{2+} concentration.

2.2.3 PTH-related peptide (PTHrP)

PTHrP is named after PTH since it shares similar protein structure, chemical properties, and some biological actions (e.g., stimulation of bone resorption). Both hormones can bind equally to PTHR1 and convey similar signaling pathway, resulting in the increased cAMP and intracellular Ca^{2+} levels (Chorev et al., 2001). However, PTH and PTHrP are not identical hormones. While PTH production is apparently limited to the parathyroid glands, PTHrP expression has been identified a number of tissues, including epithelia, mesenchymal tissues, endocrine glands, placenta, and central nervous system (Strewler, 2000; Watson et al., 2000). This indicates broader physiological functions of PTHrP in local tissues (i.e., paracrine) rather than the systemic role on Ca^{2+} homeostasis. PTHrP secretion does not depend on the plasma Ca^{2+} levels (Strewler, 2000). Unlike PTH, PTHrP normally regulates cell proliferation similar to other growth factors, e.g., epidermal growth factor (EGF), transforming growth factor-β (TGF-β), and insulin-like growth factor-I (IGF-I) whereas PTH does not (Wysolmerski and Stewart, 1998).

2.3 Intestinal anion secretion

Intestinal anion secretion is required for the maintenance of the optimal conditions for digestion and absorption of nutrients by regulating pH and fluidity of the lumen. This process is accomplished by the active Cl^- and HCO_3^- secretion mainly through the transcellular pathway (Figure 2.6). Intestinal anion secretion is activated by various secretagogues which increase the intracellular cAMP levels such as forskolin, epinephrine, prostaglandin E_1 (PGE_1), vasoactive intestinal peptide (VIP), and vasopressin (Dharmsathaphorn and Pandol, 1986; Fukuda et al., 2000; Grasset et al., 1985; Weymer et al., 1985). An increase in cAMP production leads to stimulation of cystic fibrosis transmembrane conductance regulator (CFTR) which provides an exit for both Cl^- and HCO_3^-. Some investigators suggest a role of Ca^{2+}-activated Cl^- channel (CaCC) in the transport of Cl^- across the apical membrane (Barrett and Keely, 2000).

In the basolateral membrane, Cl^- and HCO_3^- enter the intestinal cell via $Na^+/K^+/Cl^-$ cotransporter-1 (NKCC1) and electrogenic Na^+/HCO_3^- cotransporter-1 (NBCe1), respectively (Figure 2.6). Both transporters require a driving force from Na^+/K^+-ATPase. K^+ is extruded down its electrochemical gradient via the basolateral K^+ channels, which can be classified as cAMP- and Ca^{2+}-activated K^+ channels (Barrett and Keely, 2000). This step recycles K^+ for the Na^+/K^+-ATPase function, and is thus crucial for the maintenance of anion secretion process (Kunzelmann and Mall, 2002). Secretion of Cl^- creates a lumen-negative voltage that favors Na^+ secretion through the paracellular pathway. Eventually, Na^+, Cl^-, and H_2O are secreted into the intestinal lumen. On the other hand, HCO_3^- secretion is involved in both fluid secretion and luminal pH regulation.

It is noted that CFTR and CaCC in the apical membrane and K^+ channels in the basolateral membrane can be regulated by the intracellular levels of cAMP and Ca^{2+}; both of which are signaling molecules of PTH. Therefore, PTH could possibly activate these transporters through cAMP- and Ca^{2+}-dependent pathways, thereby leading to intestinal anion secretion.

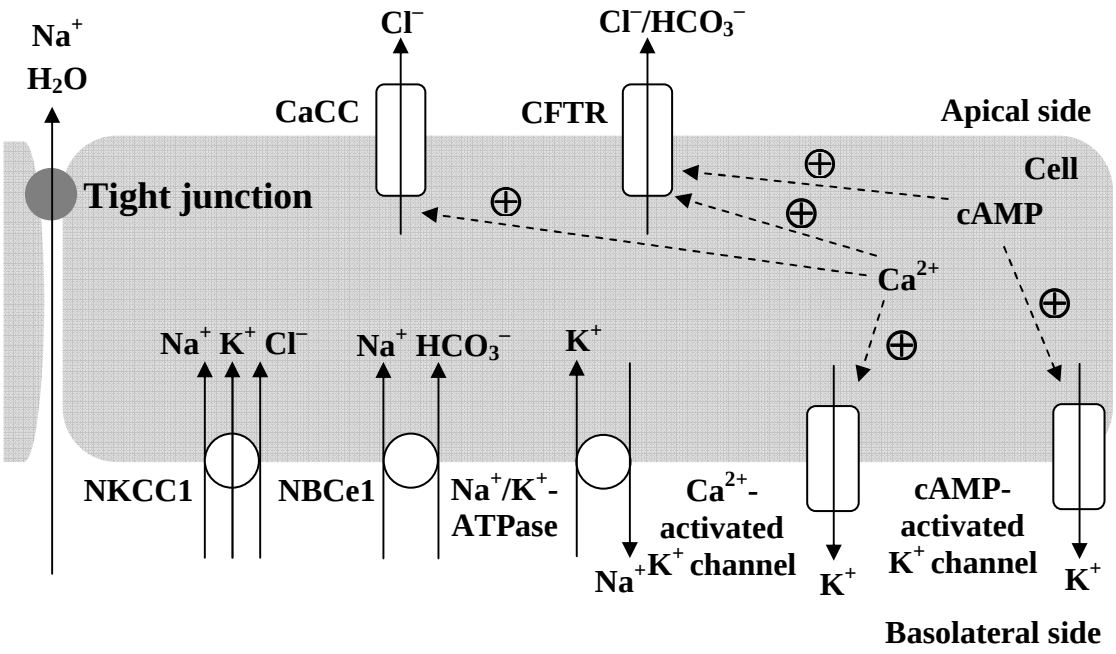

Figure 2.6 A schematic model of the intestinal anion secretion. In the basolateral membrane, Cl^- enters the cell through $Na^+/K^+/Cl^-$ cotransporter-1 (NKCC1), while HCO_3^- enters the cell through the electrogenic Na^+/HCO_3^- cotransporter-1 (NBCe1). Both transporters are driven by Na^+ gradient created by Na^+/K^+-ATPase. K^+ is recycled to the basolateral side through Ca^{2+}- and cAMP-activated K^+ channels, which, in turn, help maintain Na^+/K^+-ATPase activity. Cl^- exits the apical membrane through cystic fibrosis transmembrane conductance regulator (CFTR) and/or Ca^{2+}-activated Cl^- channel (CaCC). Na^+ and H_2O move into the lumen down the electrical and osmotic gradients, respectively. HCO_3^- is also secreted into the lumen through CFTR. Cyclic adenosine monophosphate (cAMP) plays a crucial role in the activation of CFTR and cAMP-activated K^+ channel, whereas Ca^{2+} activates CFTR, CaCC and Ca^{2+}-activated K^+ channel.

2.4 Intestinal epithelium-like Caco-2 cells

Caco-2 cells are derived from the human colorectal adenocarcinoma (Fogh et al., 1977). After confluence in a culture system, Caco-2 cells stop proliferation and gradually differentiate into enterocyte-like cells. The cells become polarized as columnar epithelial cells, form a monolayer (Le Bivic et al., 1990), and later show important characteristics of typical small intestinal cells, e.g., microvilli, tight junction, villin expression, and dome formation (Chantret et al., 1988; Hidalgo et al., 1989). Several studies support a structural and functional resemblance between Caco-2 and small intestinal absorptive cells (Bailey et al., 1996; Hilgers et al., 1990; Sambuy et al., 2005). Various enzymatic markers of the small intestine are abundantly expressed in the apical membrane of differentiated Caco-2 cells, including sucrase, isomaltase, lactase, alkaline phosphatase, γ-glutamyltransferase, aminopeptidease N, N-acetyltransferase, and dipeptidyl-peptidase IV (Chantret et al., 1988; Jumarie and Malo, 1991; Yoshioka et al., 1991). Moreover, Caco-2 cells have been used in several studies of electrolyte transport, including Cl^- and HCO_3^- secretion through the apical CFTR (Grasset et al., 1985; Inoue et al., 1997; Zhu et al., 2004 and 2005). Therefore, Caco-2 monolayer was used in the present PTH study.

CHAPTER III
MATERIALS AND METHODS

3.1 Cell culture

Human colorectal adenocarcinoma Caco-2 cell line (ATCC number: HTB-37) was a gift from the Institute of Nutrition, Mahidol University, and was stored and propagated at the Department of Physiology, Faculty of Science, Mahidol University, Thailand.

3.1.1 Maintenance

Caco-2 cells were grown in a 75-cm^2 T-flask (Corning, Corning, NY, USA) containing Dulbecco's modified Eagle's medium (DMEM; Sigma, St. Louis, MO, USA) supplemented with 15% heat-inactivated fetal bovine serum (FBS; GIBCO, Grand Island, NY, USA), 1% nonessential amino acid (NEAA; Sigma), 1% L-glutamine (GIBCO), and 100 U/mL penicillin-streptomycin (GIBCO). Culture medium was replaced everyday and the cells were passaged every 7 days or when cell confluence reached approximately 80%. The cells were maintained at 37 °C under a humidified 5% CO_2 atmosphere.

3.1.2 Experiments

In electrophysiological studies, Caco-2 cells (passage number 25–40) were seeded on a polyester Snapwell insert (12-mm diameter, 0.4-μm pore size, Corning) at 5×10^5 cells/well. Culture medium was replaced everyday for 14 days. The cells were cultured under a humidified 5% CO_2 atmosphere containing at 37 °C.

For mRNA isolation, Caco-2 cells (passage number 25–40) were cultured in a polystyrene 6-well culture plate (Corning) at 5×10^5 cells/well. Culture medium was replaced everyday for 14 days. The cells were grown under a humidified 5% CO_2 atmosphere containing at 37 °C.

3.2 Polymerase chain reaction (PCR)

3.2.1 mRNA isolation and reverse transcription

Total RNA from Caco-2 cells was extracted using TRIzol reagent (Invitrogen, Carlsbad, CA, USA) according to the manufacturer's instruction. RNA was treated with RQ1 DNase (Promega, Madison, WI, USA) and purified with RNeasy Mini kit (Qiagen, Valencia, CA, USA). Quantity and purity of the RNA were determined by measuring a ratio of 260/280 nm absorbance. One microgram of the total RNA was reverse-transcribed with Oligo-dT_{20} primer and iScript kit (Bio-rad, Hercules, CA, USA) by a thermal cycler (model MyCycler; Bio-rad). All samples were processed along with a house-keeping gene, glyceraldehydes-3-phosphate dehydrogenase (GAPDH), for normalization and checking reverse transcription consistency.

3.2.2 Conventional PCR and sequencing

All primers used in this study are shown in Table 3.1. The amplification reaction was performed by Bio-rad MyCycler (Bio-rad) with GoTaq Green Master Mix (Promenade, Madison, WI, USA). PCR products were electrophoresed on a 2% agarose gel and stained with 1 μg/mL ethidium bromide. The products were visualized under a UV transilluminator (Alpha Innotech, San Leandro, CA, USA). The resulting PCR products were also extracted by HiYield Gel/PCR DNA Extraction kit (Real Biotech Corporation, Taipei, Taiwan) and subsequently sequenced by ABI Prism 3100 Genetic Analyzer (Applied Biosystems, Foster City, CA, USA) to confirm the accuracy of the amplified sequences.

Table 3.1 Primers used in PCR experiments.

Gene (Accession number)	Primers (forward/reward)	Product length (bp)
PTHR1 (NM_000316)	5′-ACCTGCACAGCCTCATCTTCA-3′ 5′-CACACAGCCACGAAGACAGC-3′	103
PTHR2 (NM_005048)	5′-TCTGGGAGACCAATGCAGTTG-3′ 5′-GGCAGGCATACGAACACGAT-3′	118
GAPDH (NM_002046)	5′-CTGGTAAAGTGGATATTGTTG-3′ 5′-GAGGCTGTTGTCATACTTCTC-3′	359

PTHR1, type 1 parathyroid hormone receptor; PTHR2, type 2 parathyroid hormone receptor; GAPDH, glyceraldehydes 3-phosphate dehydrogenase.

3.3 Bathing solutions

3.3.1 Normal bathing solution

Normal bathing solution was composed of (in mmol/L) 118 NaCl, 4.7 KCl, 1.1 $MgSO_4$, 1.25 $CaCl_2$, 23 $NaHCO_3$, 12 D-glucose, 2.5 L-glutamine, and 2 mannitol (all chemicals were purchased from Sigma). The solution was continuously gassed with humidified 5% CO_2 in 95% O_2 and maintained temperature at 37 °C and pH 7.4. Osmolality of the solution was 290–295 mmol/kg H_2O, measured by a freezing point-based osmometer (model 3320; Advanced Instruments, Norwood, MA, USA). Water used in all solution formulae had a resistance more than 18.3 MΩ·cm and organic carbon less than 10 μg/L.

3.3.2 Cl^--depleted bathing solution

NaCl and KCl in the normal bathing solution were replaced by $NaC_6H_{11}O_6$ (sodium gluconate; Unilab, Sevenhills, NSW, Australia) and $KC_6H_{11}O_6$ (potassium gluconate; Sigma), respectively. To overcome Ca^{2+}-buffering capacity of the gluconate, $CaCl_2$ was raised to 2.5 mmol/L. The solution was gassed with humidified

5% CO_2 in 95% O_2 and maintained temperature at 37 °C and pH 7.4. Osmolality of the solution was 290–295 mmol/kg H_2O, measured by a freezing point-based osmometer.

3.3.3 HCO_3^--depleted bathing solution

HCO_3^- in the normal bathing solution was replaced by HEPES-Na (Sigma) and the concentration of Na^+ was adjusted by $NaC_6H_{11}O_6$. The solution was gassed with humidified 100% O_2 and maintained temperature at 37 °C and pH 7.4. Osmolality of the solution was 290–295 mmol/kg H_2O, measured by a freezing point-based osmometer.

3.3.4 Cl^-/HCO_3^--depleted bathing solution

NaCl, KCl, and HCO_3^- in the normal bathing solution were replaced by $NaC_6H_{11}O_6$, $KC_6H_{11}O_6$, and HEPES-Na, respectively. The concentration of Na^+ was adjusted by $NaC_6H_{11}O_6$. The solution was gassed with humidified 100% O_2 and maintained temperature at 37 °C and pH 7.4. Osmolality of the solution was 290–295 mmol/kg H_2O, measured by a freezing point-based osmometer.

3.4 Measurement of electrical parameters

3.4.1 Ussing chamber setup

Electrical parameters, i.e., transepithelial voltage (V_t), short-circuit current (I_{sc}), and transepithelial resistance (R_t), were determined by Ussing chamber technique (Figure 3.1). Snapwell containing 14-day-old Caco-2 monolayer was placed in between the 2 hemichambers. Two pairs of 2 mol/L KCl 2% agar bridges which were connected to Ag/AgCl electrodes were fitted adjacent to the monolayer (V_1 and V_2) for V_t measurement and at the end of each hemichamber (I_1 and I_2) for applying direct current. These Ag/AgCl electrodes were connected to a preamplifier/current generating unit (model ECV-4000, World Precision Instrument, Sarasota, FL, USA) and PowerLab/4SP (ADInstruments, Colorado Springs, CO, USA). The PowerLab/4SP was operated with Chart version 5.4.1 for Windows (ADInstruments).

3.4.2 Open-circuit experiment

Ussing chamber experiments were carried out under an open-circuit condition, as previously described by Kunzelmann and coworkers (2000). V_t was measured by V_1 and V_2 using V_2 on the basolateral side as a reference electrode (Figure 3.1). I_1 and I_2 were used to create desirable currents. To determine R_t and I_{sc} (herein, I_{sc} means "equivalent" short-circuit current), current pulses (I; 3 μA amplitude, 800 ms pulse duration, 0.1 Hz frequency) were continuously applied across the monolayer. The corresponding V_t deflection (ΔV_t) was used to calculate R_t according to Ohm's law;

$$R_t = \Delta V_t / I \quad (12)$$

I_{sc} was then calculated from V_t and R_t (Equation 13) according to Ohm's law,

$$I_{sc} = V_t / R_t \quad (13)$$

To mimic physiological conditions, temperature inside the Ussing chamber was maintained at 37 °C throughout the experiment. Bathing solution was continuously gassed with humidified 5% CO_2 in 95% O_2 to maintain fluid mixing, O_2 supply for the cells, and pH of 7.4.

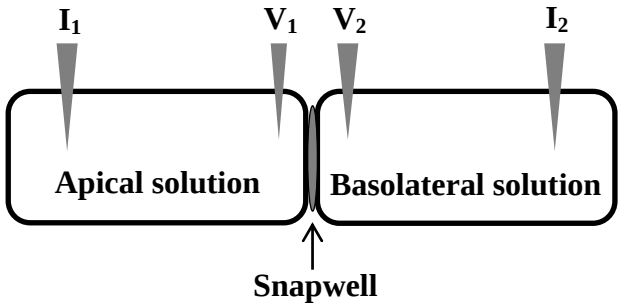

Figure 3.1 A model of Ussing chamber used in the present study. The chamber was composed of 2 hemichambers. A Snapwell containing cell monolayer was placed in between hemichambers. Four electrodes, I_1, I_2, V_1, and V_2, were placed as shown in the figure.

3.5 Impedance analysis

Snapwell containing 14-day-old cell monolayer was mounted in the modified Ussing chamber as shown in Figure 3.1. The electrode arrangement was the same as described in the measurement of electrical parameters. Impedance analysis was performed by using a 1255B frequency response analyzer and a 1287A electrochemical interface (Solartron, Farnborough Hampshire, UK). Sine-wave currents (35 $\mu A/cm^2$) were applied to the Caco-2 monolayer at different time points, i.e., before adding PTH or forskolin, at 1, 5, 10, 15, 20, 25, 30, 35, and 40 min after adding PTH or forskolin. Frequency used in all experiments was 0.5 Hz – 10 kHz. The data was processed and plotted in Nyquist and Bode diagrams by Zplot with Zview (version 3.0; Scribner Associates, Inc., Southern Pines, NC, USA), which incorporates a non-linear least-squares fitting algorithm.

An equivalent circuit was analyzed with regard to the lumped model as shown in Figure 2.3. The circuit is comprised of 4 resistors and 2 capacitors. Electrical elements of the apical and basolateral membranes consist of 2 parallel R-C combinations, i.e., R_a-C_a and R_b-C_b. R_p, a paracellular resistance, connects in parallel to the R-C combinations. These components constitute a circuit of the cell. Additionally, R_s which represents a resistance of the solution and Snapwell links in series to the cell circuit.

In order to calculate the circuit parameters, i.e., R_a, R_b, C_a, C_b, it is required an independent estimate of R_p. R_p was acquired from *y*-interception of a plot between transepithelial conductance (G_t) and I_{sc} as described by Wills et al. (Wills et al., 1979).

$$G_t = I_{sc}/E_b + G_p \quad (14)$$

G_p is transepithelial conductance which is reciprocal to R_p while E_b is electromotive force of the basolateral membrane. We used the data during cell response to PTH or forskolin to plot G_t vs. I_{sc} and the graph was subsequently analyzed by linear regression (Singh et al., 2002). The calculation was based on the assumption that R_p was constant during PTH stimulation. This assumption was

validated by mannitol flux and the nystatin-induced membrane permeabilization method (Wills et al., 1979). The calculated R_p with the impedance data was fitted by Zplot with Zview to obtain R_a, R_b, C_a, and C_b. The quality of the graph fitting was appraised by using normalized error (norm) which is the percent difference between measured and fitted data at each frequency.

For the membrane permeabilization experiment, the monolayer was stimulated with PTH for 10 min as shown in Figure 3.2. After the electrical parameters were stable, 10 μg/mL nystatin (Calbiochem, San Diego, CA, USA) was added every 5 min 6 times, and the values of I_{sc} and G_t measured at 11 time points were used to calculate G_p.

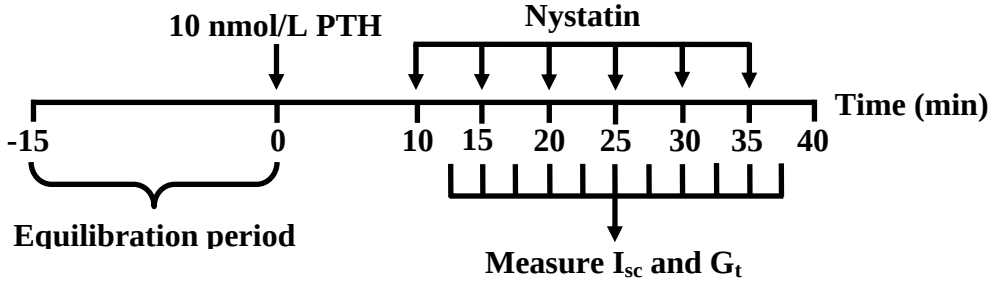

Figure 3.2 Experimental protocol of the nystatin-induced membrane permeabilization. A Caco-2 monolayer was equilibrated in normal bathing solution for 15 min. Parathyroid hormone (PTH; 10 nmol/L) was added to the basolateral side of the monolayer at 0 min. After the electrical parameters remained stable for 10 min, 10 μg/mL nystatin was added to the apical side of the monolayer every 5 min for 30 min, and I_{sc} and G_t were measured at 11 time points.

3.6 Mannitol flux

Measurement of mannitol flux was performed by the method of Tanrattana and colleagues (2004) as shown in Figure 3.3. A Caco-2 monolayer was incubated for 15 min in normal bathing solution. Then, one side of the chamber (hot side) was

replaced with ^{3}H-mannitol-containing bathing solution (specific activity of ~70 mCi/mol; Amersham, Buckinghamshire, UK), while the other side (cold side) was replaced with fresh normal bathing solution. PTH was added to the basolateral side of the monolayer at 10 min. Thereafter, a 100 μL sample was collected from each side of the chamber every 10 min for 5 times. Radioactivity of ^{3}H-mannitol was analyzed by liquid scintillation spectrophotometer (model Tri-Carb 3100 TR; Perkin-Elmer, Shelton, CT, USA).

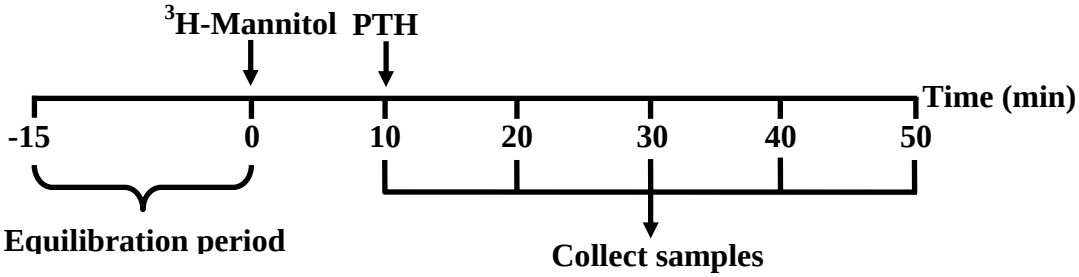

Figure 3.3 The experimental protocol of mannitol flux measurement. A Caco-2 monolayer was equilibrated in normal bathing solution for 15 min. Then, the solution was replaced with ^{3}H-mannitol-containing solution on one side of the chamber (hot side), while the other side (cold side) was replaced with fresh normal bathing solution. PTH (10 nmol/L) was added to the basolateral side at 10 min after solution replacement. Samples (100 μL) were collected from each side of the chamber every 10 min for 50 min.

Hot-to-cold unidirectional flux ($J_{H\rightarrow C}$) of mannitol was calculated as follow,

$$J_{H\rightarrow C} = R_{H\rightarrow C}/(S_H \times a) \quad (15)$$

where $J_{H\rightarrow C}$ is hot-to-cold unidirectional flux (nmol/h/cm^2)

$R_{H\rightarrow C}$ is a rate of tracer appearance in the cold side (cpm/h)

S_H is a specific activity of the hot side (cpm/nmol)

a is surface area of a Snapwell (cm^2)

S_H was calculated from Equation 16.

$$S_H = C_H/C_T \quad (16)$$

where S_H is a specific activity of the hot side (cpm/nmol)
C_H is a mean radioactivity in the hot side (cpm)
C_T is the total concentration of mannitol in the hot side (nmol)

3.7 Experimental protocols

3.7.1 Measurement of the plasma membrane capacitance and resistance of Caco-2 monolayer by impedance analysis

3.7.1.1 Basal membrane capacitance and resistance of Caco-2 monolayer

Caco-2 cells were grown on a Snapwell as a monolayer for 14 days. After reaching confluency, the monolayer was mounted in the Ussing chamber setup. The monolayer was equilibrated for 15 min, after which basal electrical parameters, i.e., V_t, I_{sc}, R_t, were determined by a DC-based procedure. Subsequently, impedance analysis was performed to determine the basal membrane capacitance and resistance of the monolayer. R_a, R_b, C_a, and C_b were calculated as described above.

3.7.1.2 Effect of forskolin on membrane capacitance and resistance of the Caco-2 monolayer

To validate the action of forskolin on the monolayer, the tracings of electrical parameters which represent ion transport across the monolayer were examined during forskolin stimulation. V_t, I_{sc}, and R_t were determined under an open-circuit condition by a DC-based procedure. After 15-min equilibration, 10 μmol/L forskolin (Sigma) was added to the basolateral side of the monolayer, and electrical parameters were determined for 15 min.

To investigate the effect of forskolin on membrane capacitance and resistance of the Caco-2 monolayer, the monolayer was grown and later mounted in the Ussing chamber setup. After 15-min equilibration, impedance analysis was performed (at 0 min) to measure basal membrane capacitance and resistance of the monolayer (Figure 3.4). Consequently, 10 μmol/L forskolin was added to the basolateral side of the monolayer, and impedance of the monolayer was measured at 1, 5, 10, 15, 20, 25, 30, 35, and 40 min after forskolin stimulation to investigate the alterations of membrane capacitance and resistance. R_a, R_b, C_a, and C_b were calculated as described in the previous section.

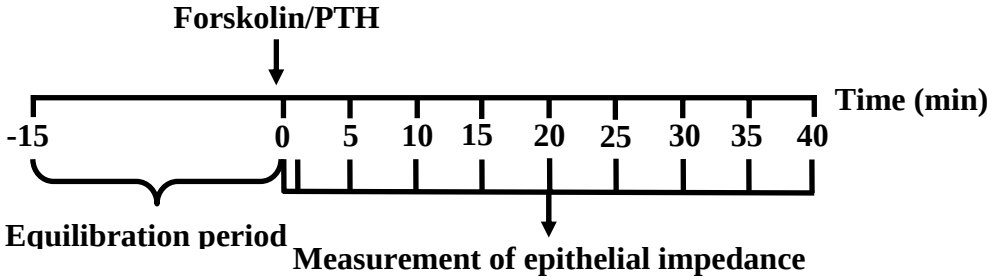

Figure 3.4 The experimental protocol of epithelial impedance measurement. A Caco-2 monolayer was equilibrated in normal bathing solution for 15 min. Forskolin (10 μmol/L) or parathyroid hormone (PTH; 10 nmol/L) was added to the basolateral side of the monolayer at 0 min. Impedance of the monolayer was measured at 0 (baseline), 1, 5, 10, 15, 20, 25, 30, 35 and 40 min after PTH treatment.

3.7.2 Effect of PTH on membrane capacitance and resistance in Caco-2 monolayer as determined by impedance analysis

3.7.2.1 PTHR mRNA expression in the Caco-2 cells

The Caco-2 cells were grown on a 6-well cell culture plate for 14 days until confluent. Then, cells were washed with phosphate buffered saline (PBS) and harvested by scraping. Total RNA extraction and reverse transcription were subsequently performed as described in the previous section. Both PTHR1 and PTHR2 mRNA expression was determined by conventional and real-time PCR.

3.7.2.2 Effect of PTH on the plasma membrane capacitance and resistance in Caco-2 monolayer

The monolayer was equilibrated for 15 min, and then impedance analysis was performed (at 0 min) to determine basal membrane capacitance and resistance of the monolayer (Figure 3.4). Subsequently, 10 nmol/L PTH (Sigma) was added to the basolateral side of the monolayer, and impedance of the monolayer was measured at 1, 5, 10, 15, 20, 25, 30, 35, and 40 min after PTH stimulation to investigate the alterations of membrane capacitance and resistance. R_a, R_b, C_a, and C_b were calculated as described in the previous section.

3.7.3 The target transporters and signaling pathways of PTH in Caco-2 cells

3.7.3.1 Effect of PTH on epithelial ion transport in Caco-2 monolayer

V_t, I_{sc}, and R_t were determined under an open-circuit condition by a DC-based procedure. After 15-min equilibration, 0.3, 1, 3, 10 or 30 nmol/L PTH was added to the basolateral side of the monolayer, and electrical parameters were determined for 15 min.

To investigate PTH site of action (basolateral vs. apical), 10 nmol/L PTH was added to either the basolateral side or apical side of the monolayer. Electrical parameters were then determined for 15 min.

To confirm the specificity of PTH, the monolayer was exposed to 10 nmol/L 1–34 PTH (active PTH), 13–34 PTH (inactive PTH; Sigma), or autoclaved 1–34 PTH in the basolateral side. All electrical parameters were then determined for 15 min. In some experiments, 1–34 PTH was incubated with polyclonal PTH antibody (CAT No. ab14164, Abcam, Cambridge, UK) at various dilutions, i.e., 1:10000, 1:1000, 1:100, or 1:10, before adding to the basolateral solution.

3.7.3.2 Effect of PTH on the paracellular resistance of Caco-2 monolayer

Effect of PTH on paracellular resistance of the Caco-2 was determined by ^{3}H-mannitol transport and the nystatin-induced membrane permeabilization technique.

3.7.3.3 Effects of Cl^- and/or HCO_3^- depletion on the PTH-stimulated ion transport in Caco-2 monolayer

The monolayer was bathed on both sides with normal, Cl^--depleted, HCO_3^--depleted or Cl^-/HCO_3^--depleted solution. Preparation of the solution was described in section C. V_t, I_{sc}, and R_t were determined under an open-circuit condition by a DC-based procedure. After 15-min equilibration, 10 nmol/L PTH was added to the basolateral side of the monolayer and electrical parameters were determined for 15 min.

3.7.3.4 The sources of HCO_3^- for the PTH-stimulated HCO_3^- secretion in Caco-2 monolayer

V_t, I_{sc}, and R_t were determined under an open-circuit condition by a DC-based procedure. After 15-min equilibration, the monolayer was preincubated with NBCe1 or carbonic anhydrase inhibitors for a specific time as described in Table 3.2. Consequently, 10 nmol/L PTH was added to the basolateral side of the monolayer, and electrical parameters were determined for 15 min.

3.7.3.5 Responsible apical ion channels for the PTH-stimulated HCO_3^- efflux in Caco-2 monolayer

V_t, I_{sc}, and R_t were determined under an open-circuit condition by a DC-based procedure. After 15-min equilibration, the monolayer was preincubated with various anion transporter inhibitors for a specific time as described in Table 3.3. Consequently, 10 nmol/L PTH was added to the basolateral side of the monolayer, and electrical parameters were determined for 15 min.

3.7.3.6 Involvement of Na^+/H^+ exchanger (NHE) in the PTH-stimulated HCO_3^- secretion in Caco-2 monolayer

V_t, I_{sc}, and R_t were determined under an open-circuit condition by a DC-based procedure. After 15-min equilibration, the monolayer was incubated with various NHE inhibitors as described in Table 3.4. Consequently, 10 nmol/L PTH was added to the basolateral side of the monolayer, and electrical parameters were determined for 15 min.

3.7.3.7 Involvement of K^+ channels in the PTH-stimulated HCO_3^- secretion in Caco-2 monolayer

V_t, I_{sc}, and R_t were determined under an open-circuit condition by a DC-based procedure. After 15-min equilibration, the monolayer was incubated with various K^+ channel inhibitors as described in Table 3.5. Consequently, 10 nmol/L PTH was added to the basolateral side of the monolayer, and electrical parameters were determined for 15 min.

3.7.3.8 Responsible signaling pathways for the PTH-stimulated HCO_3^- secretion in Caco-2 monolayer

V_t, I_{sc}, and R_t were determined under an open-circuit condition by a DC-based procedure. After 15-min equilibration, the monolayer was incubated with PKA, PI3K or Ca^{2+}/PKC inhibitors as described in Table 3.6. Consequently, 10 nmol/L PTH was added to the basolateral side of the monolayer, and electrical parameters were determined for 15 min.

3.8 Statistical analysis

Results are expressed as means ± standard errors (SE). Multiple sets of data were compared by one-way analysis of variance (ANOVA) followed by Dunnett's multiple comparison test, or Newman-Keuls' test when appropriate. Comparisons between 2 sets of data were analyzed by paired Student's *t*-test, unpaired Student's *t*-test, or Mann-Whitney *U*-test when appropriate. A dose-response relationship of PTH was plotted by nonlinear least squares fitting method. Differences were considered significant when $P < 0.05$. All statistical tests were performed by GraphPad Prism 5.0 for Windows (GraphPad Software, San Diego, CA, USA).

Table 3.2 Inhibitors used in protocol G3.4.

Abbreviated name	Chemical name	Target	Concentration used	Side of exposure	Incubation time	Manufacturer
Bumetanide	3-(aminosulfonyl)-5-(butylamino)-4-phenoxybenzoic acid	NKCC1	100 µmol/L	Basolateral	15 min	Sigma, St. Louis, MO, USA
DIDS	4,4′-diisothiocyanatostilbene-2,2′-disulfonic acid disodium salt hydrate	NBCe1	500 µmol/L	Basolateral	15 min	Sigma, St. Louis, MO, USA
Ouabain	acocantherine, G-strophanthin, 1β, 3β,5β,11α,14,19-hexahydroxycard-20(22)-enolide 3-(6-deoxy-α-L-manno pyranoside)	Na^+/K^+-ATPase	1 mmol/L	Basolateral	30 min	Sigma, St. Louis, MO, USA
Methazolamide	N-(4-methyl-2-sulfamoyl-Δ^2-1,3,4-thiadiazolin-5-ylidene) acetamide	Carbonic anhydrase	1 mmol/L	Apical and basolateral	30 min	Sigma, St. Louis, MO, USA

NKCC1, $Na^+/K^+/Cl^-$ cotransporter 1; NBCe1, electrogenic Na^+/HCO_3^- cotransporter-1.

Table 3.3 Inhibitors used in protocol G3.5.

Abbreviated name	Chemical name	Target	Concentration used	Side of exposure	Incubation time	Manufacturer
NPPB	5-nitro-2-(3-phenyl propylamino) benzoic acid	Cl^- channels	20, 50, 100, 200 µmol/L	Apical	15 min	Sigma, St. Louis, MO, USA
$CFTR_{inh}$-172	5-[(4-carboxy phenyl)methylene]-2-thioxo-3-[(3-trifluoromethyl)phenyl -4-thiazolidinone	CFTR	2, 5, 10, 20 µmol/L	Apical	15 min	Calbiochem, San Diego, CA, USA
GlyH-101	N-(2-naphthalenyl)-((3,5-dibromo-2,4-dihydroxyphenyl) methylene)glycine hydrazide	CFTR	50 µmol/L	Apical	15 min	Calbiochem, San Diego, CA, USA
DIDS	4,4′-diisothiocya natostilbene-2,2′-disulfonic acid disodium salt hydrate	CaCC and Cl^-/HCO_3^- exchangers	500 µmol/L	Apical	15 min	Sigma, St. Louis, MO, USA

CFTR, cystic fibrotic transmembrane conductance regulator; CaCC, Ca^{2+}-activated Cl^- channel.

Table 3.4 Inhibitors used in protocol G3.6.

Abbreviated name	Chemical name	Target	Concentration used	Side of exposure	Incubation time	Manufacturer
Amiloride	N-amidino-3,5-diamino-6-chloropyrazinecarboxamide	ENaC and NHE3	10, 100, 1000 µmol/L	Apical	15 min	Sigma, St. Louis, MO, USA
Amiloride	N-amidino-3,5-diamino-6-chloropyrazinecarboxamide	NHE1	1000 µmol/L	Basolateral	15 min	Sigma, St. Louis, MO, USA
EIPA	5-(N-ethyl-N-isopropyl) amiloride	NHE3	10, 20, 50 µmol/L	Apical	15 min	Sigma, St. Louis, MO, USA
EIPA	5-(N-ethyl-N-isopropyl) amiloride	NHE1	50 µmol/L	Basolateral	15 min	Sigma, St. Louis, MO, USA

ENaC, epithelial Na^+ channel; NHE1, Na^+/H^+ exchanger-1; NHE3, Na^+/H^+ exchanger-3.

Table 3.5 Inhibitors used in protocol G3.7.

Abbreviated name	Chemical name	Target	Concentration used	Side of exposure	Incubation time	Manufacturer
Chromanol 293B	Trans-N-[6-cyano-3,4-dihydro-3-hydroxy-2,2-dimethyl-2H-1-benzopyran-4-yl]-N-methyl-ethane sulfonamide	cAMP-activated K^+ channel	100 µmol/L	Basolateral	15 min	Sigma, St. Louis, MO, USA
Charybdotoxin	Glu-Phe-Thr-Asn-Val-Ser-Cys-Thr-Thr-Ser-Lys-Glu-Cys-Trp-Ser-Val-Cys-Gln-Arg-Leu-His-Asn-Thr-Ser-Arg-Gly-Lys-Cys-Met-Asn-Lys-Lys-Cys-Arg-Cys-Tyr-Ser	Ca^{2+}-activated K^+ channel	100 nmol/L	Basolateral	15 min	Sigma, St. Louis, MO, USA

Table 3.6 Inhibitors used in protocol G3.8.

Abbreviated name	Chemical name	Target	Concentration used	Side of exposure	Incubation time	Manufacturer
PKI 14–22	PKA inhibitor 14-22 amide, myristoylated	PKA	10 µmol/L	Apical and basolateral	30 min	Calbiochem, San Diego, CA, USA
BAPTA-AM	1,2-Bis(*o*-amino phenoxy)ethane-N,N,N′,N′-tetraacetic acid tetra (acetoxy methyl) ester	Intracellular Ca^{2+}	50 µmol/L	Apical and basolateral	30 min	Calbiochem, San Diego, CA, USA
GF-109203X	GF-109203X	PKC	1 µmol/L	Apical and basolateral	30 min	A.G. Scientific, San Diego, CA, USA
Wortmannin	(1S,6bR,9aS,11R,11bR) 11-(acetyloxy)-1,6b,7,8,9a,10,11,11b-octahydro-1-(methoxymethyl)-9a,11b-dimethyl-3H-furo[4,3,2-de]indeno[4,5,-h]-2-h]-2-benzopyran-3,6,9-trione	PI3K	200 nmol/L	Apical and basolateral	30 min	Tocris Bioscience, Bristol, UK
LY-294002	2-(4-morpholinyl)-8-phenyl-4H-1-benzopyran-4-one hydrochloride	PI3K	75 µmol/L	Apical and basolateral	30 min	Tocris Bioscience, Bristol, UK

PKA, protein kinase A; PKC, protein kinase C; PI3K, phosphoinositide-3-kinase.

CHAPTER IV
RESULTS

4.1 Measurement of the plasma membrane capacitance and resistance in Caco-2 monolayer by impedance analysis

DC analysis of epithelial circuitry could not determine the electrical elements of epithelium, i.e., R_a, R_b, C_a, and C_b. These electrical parameters were, therefore, determined by AC-based impedance analysis.

4.1.1 Basal membrane capacitance and resistance of Caco-2 monolayer

Basal electrical parameters of Caco-2 monolayer measured by DC-based technique were shown in Table 4.1. The confluent Caco-2 monolayer exhibited a basal V_t of 0.59 ± 0.09 mV (apical negative; n = 15), with a basal R_t of 232.74 ± 12.77 $\Omega \cdot cm^2$ (n = 15) and I_{sc} of 2.60 ± 0.40 $\mu A/cm^2$ (n = 15).

Thereafter, impedance analysis was used to determine membrane capacitance and resistance of the monolayer. An equivalent circuit was analyzed with regard to the lumped model as shown in Figure 2.2. The circuit is comprised of 4 resistors and 2 capacitors. Electrical elements of the apical and basolateral membranes consist of parallel R-C combinations. This transcellular circuit connects in parallel to a paracellular resistor (R_p), which is mainly determined by the tight junction. In addition, a resistor of the solution and Snapwell (R_s) is linked in series to the circuit of the cell.

Impedance results of the monolayer in the basal condition are illustrated in the Nyquist plot (Figure 4.1A) showing a relationship between real (Z_R) and imaginary (Z_I) terms of the impedance. Plots of frequency vs. magnitude of the impedance ($|Z|$) and frequency vs. phase difference (θ) are shown by Bode magnitude plot (Figure 4.1B) and Bode phase plot (Figure 4.1C), respectively. These parameters were used to

calculate the plasma membrane capacitance and resistance of the monolayer using impedance analysis software. The calculated plasma membrane capacitance and resistance are shown in Table 4.2. The Caco-2 monolayer had R_a and R_b of 2141.30 ± 222.50 and 993.96 ± 60.96 $\Omega \cdot cm^2$, respectively. These values are comparable to the study of Caco-2 membrane resistance using a microelectrode recording by Grasset and colleagues (1984). C_a and C_b of the monolayer were 28.98 ± 0.69 and 12.36 ± 0.23 $\mu F/cm^2$, respectively, consistent with those found in mammalian colon (Wills and Clausen, 1987).

These results indicated that the AC-based impedance analysis was able to determine the plasma membrane capacitance and resistance of Caco-2 monolayer.

Table 4.1 Basal electrical parameters of Caco-2 monolayer as measured by DC-based Ussing system.

Electrical parameters	Values	Unit	n
V_t	0.59 ± 0.09	mV	15
I_{sc}	2.60 ± 0.40	$\mu A/cm^2$	15
R_t	232.74 ± 12.77	$\Omega \cdot cm^2$	15

V_t, transepithelial voltage (potential) difference; I_{sc}, short-circuit current; R_t, transepithelial resistance.

Table 4.2 Basal membrane capacitance and resistance of Caco-2 monolayer as measured by AC-based impedance analysis.

Electrical parameters	Values	Unit	n
R_a	2141.30 ± 222.50	$\Omega \cdot cm^2$	10
R_b	993.96 ± 60.96	$\Omega \cdot cm^2$	10
C_a	28.98 ± 0.69	$\mu F/cm^2$	10
C_b	12.36 ± 0.23	$\mu F/cm^2$	10

R_a, apical membrane resistance; R_b, basolateral membrane resistance; C_a, apical membrane capacitance; C_b, basolateral membrane capacitance.

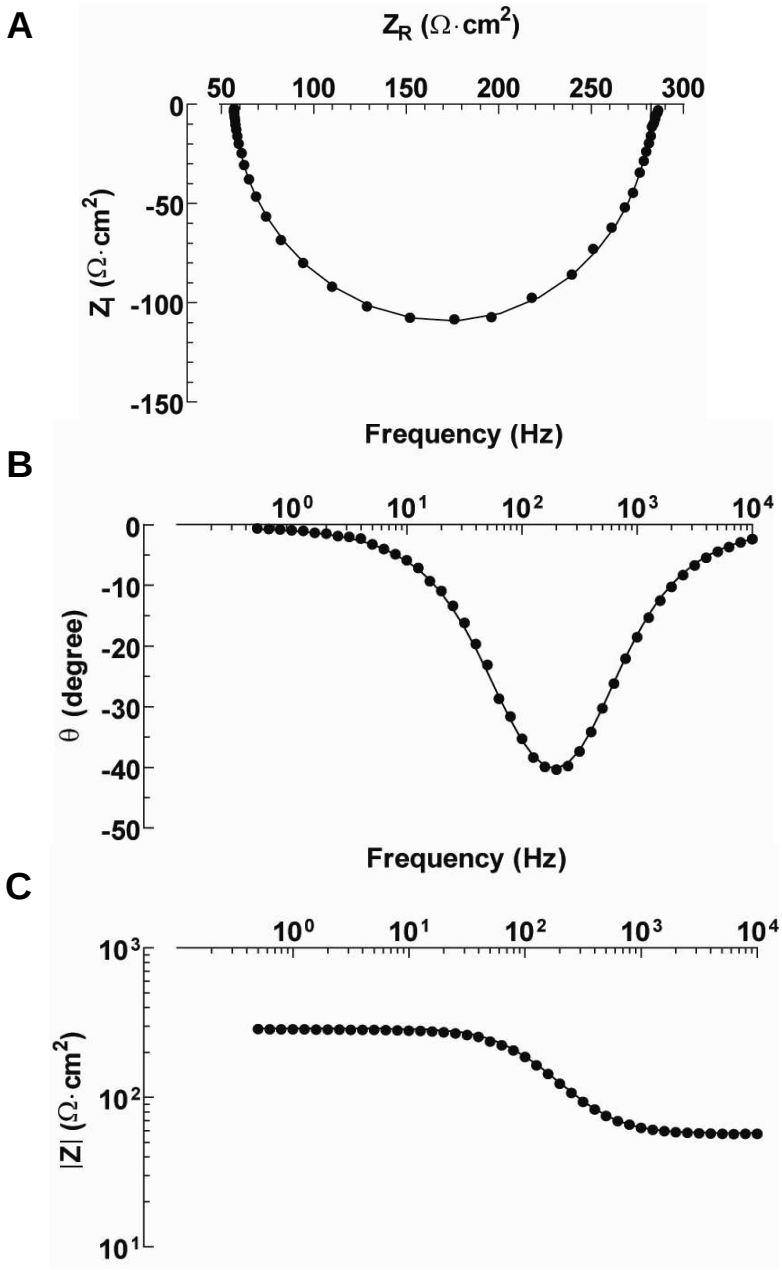

Figure 4.1 A representative transepithelial impedance of the Caco-2 monolayer. The data is presented in **(A)** Nyquist plot, **(B)** Bode phase plot, and **(C)** Bode magnitude plot. The impedance results were fitted by the lumped model, and are shown in solid lines. The parameters are as followed; apical membrane resistance (R_a) = 2028.00 $\Omega \cdot cm^2$, basolateral membrane resistance (R_b) = 1004.00 $\Omega \cdot cm^2$, apical membrane capacitance (C_a) = 27.43 $\mu F/cm^2$, basolateral membrane capacitance (C_b) = 12.84 $\mu F/cm^2$. All parameters were automatically obtained from the impedance analysis software (see Materials and Methods). Z_R, real term of impedance; Z_I, imaginary term of impedance; |Z|, magnitude of impedance.

4.1.2 Effect of forskolin on the plasma membrane capacitance and resistance in Caco-2 monolayer

To further assure that the plasma membrane capacitance and resistance can be accurately determined by impedance analysis, changes in the membrane electrical properties caused by forskolin were observed using this technique. Forskolin is an adenylyl cyclase activator which increases the intracellular cAMP level. This subsequently stimulates CFTR and, in turn, anion secretion. Activation of apical CFTR has been reported to decrease the apical membrane resistance (Bajnath et al., 1991; Grasset et al., 1985; Moser et al., 2007; Singh et al., 2002).

Action of forskolin on electrolyte transport in the Caco-2 monolayer was demonstrated by DC-based Ussing technique which was carried out under an open-circuit condition as shown in Figure 4.2. Exposure to 10 μmol/L forskolin on the basolateral side led to a rapid increase in I_{sc} (apical negative) which reached the peak within 2 min (ΔI_{sc} = 13.74 ± 1.20 μA/cm^2). I_{sc} then slightly declined and reached a new sustained level which continued throughout the experiment (>45 min; ΔI_{sc} = 6.71 ± 0.89 μA/cm^2). This result indicated that forskolin activated membrane transporters and induced anion secretion in Caco-2 monolayer.

Impedance analysis was exploited to show the forskolin-induced changes in the plasma membrane electrical properties. The results were illustrated in Nyquist (Figure 4.3A) and Bode (Figure 4.3B and 4.3C) plots. At 1 min after adding 10 μmol/L forskolin, transepithelial impedance of the monolayer was decreased as shown in Nyquist (Figure 4.3A) and Bode (Figure 4.3B) plots. A left shift of the intersection on the real-impedance (Z_R) axis at the low frequency indicated a decreased in R_t of the monolayer (Figure 4.3A). This R_t reduction was accompanied by pronounced decreases in R_a (2249.57 ± 91.48 to 790.67 ± 90.12 Ω·cm^2; Figure 4.4A) and R_b (1044.99 ± 85.10 to 234.33 ± 15.42 Ω·cm^2; Figure 4.4A). These alterations of the membrane resistance were consistent with an increase in I_{sc} as measured by DC-based Ussing chamber technique. The maximal I_{sc} response was observed at 1 min after adding forskolin, and the patterns of the change in membrane resistance and I_{sc} were also similar (Figures 4.2 and 4.4A). Forskolin had no effect on C_a (27.09 ± 1.79 vs. 27.08 ± 1.84 μF/cm^2 in control and forskolin-treated group, respectively; Figure 4.4B)

and C_b (12.44 ± 0.48 vs. 12.08 ± 0.44 μF/cm^2 in control and forskolin-treated group, respectively; Figure 4.4B) of Caco-2 monolayer.

These results confirmed that changes in the plasma membrane capacitance and resistance by a cAMP-producing agent could be determined by AC-based impedance analysis. Thus, this technique may be used to determine the plasma membrane capacitance and resistance changes after stimulation by PTH, which is also known to increase intracellular cAMP levels (Lee and Partridge, 2009; Tovey et al., 2006).

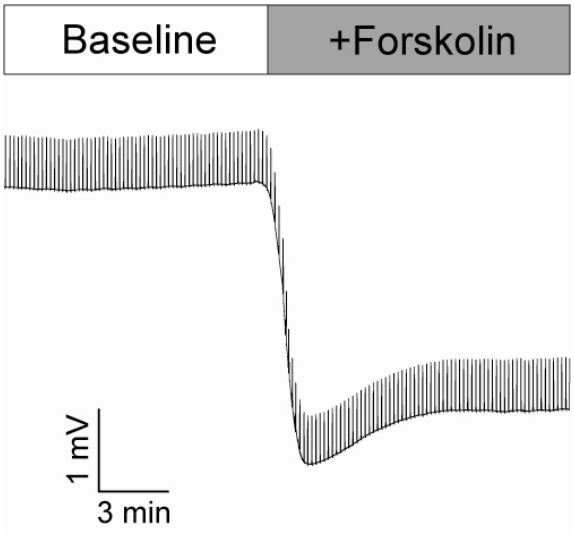

Figure 4.2 A representative recording of transepithelial potential difference (V_t) showing the action of forskolin on electrolyte transport in Caco-2 monolayer. Caco-2 cells were grown for 14 days into a monolayer on a permeable membrane (Snapwell) which was then mounted in Ussing chamber. Experiment was performed under an open-circuit condition. Forskolin (10 μmol/L) was added to the basolateral solution.

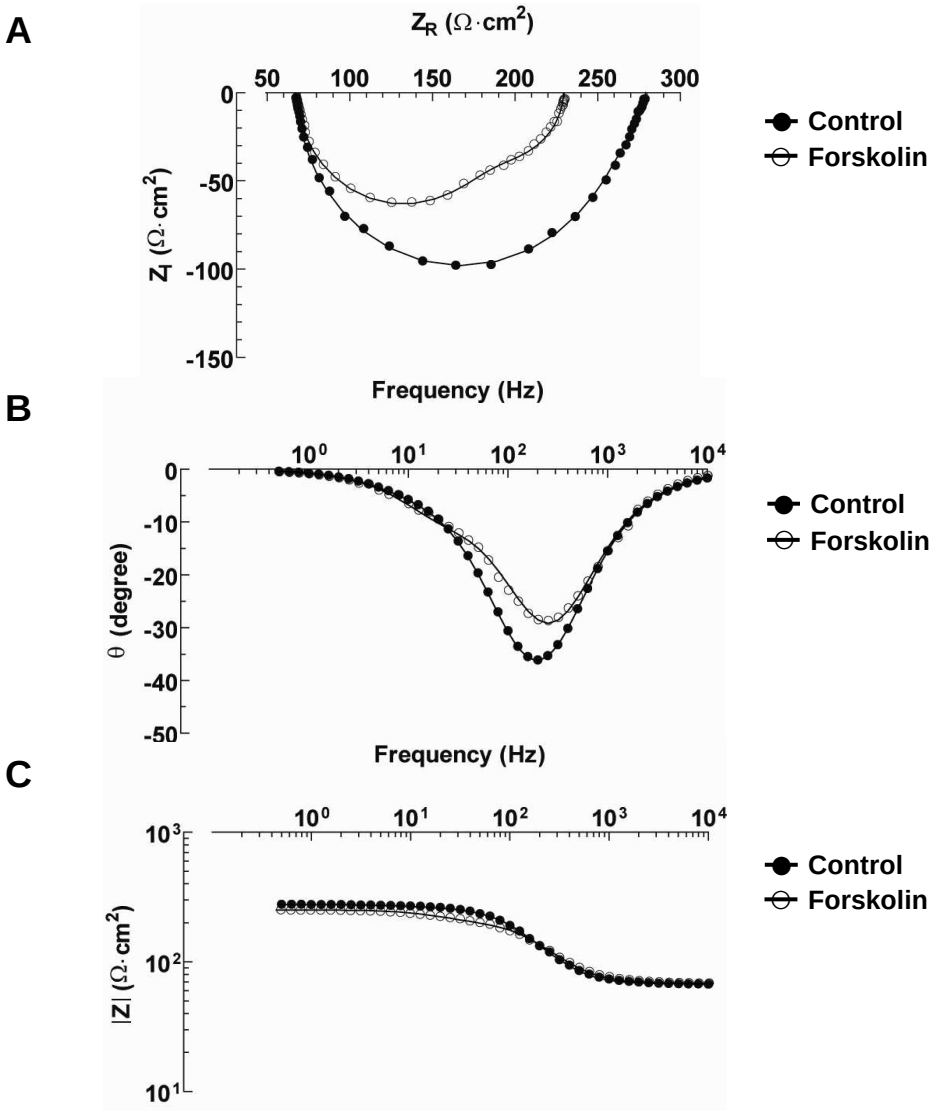

Figure 4.3 Electrical impedance in the control and forskolin-treated Caco-2 monolayers. The data is presented in **(A)** Nyquist plot, **(B)** Bode phase plot, and **(C)** Bode magnitude plot. Closed and open circles represent the data measured in the basal period and at 1 min after adding 10 μmol/L forskolin, respectively. The impedance data were automatically fitted with the lumped model, and the curves are shown in solid lines. The obtained parameters were as followed; baseline, apical membrane resistance (R_a) = 1933.00 $\Omega \cdot cm^2$, basolateral membrane resistance (R_b) = 614.90 $\Omega \cdot cm^2$, apical membrane capacitance (C_a) = 21.44 $\mu F/cm^2$, and basolateral membrane capacitance (C_b) = 13.02 $\mu F/cm^2$; 1 min after adding 10 μmol/L forskolin, R_a = 737.30 $\Omega \cdot cm^2$, R_b = 196.30 $\Omega \cdot cm^2$, C_a = 32.23 $\mu F/cm^2$, and C_b = 11.76 $\mu F/cm^2$. Z_R, real term of impedance; Z_I, imaginary term of impedance; |Z|, magnitude of impedance.

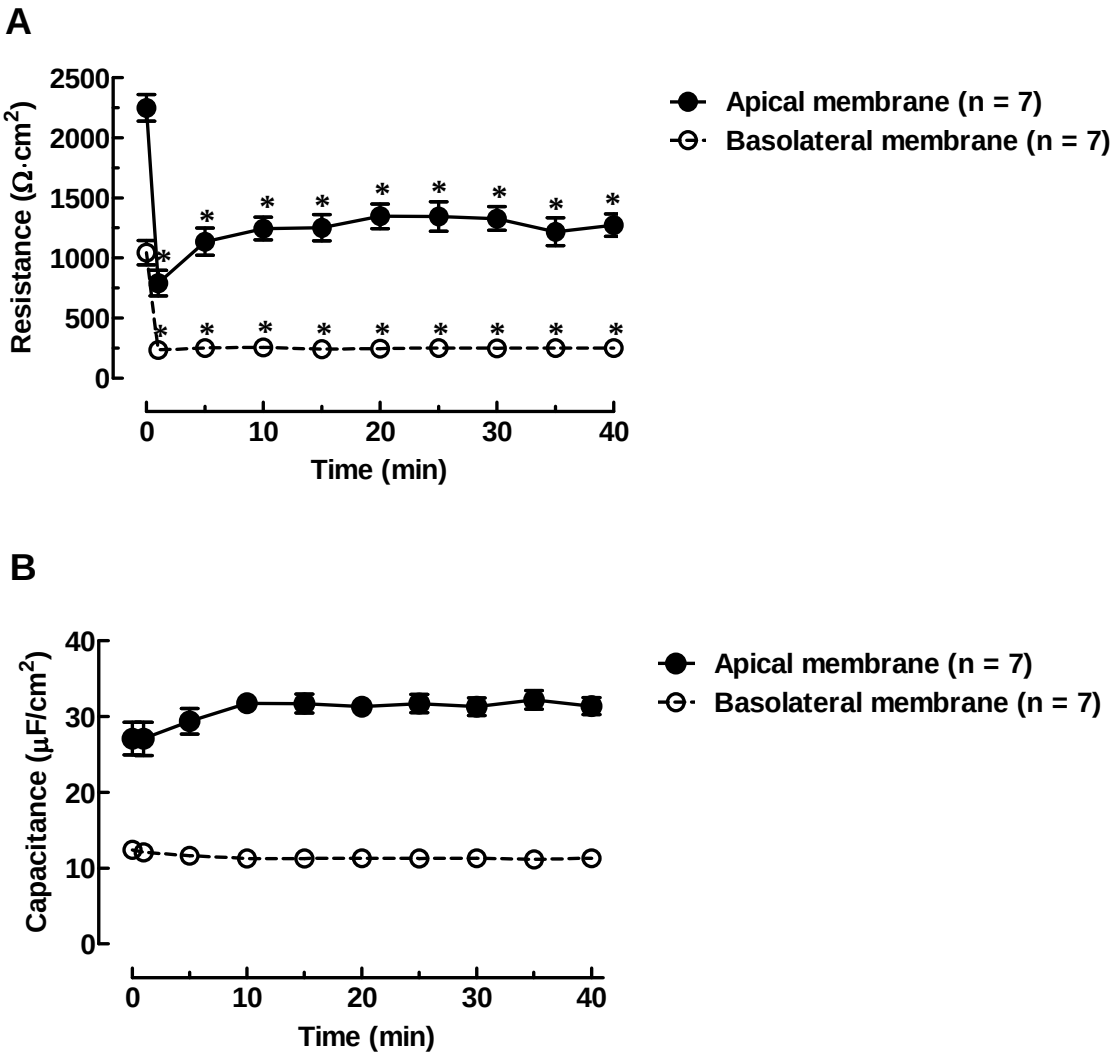

Figure 4.4 Effects of forskolin on membrane electrical properties of Caco-2 monolayer. The monolayer was exposed on the basolateral side to 10 μmol/L forskolin. The membrane capacitance and resistance were analyzed by impedance analysis at 0 (baseline), 1, 5, 10, 15, 20, 25, 30, 35, and 40 min. **(A)** Apical (R_a) and basolateral (R_b) resistance of the monolayer. **(B)** Apical (C_a) and basolateral (C_b) conductance of the monolayer. *$P < 0.05$ (paired *t*-test) compared with their respective baseline values at 0 min. Numbers in parentheses represent the number of independent monolayers in each group.

4.2 Effect of PTH on membrane capacitance and resistance in Caco-2 monolayer as determined by impedance analysis

The aim of these experiments was to demonstrate the application of impedance analysis to predict the responses of Caco-2 cells to PTH; the action of which was unknown in the intestine. This impedance analysis could provide a novel approach to predict the biological responses of the cells to drugs and hormones.

4.2.1 PTHR mRNA expression in the Caco-2 cells

Caco-2 cells were investigated for PTH receptor expression by RT-PCR. On day 14 after plating, type 1 but not type 2 parathyroid hormone receptor (PTHR) mRNAs was found to be expressed in this cell type (Figure 4.5). Although PTHR2 was not observed in conventional PCR followed by gel electrophoresis, real-time PCR could detect a modest expression of PTHR2 in Caco-2 cells (Tulalamba and Laohapitakworn, unpublished observation). The correct amplicon of PTHR1 was confirmed by sequencing.

These results confirmed that Caco-2 cells could respond to PTH.

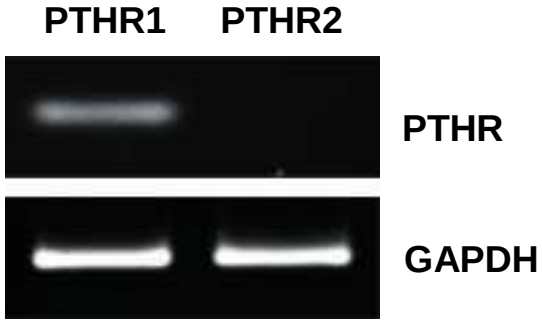

Figure 4.5 Expression of type 1 parathyroid hormone receptors (PTHR1) in Caco-2 cells, as determined by conventional PCR followed by agarose gel electrophoresis. PTHR2 expression was not observed by this technique. However, real-time PCR could reveal a modest expression of PTHR2 (Tulalamba and Laohapitakworn, unpublished observation). GAPDH, glyceraldehydes 3-phosphate dehydrogenase.

4.2.2 Effect of PTH on the plasma membrane capacitance and resistance in Caco-2 monolayer

To explore the alterations in plasma membrane electrical properties induced by PTH, impedance analysis was performed before and after PTH application to the Caco-2 monolayer. Impedance results of the monolayer at 0 (baseline) and 1 min after adding 10 μmol/L PTH to the basolateral bathing solution were illustrated in the Nyquist plot (Figure 4.6A), Bode phase plot (Figure 4.6B), and Bode magnitude plot (Figure 4.6C). PTH decreased epithelial impedance of the monolayer, and revealed a split semicircle in the Nyquist plot (Figure 4.6A) and different peaks in the Bode phase plot (Figure 4.6B). In addition, PTH also decreased R_t as shown by a left shift of the intersection on Z_R axis at low frequency (Figure 4.6A). These alterations were accompanied by a pronounced reduction in R_a (2141.30 ± 222.50 to 1182.08 ± 63.94 $\Omega \cdot cm^2$; Figure 4.7A) and R_b (993.96 ± 60.96 to 128.71 ± 9.18 $\Omega \cdot cm^2$; Figure 4.7A). No change in C_a (28.98 ± 0.69 vs. 28.97 ± 0.46 $\mu F/cm^2$ in control and PTH-treated groups, respectively; Figure 4.7B) and C_b (12.36 ± 0.23 vs. 12.43 ± 0.16 $\mu F/cm^2$; Figure 4.7B) was observed.

Further analysis of the membrane electrical properties at different time points after PTH treatment showed that alterations in R_a and R_b were transient and reversible despite a continual exposure to PTH. The decreased R_a rapidly recovered to the near-baseline level within 5 min and then remained steady (Figure 4.7A). Conversely, the recovery of R_b appeared to be slower. Neither C_a nor C_b was affected throughout the course of PTH stimulation (Figure 4.7B).

These results implicated that PTH activated transporters in both apical and basolateral membranes of Caco-2 monolayer, leading to significant decreases in R_a and R_b. **Thus, impedance analysis was capable of predicting the mechanism of action of PTH.** Transporters and signaling pathways involved in this response were then determined by Ussing chamber technique in the next series of experiments.

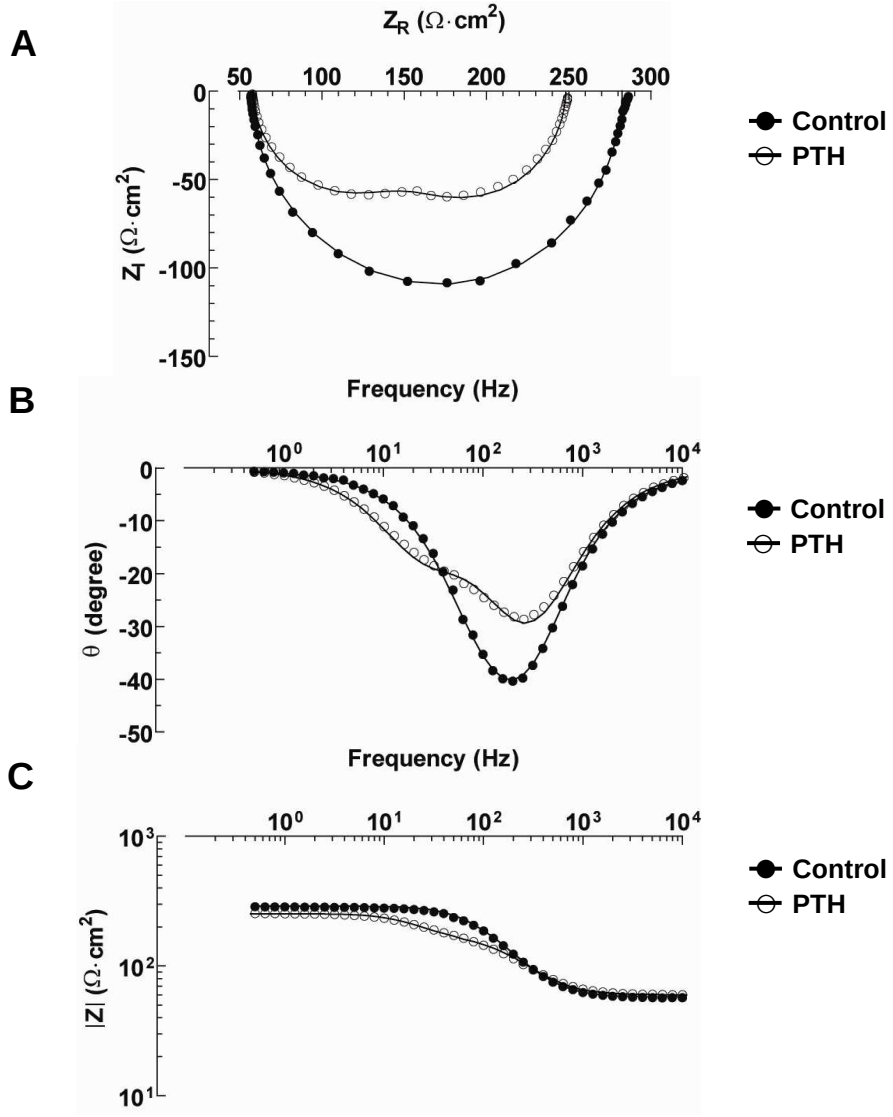

Figure 4.6 Electrical impedance in the control and PTH-treated Caco-2 monolayer. The data is presented in **(A)** Nyquist plot, **(B)** Bode phase plot, and **(C)** Bode magnitude plot. Closed and open circles represent results measured in the basal period and at 1 min after adding 10 nmol/L PTH, respectively. The impedance data were automatically fitted with the lumped model, and the curves are shown in solid lines. The obtained parameters were as followed; baseline, apical membrane resistance (R_a) = 2028.00 $\Omega \cdot cm^2$, basolateral membrane resistance (R_b) = 1044.00 $\Omega \cdot cm^2$, apical membrane capacitance (C_a) = 27.43 $\mu F/cm^2$, basolateral membrane capacitance (C_b) = 12.84 $\mu F/cm^2$; 1 min after adding 10 nmol/L PTH, R_a = 1077.00 $\Omega \cdot cm^2$, R_b = 111.40 $\Omega \cdot cm^2$, C_a = 29.30 $\mu F/cm^2$, C_b = 12.80 $\mu F/cm^2$. Z_R, real term of impedance; Z_I, imaginary term of impedance; |Z|, magnitude of impedance.

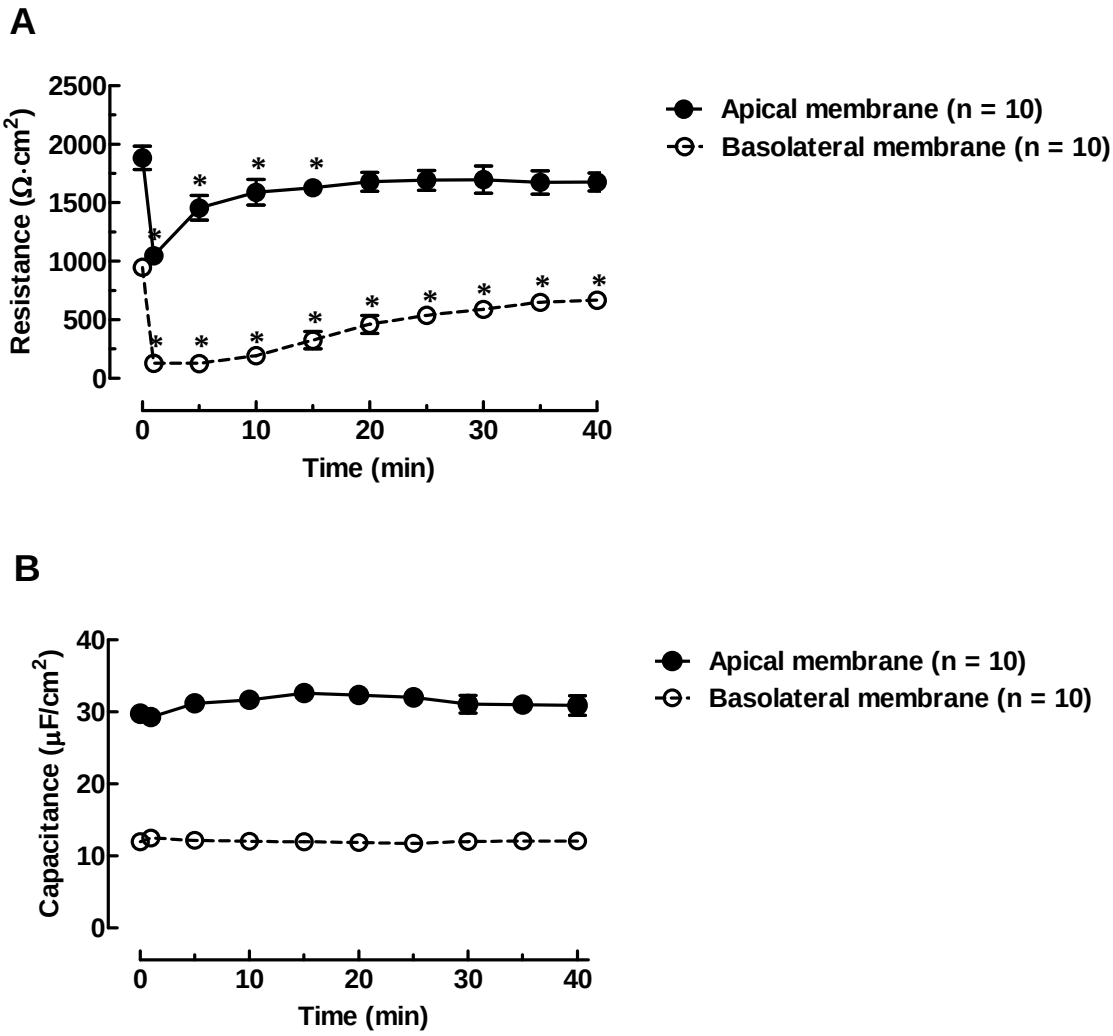

Figure 4.7 Effect of PTH on the plasma membrane electrical properties in Caco-2 monolayer. The monolayer was exposed on the basolateral side to 10 nmol/L PTH. The membrane capacitance and resistance were analyzed by impedance analysis at 0 (baseline), 1, 5, 10, 15, 20, 25, 30, 35, and 40 min after PTH exposure. **(A)** Apical (R_a) and basolateral (R_b) resistance of the monolayer. **(B)** Apical (C_a) and basolateral (C_b) conductance of the monolayer. *$P < 0.05$ (paired *t*-test) compared with their respective baseline values at 0 min. Numbers in parentheses represent the number of monolayers in each group.

4.3 The target transporters and signaling pathways of PTH in Caco-2 cells

Since the results from impedance analysis indicated that PTH activated the transcellular transporters in both apical and basolateral membranes, the present experiments were to examine the effect of PTH on transcellular ion transport as well as the responsible transporters and signaling pathways.

4.3.1 Effect of PTH on epithelial ion transport in Caco-2 monolayer

To study the action of PTH on ion transport, electrical parameters, i.e., V_t, I_{sc}, and R_t, of the Caco-2 monolayer were measured by Ussing chamber technique under a DC-based open-circuit condition. Exposure to 10 nmol/L PTH induced an increase in I_{sc} (apical negative) that peaked within 1 min (ΔI_{sc} = 14.42 ± 1.51 μA/cm^2), followed by a slow decay (Figure 4.8A). Thereafter, I_{sc} was sustained at a level above the baseline for >45 min. This response of Caco-2 monolayer resembled anion secretion caused by forskolin (Figure 4.2). The peak I_{sc} response (ΔI_{sc}) was dose-dependent, which confirmed specificity of PTH (Figure 4.8B). The concentration which caused half-maximal response (EC_{50}) was at 3 nmol/L. The maximal response was observed at 10 nmol/L and this concentration was used throughout the study. PTH exposure on the apical side exhibited a much lower peak I_{sc} response when compared to basolateral exposure (2.38 ± 0.72 vs. 18.63 ± 2.83 μA/cm^2; Figure 4.8C).

To confirm the specificity of PTH, action of 1–34 PTH (active form of PTH) was compared to 13–34 PTH (inactive form of PTH) or autoclaved 1–34 PTH. The result showed that both 13–34 PTH and autoclaved 1–34 PTH had no effect on Caco-2 monolayer (1–34 PTH vs. 13–34 PTH vs. autoclaved 1–34 PTH; 13.09 ± 1.01 vs. 0.54 ± 0.10 vs. 0.40 ± 0.19 μA/cm^2; Figure 4.9). Furthermore, the response of the monolayer to PTH was abolished when PTH was preincubated with various concentrations of PTH antibody in a dose-dependent manner. This result indicated that the response of the monolayer was specific to PTH.

Taken together, it could be concluded that PTH activated ion secretion in Caco-2 monolayer.

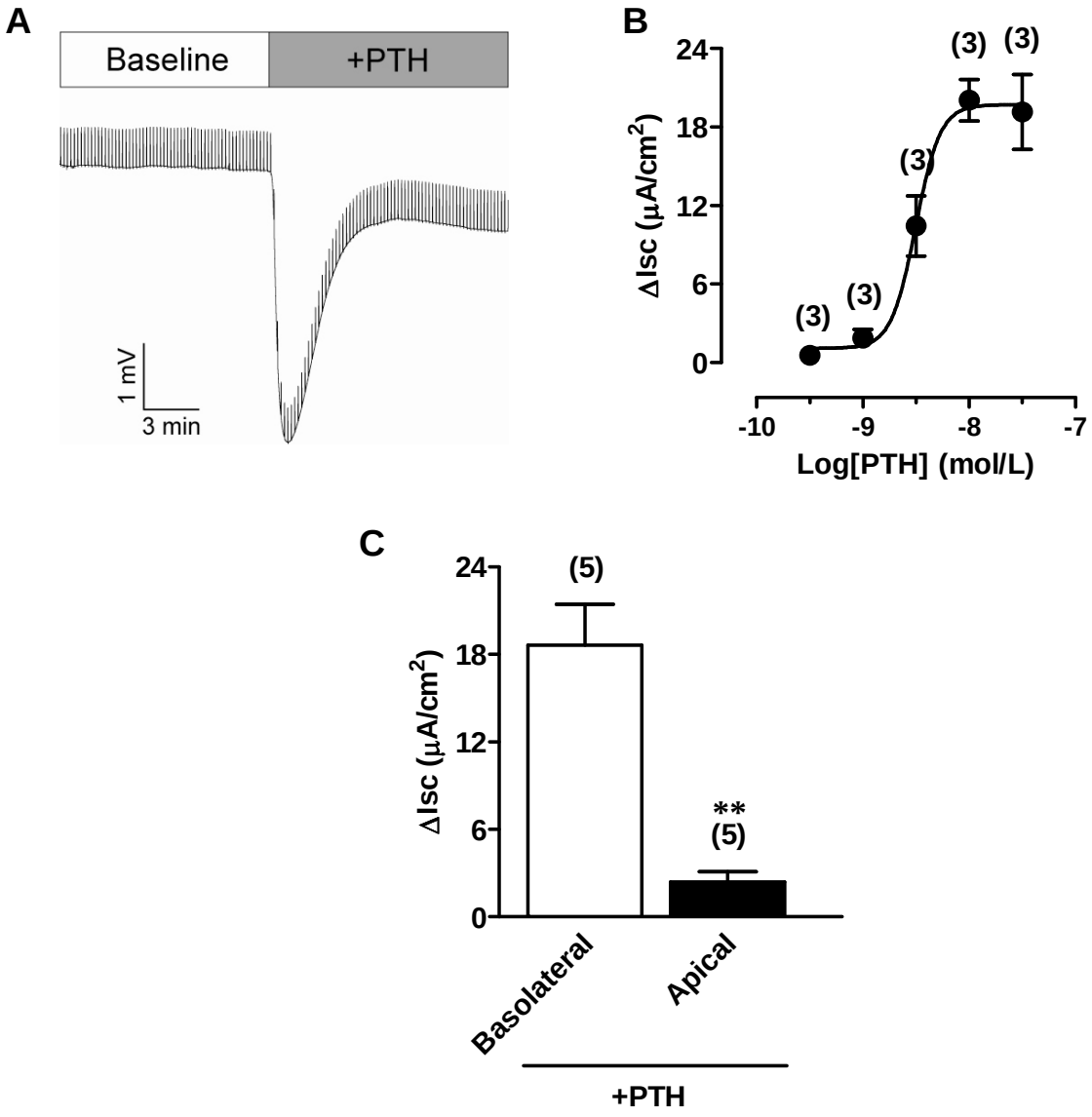

Figure 4.8 Effect of PTH on ion transport in Caco-2 monolayer. **(A)** A representative tracing of transepithelial potential difference (V_t) showing the response of Caco-2 monolayer to 10 nmol/L PTH added in the basolateral solution. **(B)** A dose-response relationship of PTH. Changes in I_{sc} were plotted against increasing doses of PTH added in the basolateral solution. Half-maximal (EC_{50}) and maximal responses were achieved at 3 and 10 nmol/L PTH, respectively. **(C)** A comparison between addition of 10 nmol/L PTH in the basolateral vs. apical solution. $^{**}P < 0.01$ (Mann-Whitney *U*-test). Numbers in parentheses represent the number of monolayers.

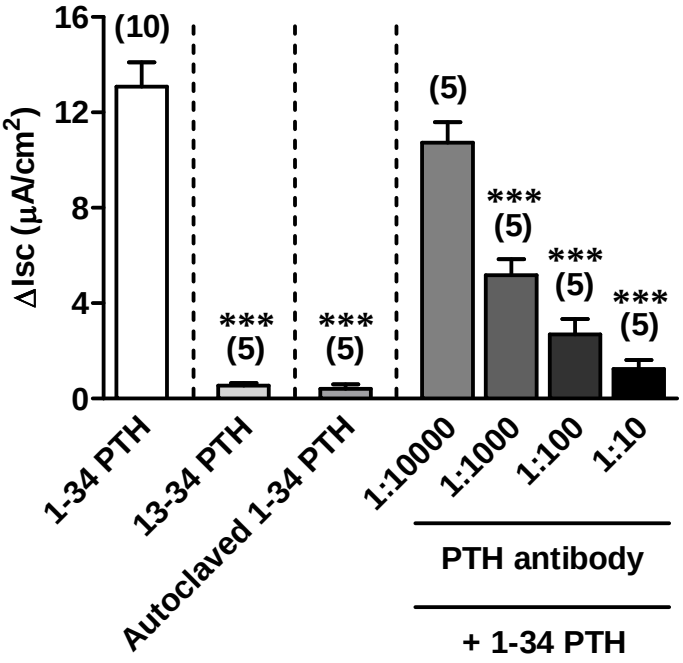

Figure 4.9 Specificity of I_{sc} response of Caco-2 monolayer to PTH. The monolayer was exposed on the basolateral side to 10 nmol/L 1–34 PTH (active form of PTH), 10 nmol/L 13–34 PTH (inactive form of PTH), or 10 nmol/L autoclaved 1–34 PTH. For PTH antibody experiment, 1–34 PTH was preincubated with PTH antibody at various dilutions (1:10000, 1:1000, 1:100, or 1:10) prior to adding the mixture in bathing solution. *** $P < 0.001$ compared with the 1–34 PTH-treated group. Numbers in parentheses represent number of monolayers in each group.

4.3.2 Effect of PTH on the paracellular resistance of Caco-2 monolayer

To study the effects of PTH on the paracellular resistance (R_p) of Caco-2 monolayer, ^{3}H-mannitol flux was first used as an indicator for the change in R_p during PTH stimulation. The results showed that ^{3}H-mannitol flux was not affected by PTH (control vs. PTH; 27.47 ± 2.26 vs. 26.22 ± 1.64 nmol/h/cm^2; Figure 4.10A). R_p was also determined using nystatin-induced membrane permeabilization method (Wills et al., 1979). R_p of both control and PTH-treated groups were found to be comparable (269.04 ± 15.48 Ω·cm^2 vs. 268.66 ± 11.43 Ω·cm^2; Figure 4.10B).

These results indicated that PTH had no effect on R_p in Caco-2 monolayer.

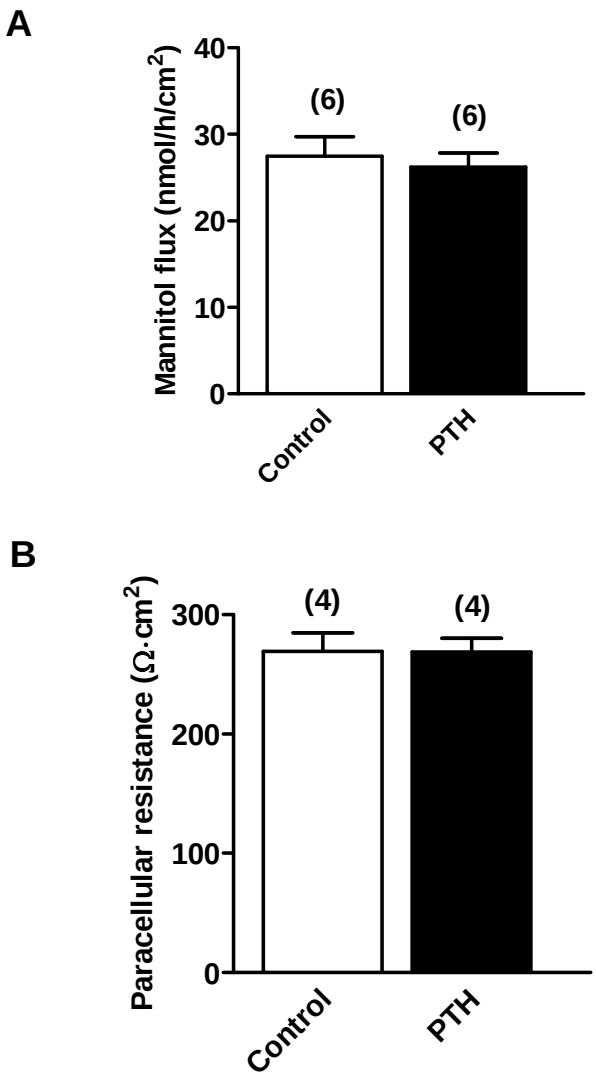

Figure 4.10 Effect of PTH on the paracellular resistance (R_p) of Caco-2 monolayer. **(A)** Transepithelial ^{3}H-mannitol flux in control and PTH-treated Caco-2 monolayer. ^{3}H-mannitol flux was an indicator of the widening of the tight junction. **(B)** R_p in control and PTH-treated Caco-2 monolayer as measured by nystatin-induced membrane permeabilization method. Numbers in parentheses represent the number of monolayers.

4.3.3 Effects of Cl^- and/or HCO_3^- depletion on the PTH-stimulated ion transport in Caco-2 monolayer

Since the results from the previous Ussing chamber experiments showed that PTH induced anion secretion in Caco-2 monolayer (Figure 4.8), the secreted ions were then examined whether they were Cl^- or HCO_3^- by the present ion substitution experiments. Cl^- or HCO_3^- in the bathing solution was replaced with gluconate or HEPES, respectively. Interestingly, Cl^--depleted solution had no effect on the PTH-stimulated I_{sc} (16.72 ± 1.32 vs. 15.08 ± 1.42 μA/cm^2; Figure 4.11), indicating that Cl^- was not involved in such PTH response. However, HCO_3^- depletion could abolish the action by ~80% (16.72 ± 1.32 vs. 3.66 ± 0.65 μA/cm^2). Depletion of both Cl^- and HCO_3^- from the bathing solution also decreased the PTH-induced I_{sc} response to PTH at the level comparable to HCO_3^- removal (2.74 ± 0.81 μA/cm^2, ~80% reduction). These results suggested that it was HCO_3^-, but not Cl^-, that was transported across the monolayer after PTH stimulation.

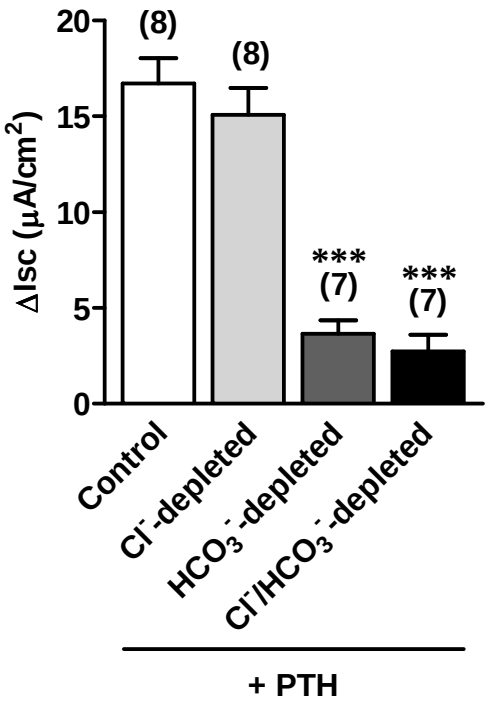

Figure 4.11 Effects of Cl^- and/or HCO_3^- depletion on the PTH-induced I_{sc} response in Caco-2 monolayer. Cl^- and/or HCO_3^- in the bathing solution were substituted with gluconate and/or HEPES, respectively. The monolayer was then exposed to 10 nmol/L PTH in the basolateral solution. ***P < 0.001 compared with the control group. Numbers in parentheses represent the number of monolayers.

4.3.4 The sources of HCO_3^- for the PTH-stimulated HCO_3^- secretion in Caco-2 monolayer

Basolateral uptake of HCO_3^- was evaluated by incubating Caco-2 monolayer with the blockers of $Na^+/K^+/Cl^-$ cotransporter-1 (NKCC1; 100 μmol/L bumetanide) or electrogenic Na^+/HCO_3^- cotransporter-1 (NBCe1; 500 μmol/L DIDS) on the basolateral side before 10 nmol/L PTH exposure. Bumetanide did not inhibit the PTH response (16.98 ± 1.09 vs. 17.95 ± 1.06 μA/cm^2; Figure 4.12), consistent with the findings from the previous experiment that the Cl^- depletion had no effect on the PTH response (Figure 4.11). However, the PTH action was markedly diminished by ~90% after exposure to DIDS (16.98 ± 1.09 vs. 1.82 ± 0.85 μA/cm^2). This result indicated that NBCe1 supplied HCO_3^- from the basolateral side. Since NBCe1 requires the activity of Na^+/K^+-ATPase for maintaining Na^+ gradient, addition of ouabain (1 mmol/L), an inhibitor of the Na^+/K^+-ATPase, to the basolateral side also inhibited the PTH action (16.98 ± 1.09 vs. 2.70 ± 0.41 μA/cm^2, ~85% reduction). Furthermore, HCO_3^- could be generated intracellularly as methazolamide (1 mmol/L), an inhibitor of carbonic anhydrase, reduced the PTH response by 60% (16.98 ± 1.09 vs. 7.08 ± 0.81 μA/cm^2; Figure 4.12).

These results suggested that NBCe1 in the basolateral membrane played a major role in PTH regulation of HCO_3^- secretion in Caco-2 cells, and carbonic anhydrase in the cytoplasm also helped generate HCO_3^- from CO_2 for the apical HCO_3^- secretion.

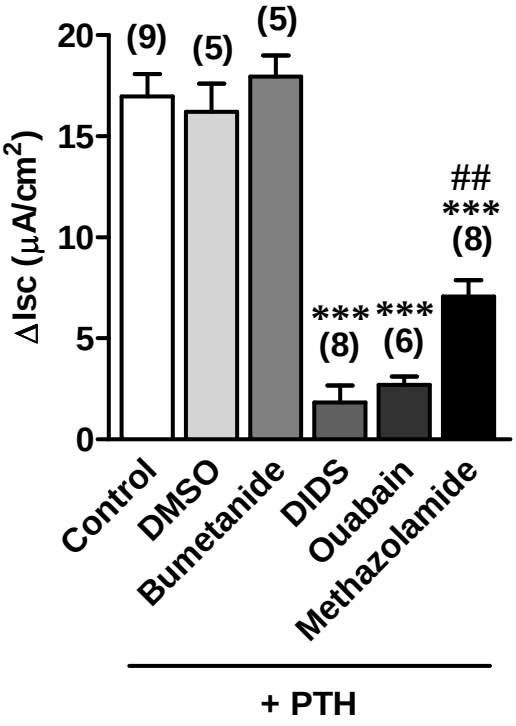

Figure 4.12 Effects of various inhibitors of basolateral membrane transporters and carbonic anhydrase on the PTH-stimulated I_{sc} response in Caco-2 monolayer. The monolayer was preincubated with $Na^+/K^+/Cl^-$ cotransporter-1 (NKCC1) inhibitor (100 μmol/L bumetanide), electrogenic Na^+/HCO_3^- cotransporter-1 (NBCe1) inhibitor [500 μmol/L 4,4′-diisothiocyanatostilbene-2,2′-disulfonic acid disodium salt hydrate (DIDS)], Na^+/K^+-ATPase inhibitor (1 mmol/L ouabain), or carbonic anhydrase inhibitor (1 mmol/L methazolamide) prior to 10 nmol/L PTH exposure. DMSO was a vehicle for inhibitor preparation. ***$P < 0.001$ compared with the control group, $^{\#\#}P <$ 0.01 compared with the ouabain-treated group. Numbers in parentheses represent the number of monolayers.

4.3.5 Responsible apical ion channels for the PTH-stimulated HCO_3^- efflux in Caco-2 monolayer

To investigate the apical transporters which mediated HCO_3^- efflux from Caco-2 cells, the monolayer was pre-treated with various anion transporter blockers. The PTH-stimulated I_{sc} response was significantly inhibited by apical exposure to a broad-spectrum Cl^- channel blocker, NPPB, in a dose-dependent manner (Figure 4.13). The PTH action was markedly abolished by the highest dose of NPPB by ~95% (200 μmol/L; 12.97 ± 0.40 vs. 0.83 ± 0.13 μA/cm^2). Moreover, the specific CFTR blockers, thiazolidinone $CFTR_{inh}$-172 and glycine hydrazide GlyH-101, were used to determine the role of CFTR, which can transport HCO_3^- across various epithelial cells including the enterocytes (Kim and Steward, 2009; Tuo et al., 2009). $CFTR_{inh}$-172 inhibited the PTH-stimulated I_{sc} response in a dose-dependent manner. The highest dose of $CFTR_{inh}$-172 (20 μmol/L) strongly blocked the PTH action ~80% (12.97 ± 0.40 vs. 2.70 ± 0.22 μA/cm^2), while GlyH-101 (50 μmol/L) showed ~80% inhibition (12.97 ± 0.40 vs. 3.07 ± 0.23 μA/cm^2). These results implied that CFTR played an important role in apical HCO_3^- secretion induced by PTH in Caco-2 monolayer. However, the PTH-stimulated I_{sc} response was not affected by apical application of anion exchanger inhibitor DIDS (500 μmol/L; 12.97 ± 0.40 vs. 12.07 ± 1.14 μA/cm^2), which can inhibit apical CaCC and Cl^-/HCO_3^- exchangers, but not CFTR.

Taken together, CFTR, but not CaCC or Cl^-/HCO_3^- exchangers, in the apical membrane mediated HCO_3^- efflux during PTH stimulation in Caco-2 monolayer.

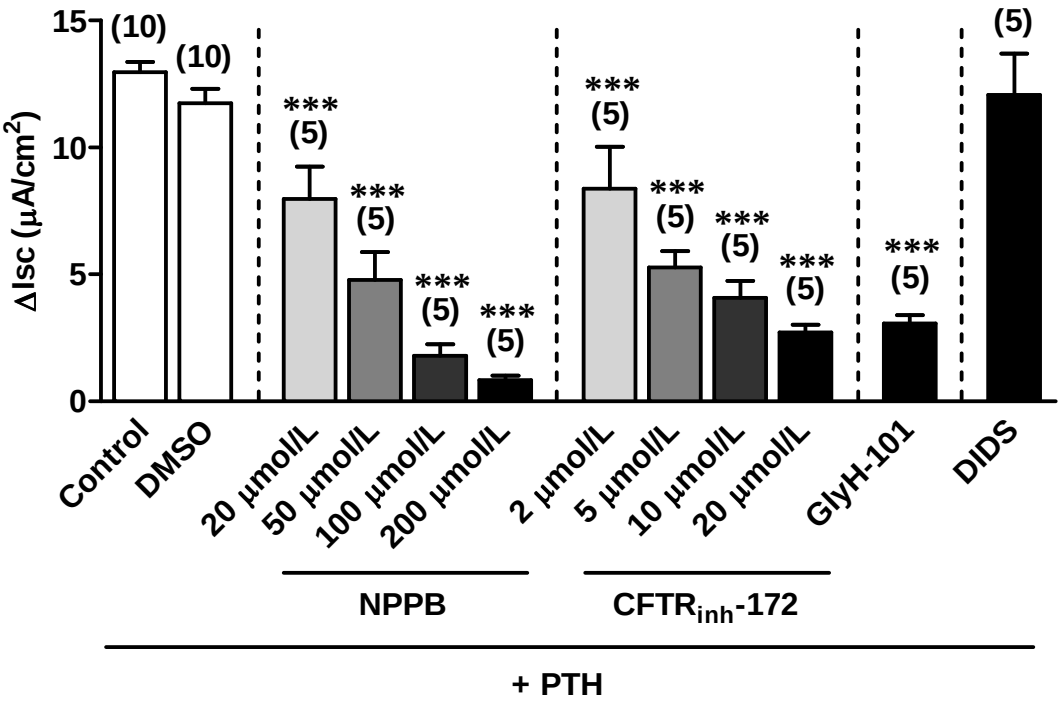

Figure 4.13 Effects of various Cl^- channel inhibitors on the PTH-induced I_{sc} response in Caco-2 monolayer. The monolayer was preincubated with the inhibitors which were added to the apical bathing solution at the following concentrations: 20, 50, 100, and 200 μmol/L of the broad-spectrum Cl^- channel inhibitor 5-nitro-2-(3-phenylpropylamino)benzoic acid (NPPB); 2, 5, 10, and 20 μmol/L of specific cystic fibrotic transmembrane conductance regulator (CFTR) inhibitor thiazolidinone $CFTR_{inh}$-172; 50 μmol/L of specific CFTR inhibitor glycine hydrazide (GlyH-101); 500 μmol/L anion exchanger inhibitor DIDS (which blocks Ca^{2+}-activated Cl^- channel (CaCC) and Cl^-/HCO_3^- exchangers, but not CFTR). DMSO was a vehicle for inhibitor preparation. ****P* < 0.001 compared with the control group. Numbers in parentheses represent the number of monolayers.

4.3.6 Involvement of Na^+/H^+ exchanger (NHE) in the PTH-stimulated HCO_3^- secretion in Caco-2 monolayer

The previous study by Laverty and coworkers (2003) showed that NHE was involved in the PTH action in chick proximal tubular cells. Moreover, NHE1 and NHE3 are expressed in the basolateral and apical membrane of Caco-2 cells, respectively (Sambuy et al., 2005). Therefore, the role of NHE in the PTH-induced HCO_3^- secretion in Caco-2 cells was investigated in this series of experiments. On the apical side, 10 μmol/L amiloride known to have no effect on NHE1 or NHE3 did not block the PTH-induced I_{sc} response (16.62 ± 0.80 vs. 16.39 ± 1.38 μA/cm^2; Figure 4.14). Nevertheless, 100 μmol/L amiloride known to fully inhibit NHE1 and block NHE3 by ~50% significantly inhibited the PTH action (16.62 ± 0.80 vs. 10.24 ± 1.15 μA/cm^2, ~40% reduction), while 1 mmol/L amiloride, which inhibits all types of NHEs, diminished the PTH action by ~70% (16.62 ± 0.80 vs. 5.40 ± 0.67 μA/cm^2). In addition, EIPA, a derivative of amiloride with NHE-inhibitory activity was used to confirm the role of NHE in the PTH action. EIPA at a concentration of 10 μmol/L known to fully inhibit NHE1 and block NHE3 by ~50%, could block the PTH-induced I_{sc} response by ~40% (16.62 ± 0.80 vs. 10.01 ± 1.15 μA/cm^2). The inhibition by EIPA was dose-dependent. The highest concentration of EIPA (50 μmol/L), which inhibits all types of NHEs, suppressed the PTH action by ~85% (16.62 ± 0.80 vs. 2.77 ± 0.64 μA/cm^2). These results suggested that NHE3 in the apical membrane was involved in the PTH-induced HCO_3^- secretion in Caco-2 cells.

Amiloride and EIPA were also preincubated on the basolateral side of the monolayer to examine the role of basolateral NHE1. Amiloride (1 mmol/L) as well as EIPA (50 μmol/L) inhibited the PTH action by ~50% (control vs. amiloride vs. EIPA, 16.62 ± 0.80 vs. 9.14 ± 0.62 vs. 8.01 ± 0.79 μA/cm^2; Figure 4.14). These results suggested that basolateral NHE1 also played a role in the action of PTH in Caco-2 monolayer.

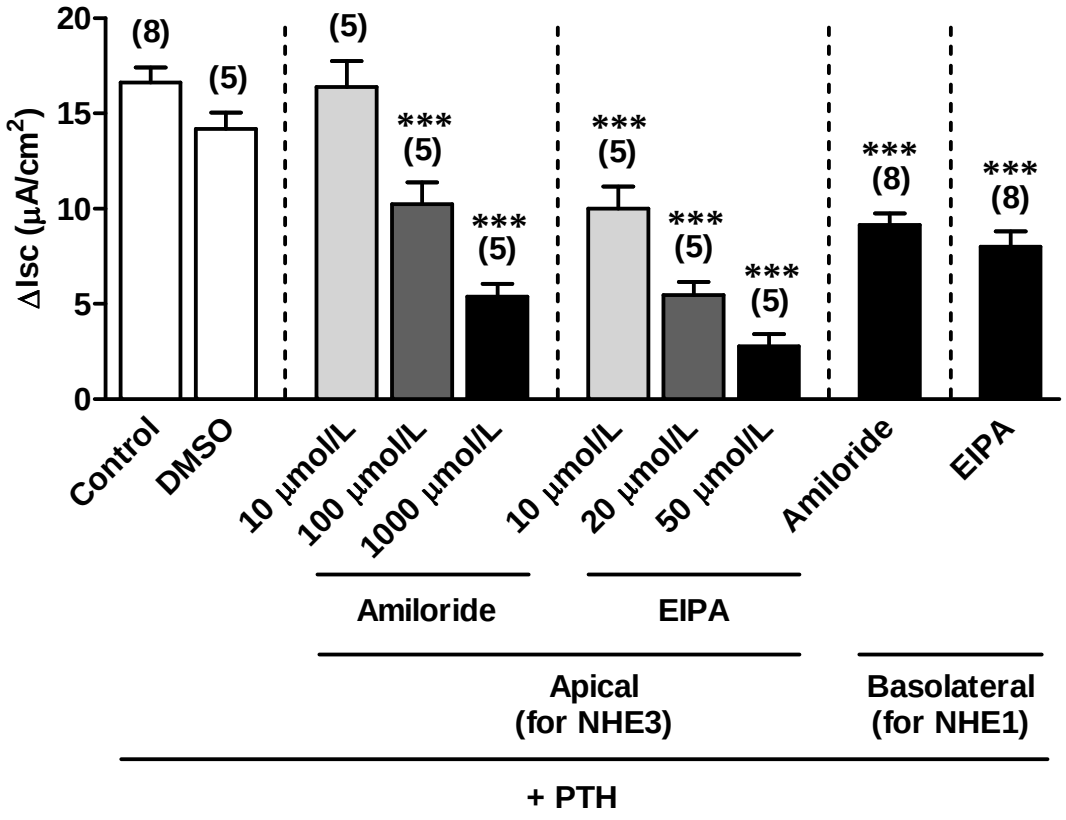

Figure 4.14 Effects of amiloride and 5-(N-ethyl-N-isopropyl) amiloride (EIPA) on the PTH-induced I_{sc} response in Caco-2 monolayer. The monolayers were preincubated with inhibitors at the following concentrations: 10, 100, and 1000 μmol/L amiloride in the apical solution; 10, 20, and 50 μmol/L EIPA in the apical solution; 1 mmol/L amiloride in the basolateral solution; or 50 μmol/L EIPA in the basolateral solution. DMSO was a vehicle for inhibitor preparation. ****P* < 0.001 compared with the control group. Numbers in parentheses represent the number of monolayers.

4.3.7 Involvement of K^+ channels in the PTH-stimulated HCO_3^- secretion in Caco-2 monolayer

To examine whether K^+ channels played roles in the response of Caco-2 monolayer to PTH, 5 mmol/L $BaCl_2$ (a nonspecific K^+ channel inhibitor), 100 μmol/L chromanol 293B (a blocker of cAMP-activated K^+ channel) and 100 nmol/L charybdotoxin (a blocker of Ca^{2+}-activated K^+ channel) were preincubated on the basolateral side of the monolayer prior 10 nmol/L PTH exposure. $BaCl_2$ reduced the PTH action by ~30% (12.10 ± 0.63 vs. 8.51 ± 0.83 μA/cm^2; Figure 4.15). However, neither chromanol 293B nor charybdotoxin inhibited the PTH-induced I_{sc} response (control vs. chromanol 293B vs. charybdotoxin, 12.10 ± 0.63 vs. 11.23 ± 0.55 vs. 11.39 ± 1.61 μA/cm^2), suggesting that K^+ channels apart from cAMP-activated and Ca^{2+}-activated K^+ channels were involved in the action of PTH in Caco-2 cells.

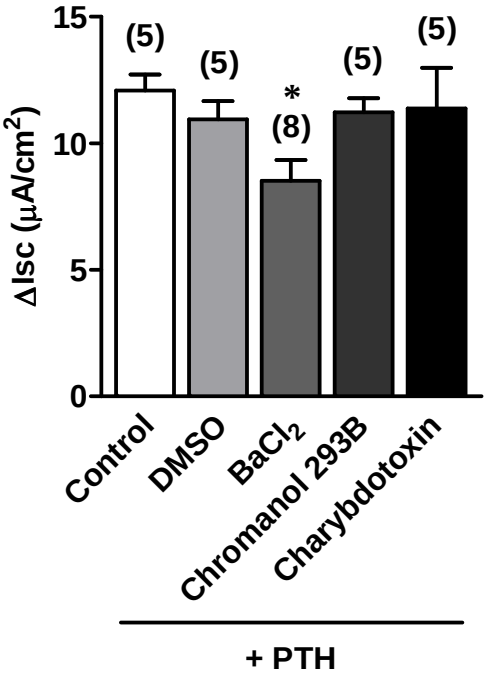

Figure 4.15 Effects of K^+ channel blockers on the PTH-induced I_{sc} response in Caco-2 monolayer. Each inhibitor was preincubated on the basolateral side of the monolayer at the following concentration: 5 mmol/L $BaCl_2$ (a nonspecific K^+ channel inhibitor); 100 μmol/L chromanol 293B (a blocker of cAMP-activated K^+ channel); or 100 nmol/L charybdotoxin (a blocker of Ca^{2+}-activated K^+ channel). DMSO was a vehicle for chromanol 293B and charybdotoxin preparation. Numbers in parentheses represent the number of monolayers.

4.3.8 Responsible signaling pathways for the PTH-stimulated HCO_3^- secretion in Caco-2 monolayer

In the last experiment, signaling pathways of PTH in Caco-2 cells were examined. Inhibitors of PTH signaling pathways were preincubated with the monolayer in both apical and basolateral sides prior to 10 nmol/L PTH exposure. A PKA inhibitor, 10 μmol/L PKI 14–22, decreased the PTH action by ~70% (17.16 ± 1.39 vs. 5.33 ± 1.02 μA/cm^2; Figure 13). However, an intracellular Ca^{2+} chelator, 50 μmol/L BAPTA-AM, and a protein kinase C (PKC) inhibitor, 1 μmol/L GF-109203X, had no effect on the PTH action (control vs. BAPTA-AM vs. GF-109203X, 17.16 ± 1.39 vs. 13.46 ± 1.82 vs. 15.89 ± 1.08 μA/cm^2), while PI3K inhibitors, 200 nmol/L wortmannin and 75 μmol/L LY-294002, inhibited the PTH-induced I_{sc} response by ~50% (control vs. wortmannin vs. LY-294002, 17.16 ± 1.39 vs. 8.47 ± 0.58 vs. 9.91 ± 0.86 μA/cm^2).

These results indicated that PTH activated HCO_3^- secretion via the PKA and PI3K pathways.

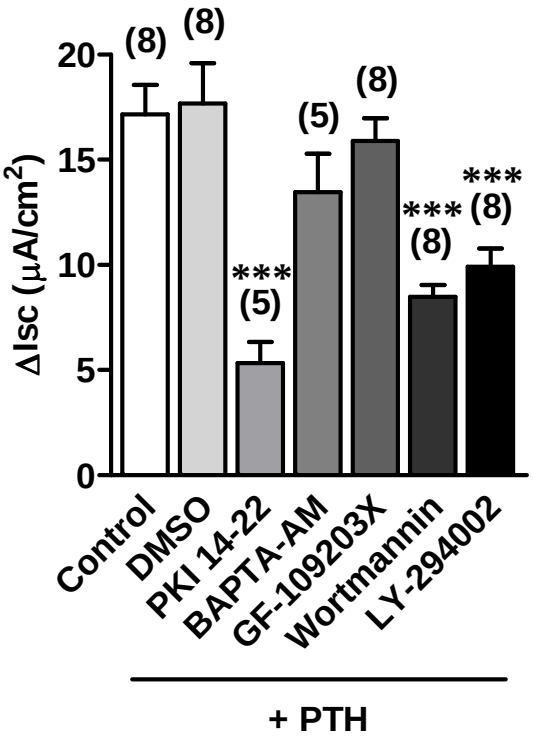

Figure 4.16 Effects of signaling pathway inhibitors on the PTH-induced I_{sc} response in Caco-2 monolayer. The monolayers were preincubated with the inhibitors added in both apical and basolateral solution at the following concentrations: a protein kinase A (PKA) inhibitor, 10 μmol/L protein kinase inhibitor 14–22 (PKI 14–22); an intracellular Ca^{2+} chelator, 50 μmol/L 1,2- bis(*o*-aminophenoxy)ethane-N,N,N′,N′-tetraacetic acid tetra (acetoxymethyl) ester (BAPTA-AM); a protein kinase C (PKC) inhibitor, 1 μmol/L GF-109203X; phosphoinositide-3-kinase (PI3K) inhibitors, 200 nmol/L wortmannin and 75 μmol/L LY-294002. DMSO was a vehicle for inhibitor preparation. ****P* < 0.001 compared with the control group. Numbers in parentheses represent the number of monolayers.

CHAPTER V
DISCUSSION

Electrical circuitry of epithelia is composed of plasma membranes and tight junctions. The properties of the plasma membrane can be described as a combination of capacitance and resistance, whereas the tight junction is represented by a single resistance. However, these electrical elements cannot be determined individually by a DC-based technique. The present study used AC-based impedance spectroscopy as a model for measuring capacitance and resistance of the plasma membrane in Caco-2 monolayer. The accuracy of this technique was confirmed by showing the forskolin-stimulated alterations of the plasma membrane electrical properties. Moreover, impedance analysis was used to measure changes in the plasma membrane capacitance and resistance induced by PTH to predict the mechanisms of PTH action. Finally, the PTH mechanisms were further investigated by identifying the responsible transporters and signaling pathways by the Ussing chamber technique. This study thus demonstrated a novel application of the impedance analysis in the prediction of the biological responses of epithelial cells to hormonal treatment.

5.1 Plasma membrane capacitance and resistance of Caco-2 monolayer

Impedance analysis has been used to determine the plasma membrane capacitance and resistance of gastric (Clausen et al., 1982), corneal (Clausen et al., 1986), gall bladder (Moser et al., 2007), renal (Wills et al., 1993), and colonic epithelia (Wills and Clausen, 1987). However, the measurement of plasma membrane electrical properties in intact epithelia is complicated by the underlying connective tissue and muscle layers, both of which also act as barriers to the applied electrical

currents. In addition, the impedance measurement is complicated by heterogeneity of cells which are structurally different and thus have distinct electrical properties. Therefore, intestinal epithelial cell line Caco-2 was used to overcome the aforementioned limitations. Caco-2 cells are suitable for this type of study because their structure and function resemble human small intestinal epithelial cells (Bailey et al., 1996; Hilgers et al., 1990; Sambuy et al., 2005).

Impedance was analyzed based on the lumped equivalent circuit (Figure 2.3). The lumped model simplifies the morphology of the epithelium into 2 separate membranes which connect in parallel with the paracellular resistance. Although some investigators suggested that the contribution of the lateral intercellular space resistance should be resolved by the distributed equivalent circuit model (Figure 2.4), the effect of distributed resistance in leaky epithelia such as intestine was not important (Clausen et al., 1979). Generally, the lumped model is adequate for determining resistive and capacitive components, as shown in the previous studies in human colonic T84 cells (Singh et al., 2002) and human bronchial epithelial cells (Kreindler et al., 2005).

During the basal period, the apical resistance R_a and the basolateral resistance R_b of Caco-2 cells was 2141.30 ± 222.50 and 993.96 ± 60.96 $\Omega \cdot cm^2$, respectively (Table 4.2). The calculated apical membrane fractional electrical resistance $[R_a/(R_a + R_b)]$ was 0.67 ± 0.01. These values were consistent with the previous report using a direct microelectrode recording in Caco-2 cells showing R_a of ~2300 $\Omega \cdot cm^2$, and the apical membrane fractional electrical resistance of 0.76 ± 0.02 (Grasset et al., 1984). The apical and basolateral capacitances, C_a and C_b, of Caco-2 cells in this study were also comparable to the values reported in mammalian colon as determined by impedance analysis [C_a, 28.98 ± 0.69 $\mu F/cm^2$ vs. 20.70 ± 1.70 $\mu F/cm^2$; C_b, 12.36 ± 0.23 vs. 9.80 ± 0.70 $\mu F/cm^2$] (Wills and Clausen, 1987). Thus, the present impedance analysis could be used to accurately determine the plasma membrane capacitance and resistance in Caco-2 monolayer.

To validate the impedance technique in Caco-2 cells, impedance of Caco-2 monolayer was determined during forskolin stimulation. Forskolin is known to increase the intracellular cAMP levels which in turn stimulate anion secretion through apical CFTR. This process normally causes a reduction in the apical and basolateral membrane resistance (Bajnath et al., 1991; Grasset et al., 1985; Moser et al., 2007;

Singh et al., 2002). In this study, decreases in both R_a and R_b after forskolin treatment were detected (Figure 4.4) and also correlated with an increase in I_{sc} as measured by DC-based Ussing technique (Figure 4.2). These results indicated that the forskolin-induced changes in plasma membrane resistance could be determined by the present impedance spectroscopic technique.

Forskolin led to anion secretion by activating transporters in both apical and basolateral membranes. Activation of apical CFTR was explained by direct phosphorylation by cAMP-dependent protein kinase (i.e., PKA), thus leading to channel opening (Gadsby and Nairn, 1999). Ameen and colleagues (2000) further showed that cAMP also induced CFTR insertion to the apical membrane. Fusion of CFTR-rich vesicles to the apical membrane could lead to a detectable change in the plasma membrane capacitance as the plasma membrane capacitance was proportional to the plasma membrane area (Clausen et al., 1982). However, the present study suggested that the reduction in R_a was caused by the increased channel opening rather than vesicle fusion since there was no change in the apical membrane capacitance. On the other hand, a decrease in R_b could result from the activation of basolateral transporters involved in forskolin-induced anion secretion, such as K^+ channels, NKCC1, NBCe1, and/or Na^+/K^+-ATPase (Figure 2.5), all of which were found to be activated by cAMP (Bachmann et al., 2003; Barrett and Keely, 2000; Carranza et al., 1998; Reynolds et al., 2007).

5.2 Application of impedance analysis in predicting biological actions of PTH in Caco-2 monolayer

Application of impedance spectroscopy in predicting the biological responses of cells to hormonal treatment was demonstrated by the study of Caco-2 cell responses to PTH.

5.2.1 Direct PTH action on Caco-2 monolayer

Several previous studies on PTH action suggested the crucial roles of PTH in regulating renal transport of various ions, including Ca^{2+} (van Abel et al., 2005), Na^{+} (Azarani et al., 1995; Bezerra et al. 2008; Fan et al., 1999; Girardi et al., 2000), Cl^{-} (Laverty et al., 2003), HPO_4^{2-} (Zhang et al., 1999), HCO_3^{-} (Bank et al. 1979; McKinney and Myers, 1980a and 1980b), and Mg^{2+} (Quamme, 1997). In human intestine, PTH usually stimulated Ca^{2+} and HPO_4^{2-} absorption indirectly through $1,25(OH)_2D_3$ action (Cross et al., 1990; Khanal and Nemere, 2008). However, the direct effect of PTH on the intestine was still unclear.

In this study, PTHR1 was found to be expressed in Caco-2 cells, consistent with previous reports of the expressions of PTHR1 mRNA and protein in rat small intestine (Urena et al., 1993; Watson et al., 2000). PTHR1 was the major isoform which mediated PTH action in bone and kidney, while PTHR2, which was less abundant in Caco-2 cells, was mainly expressed in the brain and did not show a physiological role in other organs (Juppner, 1999; Szabo et al., 2010; Usdin et al., 1995). Apart from PTHR expression, Massheimer and coworkers (2000) demonstrated that PTH could activate cAMP/PKA and PLC/IP_3/intracellular Ca^{2+} pathways in rat enterocytes. In chick enterocytes, PTH also bound to PTHR which in turn activated PKA (Nemere, 1996 and 1999). Therefore, it was suggested that PTH had a direct ion regulatory action in the intestine independent of $1,25(OH)_2D_3$.

5.2.2 PTH-induced changes in plasma membrane resistance in Caco-2 monolayer

PTH action was further examined by impedance spectroscopy in Caco-2 cells. R_a and R_b were decreased at 1 min after PTH administration (Figure 4.7A). This response was correlated with the rapidly increased I_{sc} revealed by DC-based Ussing chamber technique (Figure 4.8A). This altered I_{sc} normally indicated electrogenic anion secretion across the monolayer. Various modulators which increased the intracellular cAMP levels and subsequently activated anion transport have been shown to lower the resistance of both apical and basolateral membranes (Moser et al., 2007; Paunescu and Helman, 2001; Singh et al., 2002). Thus, the decreased R_a and R_b in Caco-2 monolayer might reflect the increased activity of apical and basolateral

transporters, which were usually under the regulation of cAMP/PKA- and PKC/Ca^{2+}-dependent signaling pathways. Moreover, the recovery of R_a and R_b even in the presence of PTH implicated possible desensitization of PTH receptors, presumably by receptor internalization as seen in the kidney and bone (Ferrari et al., 1999; Pun et al., 1990; Vilardaga et al., 2002).

Since PTH was found to induce anion secretion in Caco-2 monolayer (Figure 4.8A), and the cAMP/PKA pathway was the classical PTH signaling in the intestine (Massheimer et al., 2000), the cAMP-dependent CFTR is the most likely ion channel in the apical membrane for PTH-induced anion secretion. cAMP directly induced phosphorylation of CFTR and later caused channel opening for anion secretion (Gadsby and Nairn, 1999). This process could explain the rapid reduction of R_a in the PTH-exposed Caco-2 cells. A decrease in R_b might result from the stimulation of basolateral transporters for anion uptake. By using DC-based Ussing chamber technique, the basolateral NBCe1, NHE1, and Na^+/K^+-ATPase were found to be involved in PTH action (Figures 4.12 and 4.14), and activation of these transporters could cause a reduction in R_b. Such basolateral transporters had also been known to be regulated by cAMP and PKA (Azarani et al., 1995; Bachmann et al., 2003; Carranza et al., 1998).

Changes in plasma membrane electrical properties are usually directly associated with membrane structure itself. Plasma membrane is composed of phospholipid bilayers which contain a hydrophobic compartment in between 2 hydrophilic surfaces resembling a sandwich structure. This structure effectively maintained a separation of charge, similar to an electronic capacitor. In general, the phospholipid bilayers resemble a parallel-plate capacitor which is composed of 2 parallel conductive plates separated by a dielectric medium. Plasma membrane capacitance was relatively unaffected by the embedded molecules (e.g., integral membrane proteins), and the value was directly proportional to the plasma membrane area [normal value of plasma membrane capacitance of a single cell was ~1 $\mu F/cm^2$] (Cole, 1972). Therefore, plasma membrane capacitance could be used as an indicator of plasma membrane surface area. Any cellular processes which altered cell surface area (e.g., endocytosis or vesicle fusion) could be indirectly determined by changes in the plasma membrane capacitance. Clausen and colleagues (1982) also elucidated the

mechanism of bullfrog gastric acid secretion by using the membrane capacitance as a representative of plasma membrane area. Specifically, the histamine-induced gastric acid secretion which resulted from insertion of transporter-rich vesicles into the apical plasma membrane was demonstrated by this technique. In the present study, PTH had no effect on C_a or C_b throughout the PTH-exposed period (Figure 4.7B), implicating that PTH did not cause new CFTR insertion through vesicle fusion to the apical plasma membrane.

5.3 Mechanisms of PTH-induced HCO_3^- secretion in Caco-2 cells

Functional study of the direct PTH action was further performed by DC-based Ussing chamber technique. PTH substantially increased I_{sc} (apical negative) in a dose-dependent manner, suggesting that PTH directly stimulated anion secretion in Caco-2 cells (Figures 4.8A and 4.8B). The findings that 13–34 PTH (an inactive form of PTH), autoclaved PTH, and neutralized PTH by specific PTH antibody did not increase I_{sc} (Figure 4.9) indicated that this response was specific to PTH. Since PTH did not change mannitol flux, an indicator of the widening of the tight junction (Krugliak et al., 1994; Madara, 1989; Perez et al., 1997), or even R_p as measured by nystatin-induced membrane permeabilization method, the PTH-stimulated anion secretion should occur solely via the transcellular pathway (Figures 4.10A and 4.10B).

HCO_3^- depletion that markedly attenuated PTH action (Figure 4.11) indicated that HCO_3^- was the major anion secreted during PTH exposure. Since depletion of Cl^- had no effect on the PTH action, Cl^- was unlikely to be involved in the PTH-induced anion secretion. Some cAMP-producing mediators also induced HCO_3^- secretion in the intestinal epithelial cells (Tuo et al., 2009; Zhu et al., 2004). In the present study, the PTH-induced HCO_3^- secretion was confirmed by the findings that DIDS (as an inhibitor of NBCe1), and not bumetanide (an inhibitor of NKCC1), in the basolateral solution blocked the PTH-induced I_{sc} changes (Figure 4.12). In the rat colon, HCO_3^- was responsible for the bumetanide-insensitive forskolin-evoked anion secretion (Schultheiss and Diener, 1998). The contribution of NBCe1 was also

confirmed by the evidence that the PTH action was diminished by the inhibitor of Na^+/K^+-ATPase, which was required for NBCe1 activity (Figure 4.12). Several studies demonstrated that HCO_3^- entered the cell through NBCe1 in the basolateral membrane (Ainsworth et al., 1996; Ishiguro et al., 1996; MacLeod et al., 1996). Although the basolateral HCO_3^- influx could also be supplied by basolateral Cl^-/HCO_3^- exchangers, such transport was not dependent on Na^+/K^+-ATPase activity, and was considered electroneutral (Romero et al., 2004). Some investigators suggested that HCO_3^- generated by intracellular carbonic anhydrase also contributed to HCO_3^- secretion (Feldman, 1994; Feldman et al., 1988; Furukawa et al., 2004; Moser et al., 2007). Since the PTH-induced HCO_3^- secretion was diminished after exposure to methazolamide, an inhibitor of carbonic anhydrase (Figure 4.12), carbonic anhydrase did help to supply HCO_3^- for the PTH-enhanced apical HCO_3^- secretion.

CFTR was the major apical HCO_3^- channel in this study as confirmed by the use of 2 different CFTR inhibitors ($CFTR_{inh}$-172 and GlyH-101; Figure 4.13). The results were consistent with the evidence that CFTR was activated through cAMP/PKA, which were also the downstream signaling molecules of PTH in most target organs (Gadsby and Nairn, 1999; Lee and Partridge, 2009; Massheimer et al., 2000). Laverty and coworkers (2003) observed similar PTH effects on CFTR stimulation in chick proximal tubule. In addition to CFTR, Ca^{2+}-activated Cl^- channel (CaCC) was expressed in Caco-2 cells, but with a lower expression compared to CFTR (Zhu et al., 2004). Indeed, Ca^{2+} was one of the second messengers downstream to PTHR in intestinal cells (Massheimer et al., 2000). Involvement of CaCC in the present study must, therefore, be excluded experimentally. Since DIDS (also an inhibitor of CaCC) in the apical solution was unable to inhibit the PTH action (Figure 4.13), CaCC was not responsible for the PTH-induced I_{sc} response. This finding was consistent to the previous report of Davenport and colleagues (1996) that CaCC was not functional in Caco-2 cells. Therefore, CFTR was the principal channel in the apical membrane for the PTH-enhanced HCO_3^- secretion in Caco-2 monolayer.

Laverty and coworkers (2003) further showed that NHE was involved in the PTH action in chick renal proximal tubular cells. The involvement of NHE in the PTH action in Caco-2 cells was evaluated using high-dose amiloride and EIPA, both of which when present in the apical solution blocked the I_{sc} response in a dose-

dependent manner (Figure 4.14). At their half-inhibitory concentrations (IC_{50}) on NHE3, the PTH actions were inhibited by ~40%. On the basolateral side, both amiloride and EIPA at concentrations known to inhibit all types of NHE (Orlowski, 1993) blocked the PTH action by ~50%. Since NHE3 and NHE1 were abundant in the apical and basolateral membrane of Caco-2 cells, respectively (Sambuy et al., 2005), both types of NHEs might indirectly contribute to PTH-induced HCO_3^- secretion, perhaps by extruding the excess H^+ produced by carbonic anhydrase.

Basolateral K^+ channels helped to recycle K^+ ions for Na^+/K^+-ATPase, which in turn provided a driving force for NBCe1. Moreover, Na^+/K^+-ATPase maintained a hyperpolarized membrane voltage (intracellular negative) that was crucial for anion secretion (Kunzelmann and Mall, 2002). Two main types of K^+ channels have been characterized in the basolateral membrane of mammalian colon, namely cAMP- and Ca^{2+}-activated K^+ channels. However, the PTH action was insensitive to chromanol 293B and charybdotoxin, which specifically inhibited cAMP- and Ca^{2+}-activated K^+ channels, respectively. Zhu and colleagues (2005) also showed that the tetramethylpyrazine-induced cAMP- and Ca^{2+}-dependent I_{sc} change in Caco-2 monolayer was not blocked by chromanol 293B or charybdotoxin. These results suggested that other K^+ channels were involved in the PTH-induced HCO_3^- secretion. Some studies demonstrated the involvement of arachidonic acid-activated K^+ channels, which showed distinct characteristics from cAMP- and Ca^{2+}-activated K^+ channels, in Cl^- secretion in T84 colonic cells (Barrett and Bigby, 1993; Devor and Frizzell, 1998). Moreover, it was also possible that Ca^{2+}-activated K^+ channels might compensate for cAMP-activated K^+ channel activity during cAMP-activated K^+ channel inhibition, and vice versa. The responsible K^+ channels for the PTH action remain to be investigated.

5.4 Signaling pathways involved in PTH-induced HCO_3^- secretion in Caco-2 monolayer

Signaling pathways of PTH through PTHR have been extensively studied in bone and kidney (Lee and Partridge, 2009; Tovey et al., 2006). PTHR, a member of GPCR superfamily, exerted its action through 2 different G-proteins, namely $G_{\alpha s}$ and $G_{\alpha q}$. $G_{\alpha s}$ increased cAMP levels which, in turn, activated PKA. Consequently, PKA phosphorylated downstream PTH targets, such as Ca^{2+} channels (Picotto et al., 1997). On the other hand, $G_{\alpha q}$ stimulated PLC which cleaved PIP_2 in the plasma membrane into DAG and IP_3. IP_3 induced Ca^{2+} release from SER and thus increased intracellular Ca^{2+}. DAG then activated PKC which further phosphorylated downstream PTH targets, such as Ca^{2+} channels (Fritsch and Chesnoy-Marchais, 1994). It was evident that PTH also exerted its action through extracellular signal-regulated kinase (ERK)/mitogen-activated protein kinase (MAPK) pathway (Swarthout et al., 2001; Verheijen and Defize, 1997). In the intestine, PTH signal transduction was similar to that in the kidney and bone, i.e., involving cAMP/PKA, PLC/DAG/PKC, PLC/IP_3/intracellular Ca^{2+}, and ERK/MAP pathways (Gentili et al., 2001; Massheimer et al., 2000; Nemere, 1999).

The present study showed that PTH-induced HCO_3^- secretion in Caco-2 cells was inhibited by PKI 14–22, wortmannin, and LY-294002, indicating the involvement of PKA and PI3K (Figure 4.16). Both pathways were found to regulate some transporters responsible for HCO_3^- secretion, e.g., NBCe1 (Bachmann et al., 2003; Yu et al., 2009), CFTR (Tuo et al., 2009), NHE3 (Akhter et al., 2002; Zhao et al., 1999), NHE1 (Putney et al., 2002), and Na^+/K^+-ATPase (Bhargava et al. 2007; Carranza et al., 1998). PTH also used cAMP/PKA pathway to induce Cl^- secretion in the renal proximal tubular cells (Laverty et al., 2003) and osteoblasts (Chesnoy-Marchais and Fritsch, 1989). On the other hand, the Ca^{2+}/PKC pathway did not contribute to the PTH action since neither intracellular Ca^{2+} chelator, BAPTA, nor PKC inhibitor, GF-109203X, inhibited the PTH-induced I_{sc} response in Caco-2 cells (Figure 4.16). ERK/MAPK pathway was not investigated in the present study, but it was unlikely to be involved in PTH-induced HCO_3^- secretion. The ERK and MAPK

usually regulated cell proliferation at the genomic level, rather than the rapid stimulation of intestinal ion transport (Chang and Karin, 2001).

Taken together, the present investigation provided evidence, for the first time, that PTH exerted its direct ion regulatory function in the intestinal cells. This PTH-induced HCO_3^- secretion may be essential for the luminal hydration and/or local pH regulation for the digestive process. However, further investigation is required to demonstrate physiological significance of this PTH action in vivo.

CHAPTER VI
CONCLUSIONS

The present study demonstrated the application of impedance measurement in the analyses of the plasma membrane capacitance and resistance in the intestinal epithelium-like Caco-2 monolayer. AC-based impedance spectroscopy was used to predict biological responses of Caco-2 cells to PTH, the action of which in the intestine was previously not known. Finally, transporters and signaling pathways responsible for the PTH action were investigated by DC-based Ussing chamber technique. Conclusions could be drawn as followed;

1. **Impedance spectroscopy was capable of determining plasma membrane capacitance and resistance of Caco-2 cells.**

    1.1 Impedance analysis could determine baseline plasma membrane capacitance and resistance of Caco-2 monolayer (C_a = 28.98 ± 0.69 μF/cm^2, C_b = 12.36 ± 0.23 μF/cm^2, R_a = 2141.30 ± 222.50 Ω·cm^2, R_b = 993.96 ± 60.96 Ω·cm^2).

    1.2 Impedance analysis could detect the forskolin-induced decrease in plasma membrane resistance.

2. **Impedance spectroscopy was capable of predicting the PTH action on Caco-2 monolayer.**

    2.1 PTH reduced the resistance of both apical and basolateral membranes, indicating that transporters in both membranes were activated by PTH.

    2.2 Plasma membrane capacitance was not affected by PTH, implying that PTH action did not induce fusion of subapical vesicle to the plasma membrane.

3. PTH exerted direct actions on Caco-2 cells by stimulating epithelial anion secretion.

3.1 Caco-2 cells predominantly expressed PTHR1 mRNA, which was the functional PTHR isoform in most target organs, such as bone and kidney.

3.2 Direct exposure to PTH induced anion secretion in a dose-dependent manner [half-maximal effective concentration (EC_{50}) = 3 nmol/L; maximal effective concentration = 10 nmol/L].

3.3 13–34 PTH (inactive form of PTH), autoclaved 1–34 PTH, and 1–34 PTH preincubated with neutralizing PTH antibody did not show anion secretion, indicating that this epithelial response was specific to PTH.

4. Mechanisms and signaling pathways responsible for the PTH-induced anion secretion.

4.1 PTH had no effect on R_p, indicating that PTH predominantly increased transcellular ion transport rather than paracellular transport.

4.2 The principal anion secreted during PTH exposure was HCO_3^-, and not Cl^-.

4.3 HCO_3^- availability was provided by HCO_3^- entry through NBCe1 in the basolateral membrane and endogenous HCO_3^- generation catalyzed by carbonic anhydrase.

4.4 HCO_3^- was secreted through CFTR in the apical membrane.

4.5 Apical NHE3 and basolateral NHE1 helped extrude excess H^+ produced by carbonic anhydrase.

4.6 Na^+/K^+-ATPase provided driving force for NBCe1, and other K^+ channels apart from cAMP-activated and Ca^{2+}-activated K^+ channels helped recycle K^+ to the basolateral solution.

4.7 PTH exerted its action through PKA- and PI3K-dependent pathways.

This PTH action and its possible mechanism are depicted in Figure 6.1.

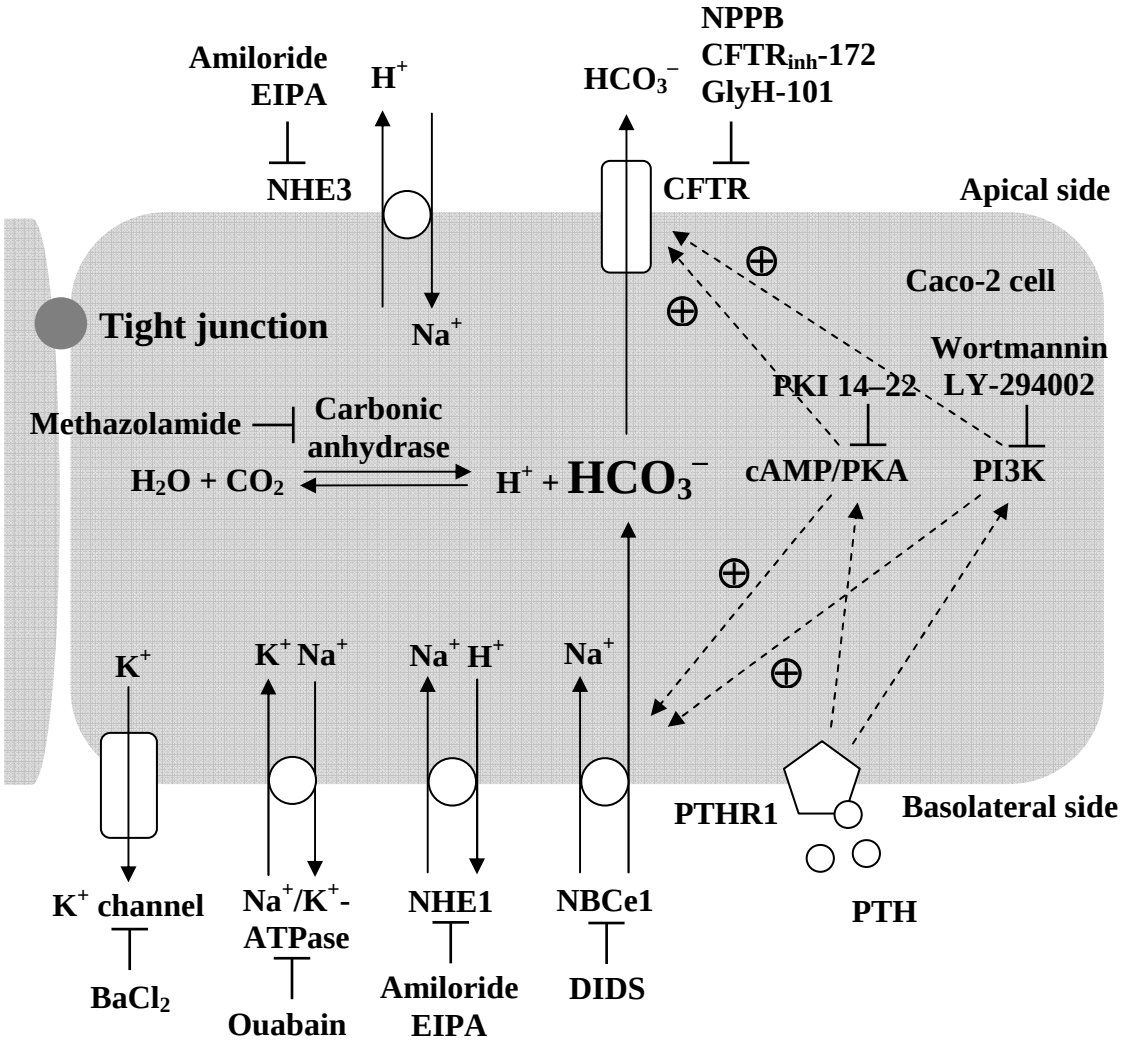

Figure 6.1 Hypothetical diagram of PTH-induced HCO_3^- secretion in Caco-2 monolayer. HCO_3^- enters the basolateral membrane through electrogenic Na^+/HCO_3^- cotransporter-1 (NBCe1). NBCe1 requires Na^+ concentration gradient which is maintained by Na^+/K^+-ATPase activity. K^+ is recycled to the basolateral side through K^+ channel. HCO_3^- is also partly generated by intracellular carbonic anhydrase. HCO_3^- leaves the cell through the apical cystic fibrosis transmembrane conductance regulator (CFTR). Excess H^+ produced by carbonic anhydrase is extruded by the apical Na^+/H^+ exchanger-3 (NHE3) and basolateral Na^+/H^+ exchanger-1 (NHE1). PTH-induced HCO_3^- secretion is mediated by cyclic adenosine monophosphate (cAMP)/protein kinase A (PKA) and phosphoinositide-3-kinase (PI3K) signaling pathways, which have been known to activate apical CFTR and basolateral NBCe1 activities (Bachmann et al., 2003; Tuo et al., 2009). Inhibitors of transporters and signaling molecules are shown in the figure.

REFERENCES

Abou-Samra AB, Juppner H, Force T, Freeman MW, Kong XF, Schipani E, Urena P, Richards J, Bonventre JV, Potts JT Jr, Kronenberg HM, Segre G. Expression cloning of a common receptor for parathyroid hormone and parathyroid hormone-related peptide from rat osteoblast-like cells: a single receptor stimulates intracellular accumulation of both cAMP and inositol trisphosphates and increases intracellular free calcium. Proc Natl Acad Sci USA 1992;89(7):2732–2736.

Agus ZS, Puschett JB, Senesky D, Goldberg M. Mode of action of parathyroid hormone and cyclic adenosine 3′,5′-monophosphate on renal tubular phosphate reabsorption in the dog. J Clin Invest 1971;50(3):617–626.

Ainsworth MA, Amelsberg M, Hogan DL, Isenberg JI. Acid-base transport in isolated rabbit duodenal villus and crypt cells. Scand J Gastroenterol 1996;31(11):1069–1077.

Akhter S, Kovbasnjuk O, Li X, Cavet M, Noel J, Arpin M, Hubbard AL, Donowitz M. Na^+/H^+ exchanger 3 is in large complexes in the center of the apical surface of proximal tubule-derived OK cells. Am J Physiol Cell Physiol 2002;283(3):C927–C940.

Ameen NA, van Donselaar E, Posthuma G, de Jonge H, McLaughlin G, Geuze HJ, Marino C, Peters PJ. Subcellular distribution of CFTR in rat intestine supports a physiologic role for CFTR regulation by vesicle traffic. Histochem Cell Biol 2000;114(3):219–228.

Arnaud CD Jr, Tenenhouse AM, Rasmussen H. Parathyroid hormone. Annu Rev Physiol 1967;29:349–372.

Azarani A, Goltzman D, Orlowski J. Parathyroid hormone and parathyroid hormone-related peptide inhibit the apical Na^+/H^+ exchanger NHE-3 isoform in renal cells (OK) via a dual signaling cascade involving protein kinase A and C. J Biol Chem 1995;270(34):20004–20010.

Azarani A, Orlowski J, Goltzman D. Parathyroid hormone and parathyroid hormone-related peptide activate the Na^+/H^+ exchanger NHE-1 isoform in osteoblastic cells (UMR-106) via a cAMP-dependent pathway. J Biol Chem 1995;270(39):23166–23172.

Bachmann O, Rossmann H, Berger UV, Colledge WH, Ratcliff R, Evans MJ, Gregor M, Seidler U. cAMP-mediated regulation of murine intestinal/pancreatic Na^+/HCO_3^- cotransporter subtype pNBC1. Am J Physiol Gastrointest Liver Physiol 2003;284(1):G37–G45.

Bailey CA, Bryla P, Malick AW. The use of the intestinal epithelial cell culture model, Caco-2, in pharmaceutical development. Adv Drug Deliver Rev 1996;22:85–103.

Bajnath RB, Augeron C, Laboisse CL, Bijman J, de Jonge HR, Groot JA. Electrophysiological studies of forskolin-induced changes in ion transport in the human colon carcinoma cell line HT-29 cl.19A: lack of evidence for a cAMP-activated basolateral K^+ conductance. J Membr Biol 1991;122(3):239–250.

Bank N, Su WS, Aynedjian HS. A micropuncture study of renal phosphate transport in rats with chronic renal failure and secondary hyperparathyroidism. J Clin Invest 1978;61(4):884–894.

Barrett KE, Bigby TD. Involvement of arachidonic acid in the chloride secretory response of intestinal epithelial cells. Am J Physiol Cell Physiol 1993;264(2 Pt 1):C446–C452.

Barrett KE, Keely SJ. Chloride secretion by the intestinal epithelium: molecular basis and regulatory aspects. Annu Rev Physiol 2000;62:535–572.

Bezerra CN, Girardi AC, Carraro-Lacroix LR, Reboucas NA. Mechanisms underlying the long-term regulation of NHE3 by parathyroid hormone. Am J Physiol Renal Physiol 2008;294(5):F1232–F1237.

Bhargava M, Lei J, Mariash CN, Ingbar DH. Thyroid hormone rapidly stimulates alveolar Na,K-ATPase by activation of phosphatidylinositol 3-kinase. Curr Opin Endocrinol Diabetes Obes 2007;14(5):416–420.

Bourdeau JE, Langman CB, Bouillon R. Parathyroid hormone-stimulated calcium absorption in cTAL from vitamin D-deficient rabbits. Kidney Int 1987;31(4):913–917.

Bringhurst FR, Segre GV, Lampman GW, Potts JT Jr. Metabolism of parathyroid hormone by Kupffer cells: analysis by reverse-phase high-performance liquid chromatography. Biochemistry 1982;21(18):4252–4258.

Bringhurst FR, Stern AM, Yotts M, Mizrahi N, Segre GV, Potts JT Jr. Peripheral metabolism of PTH: fate of biologically active amino terminus in vivo. Am J Physiol Endocrinol Metab 1988;255(6 Pt 1):E886–E893.

Brown EM, Vassilev PM, Quinn S, Hebert SC. G-protein-coupled, extracellular Ca^{2+}-sensing receptor: a versatile regulator of diverse cellular functions. Vitam Horm 1999;55:1–71.

Carranza ML, Rousselot M, Chibalin AV, Bertorello AM, Favre H, Feraille E. Protein kinase A induces recruitment of active Na^{+},K^{+}-ATPase units to the plasma membrane of rat proximal convoluted tubule cells. J Physiol 1998;511(Pt 1):235–243.

Chang L, Karin M. Mammalian MAP kinase signalling cascades. Nature 2001;410(6824):37–40.

Chantret I, Barbat A, Dussaulx E, Brattain MG, Zweibaum A. Epithelial polarity, villin expression, and enterocytic differentiation of cultured human colon carcinoma cells: a survey of twenty cell lines. Cancer Res 1988;48(7):1936–1942.

Chesnoy-Marchais D, Fritsch J. Chloride current activated by cyclic AMP and parathyroid hormone in rat osteoblasts. Pflugers Arch 1989;415(1):104–114.

Chorev M, Alexander J, Rosenblatt M. Interactions of parathyroid hormone and parathyroid homone-related protein with their receptors. In: Bilezikian JP, Levine MA, Marcus R, eds. *The parathyroids: basic and clinical concepts*. 2 ed. Calif: Academic Press 2001:31–52.

Chung U, Igarashi T, Nishishita T, Iwanari H, Iwamatsu A, Suwa A, Mimori T, Hata K, Ebisu S, Ogata E, Fujita T, Okazaki T. The interaction between Ku

antigen and REF1 protein mediates negative gene regulation by extracellular calcium. J Biol Chem 1996;271(15):8593–8598.

Clausen C. Impedance analysis in tight epithelia. Methods Enzymol 1989;171:628–642.

Clausen C, Lewis SA, Diamond JM. Impedance analysis of a tight epithelium using a distributed resistance model. Biophys J 1979;26(2):291–317.

Clausen C, Machen TE, Diamond JM. Changes in the cell membranes of the bullfrog gastric mucosa with acid secretion. Science 1982;217(4558):448–450.

Clausen C, Reinach PS, Marcus DC. Membrane transport parameters in frog corneal epithelium measured using impedance analysis techniques. J Membr Biol 1986;91(3):213–225.

Cohn DV, Macgregor RR, Chu LL, Kimmel JR, Hamilton JW. Calcemic fraction-A: biosynthetic peptide precursor of parathyroid hormone. Proc Natl Acad Sci USA 1972;69(6):1521–1525.

Cole KS. Membrane, ions, and impulses. In: Davson H ed. *A textbook of general physiology*. Calif: University of California Press 1972:12–59.

Cross HS, Debiec H, Peterlik M. Mechanism and regulation of intestinal phosphate absorption. Miner Electrolyte Metab 1990;16(2–3):115–124.

Davenport SE, Mergey M, Cherqui G, Boucher RC, Gespach C, Gabriel SE. Deregulated expression and function of CFTR and Cl^- secretion after activation of the Ras and Src/PyMT pathways in Caco-2 cells. Biochem Biophys Res Commun 1996;229(2):663–672.

Devor DC, Frizzell RA. Modulation of K^+ channels by arachidonic acid in T84 cells. II. Activation of a Ca^{2+}-independent K^+ channel. Am J Physiol Cell Physiol 1998;274(1 Pt 1):C149–C160.

Dharmsathaphorn K, Pandol SJ. Mechanism of chloride secretion induced by carbachol in a colonic epithelial cell line. J Clin Invest 1986;77(2):348–354.

Dorner AJ, Kemper B. Conversion of pre-proparathyroid hormone to proparathyroid hormone by dog pancreatic microsomes. Biochemistry 1978;17(25):5550–5555.

Endres DB, Villanueva R, Sharp CF Jr, Singer FR. Immunochemiluminometric and immunoradiometric determinations of intact and total immunoreactive parathyrin: performance in the differential diagnosis of hypercalcemia and hypoparathyroidism. Clin Chem 1991;37(2):162–168.

Fan L, Wiederkehr MR, Collazo R, Wang H, Crowder LA, Moe OW. Dual mechanisms of regulation of Na/H exchanger NHE-3 by parathyroid hormone in rat kidney. J Biol Chem 1999;274(16):11289–11295.

Feldman GM. HCO3- secretion by rat distal colon: effects of inhibitors and extracellular Na^+. Gastroenterology 1994;107(2):329–338.

Feldman GM, Berman SF, Stephenson RL. Bicarbonate secretion in rat distal colon in vitro: a measurement technique. Am J Physiol Cell Physiol 1988;254(3 Pt 1):C383–C390.

Ferrari SL, Behar V, Chorev M, Rosenblatt M, Bisello A. Endocytosis of ligand-human parathyroid hormone receptor 1 complexes is protein kinase C-dependent and involves β-arrestin2. Real-time monitoring by fluorescence microscopy. J Biol Chem 1999;274(42):29968–29975.

Fogh J, Fogh JM, Orfeo T. One hundred and twenty-seven cultured human tumor cell lines producing tumors in nude mice. J Natl Cancer Inst 1977;59(1):221–226.

Fritsch J, Chesnoy-Marchais D. Dual modulation of the L-type calcium current of rat osteoblastic cells by parathyroid hormone: opposite effects of protein kinase C and cyclic nucleotides. Cell Signal 1994;6:645–655.

Fukuda M, Ohara A, Bamba T, Saek Y. Activation of transepithelial ion transport by secretin in human intestinal Caco-2 cells. Jpn J Physiol 2000;50(2):215–225.

Furukawa O, Bi LC, Guth PH, Engel E, Hirokawa M, Kaunitz JD. NHE3 inhibition activates duodenal bicarbonate secretion in the rat. Am J Physiol Gastrointest Liver Physiol 2004;286(1):G102–G109.

Gadsby DC, Nairn AC. Control of CFTR channel gating by phosphorylation and nucleotide hydrolysis. Physiol Rev 1999;79:S77–S107.

Garabedian M, Holick MF, Deluca HF, Boyle IT. Control of 25-hydroxycholecalciferol metabolism by parathyroid glands. Proc Natl Acad Sci USA 1972;69(7):1673–1676.

Gardella TJ, Wilson AK, Keutmann HT, Oberstein R, Potts JT Jr, Kronenberg M, Nussbaum SR. Analysis of parathyroid hormone's principal receptor-binding region by site-directed mutagenesis and analog design. Endocrinology 1993;132(5):2024–2030.

Gensure RC, Gardella TJ, Juppner H. Parathyroid hormone and parathyroid hormone-related peptide, and their receptors. Biochem Biophys Res Commun 2005;328(3):666–678.

Gentili C, Morelli S, Boland R, de Boland AR. Parathyroid hormone activation of map kinase in rat duodenal cells is mediated by 3′,5′-cyclic AMP and Ca^{2+}. Biochim Biophys Acta 2001;1540(3):201–212.

Girardi AC, Titan SM, Malnic G, Reboucas NA. Chronic effect of parathyroid hormone on NHE3 expression in rat renal proximal tubules. Kidney Int 2000;58(4):1623–1631.

Gordon LG, Kottra G, Fromter E. Electrical impedance analysis of leaky epithelia: theory, techniques, and leak artifact problems. Methods Enzymol 1989;171:642–663.

Grasset E, Bernabeu J, Pinto M. Epithelial properties of human colonic carcinoma cell line Caco-2: effect of secretagogues. Am J Physiol Cell Physiol 1985;248(5 Pt 1):C410–C418.

Grasset E, Pinto M, Dussaulx E, Zweibaum A, Desjeux JF. Epithelial properties of human colonic carcinoma cell line Caco-2: electrical parameters. Am J Physiol Cell Physiol 1984;247(3 Pt 1):C260–C267.

Habener JF, Amherdt M, Ravazzola M, Orci L. Parathyroid hormone biosynthesis. Correlation of conversion of biosynthetic precursors with intracellular protein migration as determined by electron microscope autoradiography. J Cell Biol 1979;80(3):715–731.

Haden ST, Brown EM, Hurwitz S, Scott J, El-Hajj Fuleihan G. The effects of age and gender on parathyroid hormone dynamics. Clin Endocrinol (Oxf) 2000;52(3):329–338.

Hidalgo IJ, Raub TJ, Borchardt RT. Characterization of the human colon carcinoma cell line (Caco-2) as a model system for intestinal epithelial permeability. Gastroenterology 1989;96(3):736–749.

Hilgers AR, Conradi RA, Burton PS. Caco-2 cell monolayers as a model for drug transport across the intestinal mucosa. Pharm Res 1990;7(9):902–910.

Iino Y, Burg MB. Effect of parathyroid hormone on bicarbonate absorption by proximal tubules in vitro. Am J Physiol Renal Physiol 1979;236(4):F387–F391.

Inoue CN, Woo JS, Schwiebert EM, Morita T, Hanaoka K, Guggino SE, Guggino WB. Role of purinergic receptors in chloride secretion in Caco-2 cells. Am J Physiol Cell Physiol 1997;272(6 Pt 1):C1862–C1870.

Ishiguro H, Steward MC, Wilson RW, Case RM. Bicarbonate secretion in interlobular ducts from guinea-pig pancreas. J Physiol 1996;495(Pt 1):179–191.

Jumarie C, Malo C. Caco-2 cells cultured in serum-free medium as a model for the study of enterocytic differentiation in vitro. J Cell Physiol 1991;149(1):24–33.

Juppner H. Receptors for parathyroid hormone and parathyroid hormone-related peptide: exploration of their biological importance. Bone 1999;25(1):87–90.

Kemper B, Habener JF, Mulligan RC, Potts JT Jr, Rich A. Pre-proparathyroid hormone: a direct translation product of parathyroid messenger RNA. Proc Natl Acad Sci USA 1974;71(9):3731–3735.

Kemper B, Habener JF, Potts JT Jr, Rich A. Proparathyroid hormone: identification of a biosynthetic precursor to parathyroid hormone. Proc Natl Acad Sci USA 1972;69(3):643–647.

Khanal RC, Nemere I. Regulation of intestinal calcium transport. Annu Rev Nutr 2008;28:179–196.

Kilav R, Silver J, Naveh-Many T. Parathyroid hormone gene expression in hypophosphatemic rats. J Clin Invest 1995;96(1):327–333.

Kim D, Steward MC. The role of CFTR in bicarbonate secretion by pancreatic duct and airway epithelia. J Med Invest 2009;56:336–342.

Kreindler JL, Jackson AD, Kemp PA, Bridges RJ, Danahay H. Inhibition of chloride secretion in human bronchial epithelial cells by cigarette smoke extract. Am J Physiol Lung Cell Mol Physiol 2005;288(5):L894–L902.

Kronenberg HM, Bringhurst FR, Segre GV, Potts JT Jr. Parathyroid hormone biosynthesis and metabolism. In: Bilezikian JP, Marcus R, Levine MA, eds. *The parathyroids: basic and clinical concepts*. New York: Raven Press 1994:125–138.

Krugliak P, Hollander D, Schlaepfer CC, Nguyen H, Ma TY. Mechanisms and sites of mannitol permeability of small and large intestine in the rat. Dig Dis Sci 1994;39(4):796–801.

Kunzelmann K, Beesley AH, King NJ, Karupiah G, Young JA, Cook DI. Influenza virus inhibits amiloride-sensitive Na^+ channels in respiratory epithelia. Proc Natl Acad Sci USA 2000;97(18):10282–10287.

Kunzelmann K, Mall M. Electrolyte transport in the mammalian colon: mechanisms and implications for disease. Physiol Rev 2002;82(1):245–289.

Laverty G, McWilliams C, Sheldon A, Arnason SS. PTH stimulates a Cl^--dependent and EIPA-sensitive current in chick proximal tubule cells in culture. Am J Physiol Renal Physiol 2003;284(5):F987–F995.

Le Bivic A, Quaroni A, Nichols B, Rodriguez-Boulan E. Biogenetic pathways of plasma membrane proteins in Caco-2, a human intestinal epithelial cell line. J Cell Biol 1990;111(4):1351–1361.

Lee M, Partridge NC. Parathyroid hormone signaling in bone and kidney. Curr Opin Nephrol Hypertens 2009;18(4):298–302.

Li H, Seitz PK, Thomas ML, Selvanayagam P, Rajaraman S, Cooper CW. Widespread expression of the parathyroid hormone-related peptide and PTH/PTHrP receptor genes in intestinal epithelial cells. Lab Invest 1995;73(6):864–870.

Li YC, Amling M, Pirro AE, Priemel M, Meuse J, Baron R, Delling G, Demay MB. Normalization of mineral ion homeostasis by dietary means prevents hyperparathyroidism, rickets, and osteomalacia, but not alopecia in vitamin D receptor-ablated mice. Endocrinology 1998;139(10):4391–4396.

Lim SK, Gardella TJ, Baba H, Nussbaum SR, Kronenberg HM. The carboxy-terminus of parathyroid hormone is essential for hormone processing and secretion. Endocrinology 1992;131(5):2325–2330.

MacLeod RJ, Redican F, Lembessis P, Hamilton JR, Field M. Sodium-bicarbonate cotransport in guinea pig ileal crypt cells. Am J Physiol Cell Physiol 1996;270(3 Pt 1):C786–C793.

Madara JL. Loosening tight junctions. Lessons from the intestine. J Clin Invest 1989;83(4):1089–1094.

Malloy PJ, Pike JW, Feldman D. The vitamin D receptor and the syndrome of hereditary 1,25-dihydroxyvitamin D-resistant rickets. Endocr Rev 1999;20(2):156–188.

Martin KJ, Hruska KA, Freitag JJ, Klahr S, Slatopolsky E. The peripheral metabolism of parathyroid hormone. N Engl J Med 1979;301(20):1092–1098.

Massheimer V, Picotto G, Boland R, De Boland AR. Effect of aging on the mechanisms of PTH-induced calcium influx in rat intestinal cells. J Cell Physiol 2000;182(3):429–437.

McKinney TD, Myers P. Bicarbonate transport by proximal tubules: effect of parathyroid hormone and dibutyryl cyclic AMP. Am J Physiol Renal Physiol 1980a;238(3):F166–F174.

McKinney TD, Myers P. PTH inhibition of bicarbonate transport by proximal convoluted tubules. Am J Physiol Renal Physiol 1980b;239(2):F127–134.

Milstein C, Brownlee GG, Harrison TM, Mathews MB. A possible precursor of immunoglobulin light chains. Nat New Biol 1972;239(91):117–120.

Moallem E, Kilav R, Silver J, Naveh-Many T. RNA-Protein binding and post-transcriptional regulation of parathyroid hormone gene expression by calcium and phosphate. J Biol Chem 1998;273(9):5253–5259.

Moser AJ, Gangopadhyay A, Bradbury NA, Peters KW, Frizzell RA, Bridges RJ. Electrogenic bicarbonate secretion by prairie dog gallbladder. Am J Physiol Gastrointest Liver Physiol 2007;292(6):G1683–G1694.

Murray TM, Rao LG, Divieti P, Bringhurst FR. Parathyroid hormone secretion and action: evidence for discrete receptors for the carboxyl-terminal region and

related biological actions of carboxyl-terminal ligands. Endocr Rev 2005;26(1):78–113.

Naveh-Many T, Marx R, Keshet E, Pike JW, Silver J. Regulation of 1,25-dihydroxyvitamin D_3 receptor gene expression by 1,25-dihydroxyvitamin D_3 in the parathyroid in vivo. J Clin Invest 1990;86(6):1968–1975.

Naveh-Many T, Rahamimov R, Livni N, Silver J. Parathyroid cell proliferation in normal and chronic renal failure rats. The effects of calcium, phosphate, and vitamin D. J Clin Invest 1995;96(4):1786–1793.

Naylor SL, Sakaguchi AY, Szoka P, Hendy GN, Kronenberg HM, Rich A, Shows TB. Human parathyroid hormone gene (PTH) is on short arm of chromosome 11. Somatic Cell Genet 1983;9(5):609–616.

Nemere I. Parathyroid hormone rapidly stimulates phosphate transport in perfused duodenal loops of chicks: lack of modulation by vitamin D metabolites. Endocrinology 1996;137(9):3750–3755.

Nemere I. 24,25-dihydroxyvitamin D_3 suppresses the rapid actions of 1,25-dihydroxyvitamin D_3 and parathyroid hormone on calcium transport in chick intestine. J Bone Miner Res 1999;14(9):1543–1549.

Nemere I, Larsson D. Does PTH have a direct effect on intestine? J Cell Biochem 2002;86(1):29–34.

Okazaki T, Igarashi, T, Kronenberg HM. 5′-Flanking region of the parathyroid hormone gene mediates negative regulation by 1,25-$(OH)_2$ vitamin D_3. J Biol Chem 1988;263(5):2203–2208.

Orlowski J. Heterologous expression and functional properties of amiloride high affinity (NHE-1) and low affinity (NHE-3) isoforms of the rat Na/H exchanger. J Biol Chem 1993;268(22):16369–16377.

Paunescu TG, Helman SI. PGE_2 activation of apical membrane Cl^- channels in A6 epithelia: impedance analysis. Biophys J 2001;81(2):852–866.

Pérez M, Barber A, Ponz F. Modulation of intestinal paracellular permeability by intracellular mediators and cytoskeleton. Can J Physiol Pharmacol 1997;75(4):287–292.

Picotto G, Massheimer V, Boland R. Parathyroid hormone stimulates calcium influx and the cAMP messenger system in rat enterocytes. Am J Physiol Cell Physiol 1997;273:C1349–C1353.

Pines M, Fukayama S, Costas K, Meurer E, Goldsmith PK, Xu X, Muallem S, Behar V, Chorev M, Rosenblatt M, Tashjian AH Jr, Suva LJ. Inositol 1-,4-,5-trisphosphate-dependent Ca^{2+} signaling by the recombinant human PTH/PTHrP receptor stably expressed in a human kidney cell line. Bone 1996;18(4):381–389.

Potts JT Jr, Tregear GW, Keutmann HT, Niall HD, Sauer R, Deftos LJ, Dawson BF, Hogan ML, Aurbach GD. Synthesis of a biologically active N-terminal tetratriacontapeptide of parathyroid hormone. Proc Natl Acad Sci USA 1971;68(1):63–67.

Powell DW. Barrier function of epithelia. Am J Physiol Gastrointest Liver Physiol 1981;241(4):G275–G288.

Pun KK, Ho PW, Nissenson RA, Arnaud CD. Desensitization of parathyroid hormone receptors on cultured bone cells. J Bone Miner Res 1990;5(12):1193–1200.

Putney LK, Denker SP, Barber DL. The changing face of the Na^+/H^+ exchanger, NHE1: structure, regulation, and cellular actions. Annu Rev Pharmacol Toxicol 2002;42:527–552.

Quamme GA. Renal magnesium handling: new insights in understanding old problems. Kidney Int 1997;52(5):1180–1195.

Reynolds A, Parris A, Evans LA, Lindqvist S, Sharp P, Lewis M, Tighe R, Williams MR. Dynamic and differential regulation of NKCC1 by calcium and cAMP in the native human colonic epithelium. J Physiol 2007;582(Pt 2):507–524.

Rodriguez M, Almaden Y, Hernandez A, Torres A. Effect of phosphate on the parathyroid gland: direct and indirect? Curr Opin Nephrol Hypertens 1996;5(4):321–328.

Romero MF, Fulton CM, Boron WF. The SLC4 family of HCO_3^- transporters. Pflugers Arch 2004;447(5):495–509.

Rosenblatt M, Segre GV, Tyler GA, Shepard GL, Nussbaum SR, Potts JT Jr. Identification of a receptor-binding region in parathyroid hormone. Endocrinology 1980;107(2):545–550.

Russell J, Silver J, Sherwood LM. The effects of calcium and vitamin D metabolites on cytoplasmic mRNA coding for pre-proparathyroid hormone in isolated parathyroid cells. Trans Assoc Am Physicians 1984;97:296–303.

Sambuy Y, De Angelis I, Ranaldi G, Scarino ML, Stammati A, Zucco F. The Caco-2 cell line as a model of the intestinal barrier: influence of cell and culture-related factors on Caco-2 cell functional characteristics. Cell Biol Toxicol 2005;21(1):1–26.

Schluter KD. PTH and PTHrP: Similar structures but different functions. News Physiol Sci 1999;14:243–249.

Schultheiss G, Diener M. K^+ and Cl^- conductances in the distal colon of the rat. Gen Pharmacol 1998;31(3):337–342.

Silver J, Naveh-Many T, Mayer H, Schmelzer HJ, Popovtzer MM. Regulation by vitamin D metabolites of parathyroid hormone gene transcription in vivo in the rat. J Clin Invest 1986;78(5):1296–1301.

Singh AK, Singh S, Devor DC, Frizzell RA, van Driessche W, Bridges RJ. Transepithelial impedance analysis of chloride secretion. Methods Mol Med 2002;70:129–142.

Strewler GJ. The physiology of parathyroid hormone-related protein. N Engl J Med 2000;342(3):177–185.

Swarthout JT, Doggett TA, Lemker JL, Partridge NC. Stimulation of extracellular signal-regulated kinases and proliferation in rat osteoblastic cells by parathyroid hormone is protein kinase C-dependent. J Biol Chem 2001;276(10):7586–7592.

Szabo FK, Snyder N, Usdin TB, Hoffman GE. A direct neuronal connection between the subparafascicular and ventrolateral arcuate nuclei in non-lactating female rats. Could this pathway play a role in the suckling-induced prolactin release? Endocrine 2010;37(1):62–70.

Tanrattana C, Charoenphandhu N, Limlomwongse L, Krishnamra N. Prolactin directly stimulated the solvent drag-induced calcium transport in the duodenum of female rats. Biochim Biophys Acta 2004;1665(1–2):81–91.

Tovey SC, Dedos SG, Taylor CW. Signaling from parathyroid hormone. Biochem Soc Trans 2006;34:515–517.

Tuo B, Wen G, Zhang Y, Liu X, Wang X, Dong H. Involvement of phosphatidylinositol 3-kinase in cAMP- and cGMP-induced duodenal epithelial CFTR activation in mice. Am J Physiol Cell Physiol 2009;297(3):C503–C515.

Urena P, Kong XF, Abou-Samra AB, Juppner H, Kronenberg HM, Potts JT Jr, Segre GV. Parathyroid hormone (PTH)/PTH-related peptide receptor messenger ribonucleic acids are widely distributed in rat tissues. Endocrinology 1993;133(2):617–623.

Usdin TB, Gruber C, Bonner TI. Identification and functional expression of a receptor selectively recognizing parathyroid hormone, the PTH2 receptor. J Biol Chem 1995;270(26):15455–15458.

Usdin TB, Hoare SR, Wang T, Mezey E, Kowalak JA. TIP39: a new neuropeptide and PTH2-receptor agonist from hypothalamus. Nat Neurosci 1999;2(11):941–943.

van Abel M, Hoenderop JG, van der Kemp AW, Friedlaender MM, van Leeuwen JP, Bindels RJ. Coordinated control of renal Ca^{2+} transport proteins by parathyroid hormone. Kidney Int 2005;68(4):1708–1721.

Verheijen MH, Defize LH. Parathyroid hormone activates mitogen-activated protein kinase via a cAMP-mediated pathway independent of Ras. J Biol Chem 1997;272(6):3423–3429.

Vilardaga JP, Krasel C, Chauvin S, Bambino T, Lohse MJ, Nissenson RA. Internalization determinants of the parathyroid hormone receptor differentially regulate β-arrestin/receptor association. J Biol Chem 2002;277(10):8121–8129.

Watson PH, Fraher LJ, Hendy GN, Chung UI, Kisiel M, Natale BV, Hodsman AB. Nuclear localization of the type 1 PTH/PTHrP receptor in rat tissues. J Bone Miner Res 2000;15(6):1033–1044.

Weymer A, Huott P, Liu W, McRoberts JA, Dharmsathaphorn K. Chloride secretory mechanism induced by prostaglandin E1 in a colonic epithelial cell line. J Clin Invest 1985;76(5):1828–1836.

Wills NK, Clausen C. Transport-dependent alterations of membrane properties of mammalian colon measured using impedance analysis. J Membr Biol 1987;95(1):21–35.

Wills NK, Lewis SA, Eaton DC. Active and passive properties of rabbit descending colon: a microelectrode and nystatin study. J Membr Biol 1979;45(1–2);81–108.

Wills NK, Purcell RK, Clausen C. Na^+ transport and impedance properties of cultured renal (A6 and 2F3) epithelia. J Membr Biol 1992;125(3):273–285.

Wills NK, Purcell RK, Clausen C, Millinoff LP. Effects of aldosterone on the impedance properties of cultured renal amphibian epithelia. J Membr Biol 1993;133(1):17–27.

Wysolmerski JJ, Stewart AF. The physiology of parathyroid hormone-related protein: an emerging role as a developmental factor. Annu Rev Physiol 1998;60:431–460.

Yoshioka M, Erickson RH, Matsumoto H, Gum E, Kim YS. Expression of dipeptidyl aminopeptidase IV during enterocytic differentiation of human colon cancer (Caco-2) cells. Int J Cancer 1991;47(6):916–921.

Yu H, Riederer B, Stieger N, Boron WF, Shull GE, Manns MP, Seidler UE, Bachmann O. Secretagogue stimulation enhances NBCe1 (electrogenic Na^+/HCO_3^-cotransporter) surface expression in murine colonic crypts. Am J Physiol Gastrointest Liver Physiol 2009;297(6):G1223–G1231.

Zhang Y, Norian JM, Magyar CE, Holstein-Rathlou NH, Mircheff AK, McDonough AA. In vivo PTH provokes apical NHE3 and NaPi2 redistribution and Na-K-ATPase inhibition. Am J Physiol Renal Physiol 1999;276(5 Pt 2):F711–F719.

Zhao H, Wiederkehr MR, Fan L, Collazo RL, Crowder LA, Moe OW. Acute inhibition of Na/H exchanger NHE-3 by cAMP. Role of protein kinase A and NHE-3 phosphoserines 552 and 605. J Biol Chem 1999;274(7):3978–3987.

Zhu JX, Yang N, He Q, Tsang LL, Zhao WC, Chung YW, Chan HC. Differential Cl^- and HCO_3^- mediated anion secretion by different colonic cell types in response to tetromethylpyrazine. World J Gastroenterol 2004;10(12):1763–1768.

Zhu JX, Zhang GH, Yang N, Rowlands DK, Wong HY, Tsang LL, Chung YW, Chan HC. Activation of apical CFTR and basolateral Ca^{2+}-activated K^+ channels by tetramethylpyrazine in Caco-2 cell line. Eur J Pharmacol 2005;510(3):187–195.

Zull JE, Lev NB. A theoretical study of the structure of parathyroid hormone. Proc Natl Acad Sci USA 1980;77(7):3791–3795.

APPENDICES

APPENDIX A
SOLUTION PREPARATION

A. Normal bathing solution

Normal bathing solution was prepared as 5× solution.

Substance	Molecular weight	Concentration in 1× solution (mmol/L)	Weight per 1000 mL 5× solution (g)
NaCl	58.44	118.0	34.47960
KCl	74.55	4.7	1.75193
$NaHCO_3$	84.01	23.0	9.66115
$MgSO_4 \cdot 7H_2O$	246.48	1.1	1.35564
D-Glucose	180.16	12.0	10.80960
L-Glutamine	146.15	12.5	1.82688
Mannitol	182.17	2.0	1.82170

$CaCl_2$ was not readily added into the 5× solution to prevent $CaCO_3$ precipitation. 25 mmol/L $CaCl_2$ was prepared separately and diluted together with 5× solution to make up 1× normal bathing solution. The final concentration of $CaCl_2$ in the 1× solution was 1.25 mmol/L.

The 1× normal bathing solution was continuously gassed with humidified 5% CO_2 in 95% O_2, and maintained at 37 °C and pH 7.4. Osmolality of the solution was 290–295 mmol/kg H_2O.

B. Cl^--depleted bathing solution

Cl^--depleted bathing solution was prepared as 5× solution.

Substance	Molecular weight	Concentration in 1× solution (mmol/L)	Weight per 1000 mL 5× solution (g)
$NaC_6H_{11}O_6$ (Sodium gluconate)	218.15	118.0	128.70850
$KC_6H_{11}O_6$ (Potassium gluconate)	234.25	4.7	5.50488
$NaHCO_3$	84.01	23.0	9.66115
$MgSO_4 \cdot 7H_2O$	246.48	1.1	1.35564
D-Glucose	180.16	12.0	10.80960
L-Glutamine	146.15	12.5	1.82688

$CaCl_2$ was not readily added into the 5× solution to prevent $CaCO_3$ precipitation. 25 mmol/L $CaCl_2$ was prepared separately and diluted together with 5× solution to make up 1× normal bathing solution. The final concentration of $CaCl_2$ in the 1× solution was 2.5 mmol/L in order to compensate for Ca^{2+}-chelating effect of gluconate. Osmolality of 1× solution was adjusted by 1 mol/L mannitol, and the final osmolality was 290–295 mmol/kg H_2O.

The 1× bathing solution was continuously gassed with humidified 5% CO_2 in 95% O_2 and maintained at 37 °C (pH 7.4).

C. HCO_3^--depleted bathing solution

HCO_3^--depleted bathing solution was prepared as 5× solution.

Substance	Molecular weight	Concentration in 1× solution (mmol/L)	Weight per 1000 mL 5× solution (g)
NaCl	58.44	118.0	34.47960
KCl	74.55	4.7	1.75193
HEPES sodium salt	260.30	10.0	13.01500
$MgSO_4 \cdot 7H_2O$	246.48	1.1	1.35564
D-Glucose	180.16	12.0	10.80960
L-Glutamine	146.15	12.5	1.82688

25 mmol/L $CaCl_2$ was prepared separately and diluted together with 5× solution to make up 1× normal bathing solution. The final concentration of $CaCl_2$ in the 1× solution was 1.25 mmol/L. Osmolality of the 1× solution was adjusted by 1 mol/L mannitol and the final osmolality was 290–295 mmol/kg H_2O.

The 1× bathing solution was continuously gassed with humidified 5% CO_2 in 95% O_2 and maintained at 37 °C (pH 7.4).

D. Cl^-/HCO_3^--depleted bathing solution

Cl^-/HCO_3^--depleted bathing solution was prepared as 5× solution.

Substance	Molecular weight	Concentration in 1× solution (mmol/L)	Weight per 1000 mL 5× solution (g)
$NaC_6H_{11}O_6$ (Sodium gluconate)	218.15	118.0	128.70850
$KC_6H_{11}O_6$ (Potassium gluconate)	234.25	4.7	5.50488
HEPES sodium salt	260.30	10.0	13.01500
$MgSO_4 \cdot 7H_2O$	246.48	1.1	1.35564
D-Glucose	180.16	12.0	10.80960
L-Glutamine	146.15	12.5	1.82688

25 mmol/L $CaCl_2$ was prepared separately and diluted together with 5× solution to make up 1× normal bathing solution. The final concentration of $CaCl_2$ in the 1× solution was 2.5 mmol/L in order to compensate for the Ca^{2+}-chelating effect of gluconate. Osmolality of the 1× solution was adjusted by 1 mol/L mannitol, and the final osmolality was 290–295 mmol/kg H_2O.

The 1× bathing solution was continuously gassed with humidified 5% CO_2 in 95% O_2 and maintained at 37 °C (pH 7.4).

APPENDIX B
PREPARATION OF BIOCHEMICALS, HORMONES AND INHIBITORS

A. Amiloride

Amiloride is a guadinidium group which contains pyridine derivative. Its protonated form directly interacts with the extracellular domain of ENaC, NHE, and Na^+/Ca^{2+} exchanger (NCX) resulting in inhibition of these transporters. Amiloride blocks ENaC at concentrations in the range of μmol/L while inhibition of NHE and NCX requires higher concentrations in the range of mmol/L. The higher concentrations of amiloride (several mmol/L) has been reported to nonspecifically inhibit other transporters, e.g., Na^+/K^+-ATPase and Na^+-coupled solute transporters. In this study, amiloride was dissolved in DMSO to obtain a final concentration of 1 mol/L (stock solution).

B. BAPTA-AM

BAPTA is a polyamino carboxylic acid compound which can chelate Ca^{2+} using its 4 carboxyl arms. To allow it permeate the plasma membrane, carboxylic acids are modified with acetoxymethyl (AM) ester groups resulting in an uncharged molecule called BAPTA-AM. Once BAPTA-AM enters the cell, the AM ester group is cleaved by nonspecific esterases, and the active BAPTA is trapped intracellularly. BAPTA-AM is generally used to chelate intracellular Ca^{2+}, thus reducing cytosolic free Ca^{2+} concentration. In this study, BAPTA-AM was dissolved in DMSO to obtain a final concentration of 10 mmol/L (stock solution).

C. Bumetanide

Bumetanide is a benzoic acid derivative which is structurally and pharmacologically similar to loop diuretic furosemide, but is more potent than furosemide. Bumetanide specifically inhibits NKCC. In this study, bumetanide was dissolved in DMSO to obtain a final concentration of 100 mmol/L (stock solution).

D. $CFTR_{inh}$-172

$CFTR_{inh}$-172 is an analog of thiazolidinone which has high potency and specificity to CFTR. It directly interacts with the cytosolic domain of CFTR, leading to an increase in the mean closed time, probably by stabilizing the closed state of the channel, without affecting the mean open time. This action is different from GlyH-101 which blocks CFTR by occluding the channel pore. In this study, $CFTR_{inh}$-172 was dissolved in DMSO to obtain a final concentration of 20 mmol/L (stock solution).

E. Charybdotoxin

Charybdotoxin is a neurotoxin from the venom of the scorpion *Leiurus quinquestriatus hebraeus*. This toxin binds to the extracellular part of the pore of Ca^{2+}-activated K^+ channel. In this study, charybdotoxin was dissolved in distilled water to obtain a final concentration of 100 μmol/L (stock solution).

F. Chromanol 293B

Chromanol 293B is a chromanol derivative which inhibits the cAMP-activated K^+ channel. It blocks the channel activity by binding to the pore of the channel. In this study, chromanol 293B was dissolved in DMSO to obtain a final concentration of 100 mmol/L (stock solution).

G. 4,4′-diisothiocya natostilbene-2,2′-disulfonic acid disodium salt hydrate (DIDS)

DIDS is a nonspecific blocker of anion transporters such as CaCC, NBCe1, and Cl^-/HCO_3^- exchangers. However, DIDS does not block CFTR. In this study, DIDS was dissolved in DMSO to obtain a final concentration of 100 mmol/L (stock solution).

H. 5-(N-ethyl-N-isopropyl) amiloride (EIPA)

EIPA is an amiloride derivative which has high specificity and potency to NHE, but low inhibitory effect on ENaC. In this study, EIPA was dissolved in DMSO to obtain a final concentration of 100 mmol/L (stock solution).

I. Forskolin

Forskolin as an activator of adenylyl cyclase is generally used to increase an intracellular cAMP level. Forskolin stimulates Cl^- and/or HCO_3^- secretion in various epithelia by activating CFTR. In this study, forskolin was dissolved in DMSO to obtain a final concentration of 10 mmol/L (stock solution).

J. GF-109203X

GF-109203X is an aminoalkyl bisindolylmaleimide derivative which has high potency and specific to PKC. GF-109203X can permeate the plasma membrane and inhibits PKC by binding to the ATP-binding site of the catalytic domain. It is a competitive inhibitor with respect to ATP. In this study, GF-109203X was dissolved in DMSO to obtain a final concentration of 0.33 mmol/L (stock solution).

K. GlyH-101

GlyH-101 is a glycine hydrazide analog which specifically blocks CFTR. It acts from the extracellular side to occlude the pore of the channel, thereby decreasing the mean open time and showing a voltage-dependent inhibition. In this study, GlyH-101 was dissolved in DMSO to obtain a final concentration of 50 mmol/L (stock solution).

L. LY-294002

LY-294002, a morpholino derivative of quercetin, is a potent and specific membrane-permeable inhibitor of PI3K. LY-294002 competitively blocks ATP binding at the ATP-binding site of the PI3K catalytic domain. It is less potent but more specific than wortmannin, another PI3K inhibitor. In this study, LY-294002 was dissolved in DMSO to obtain a final concentration of 25 mmol/L (stock solution).

M. Methazolamide

Methazolamide, a sulfonamide-containing inhibitor of the Zn-containing carbonic anhydrase, directly binds to the metal center of this enzyme, and also interacts with amino acids around that area. This enzyme normally catalyzes the following reaction;

$$H_2O + CO_2 \leftrightharpoons H^+ + HCO_3^-$$

Methazolamide is more permeable to the plasma membrane than its analog, acetazolamide. In this study, methazolamide was dissolved in DMSO to obtain a final concentration of 1 mol/L (stock solution).

N. 5-nitro-2-(3-phenylpropylamino)benzoic acid (NPPB)

NPPB is a potent nonspecific Cl^- channel blocker. It inhibits various types of Cl^- channels including CFTR and CaCC. In this study, NPPB was dissolved in DMSO to obtain a final concentration of 100 mmol/L (stock solution).

O. Nystatin

Nystatin is a pore-forming antifungal drug. It binds to sterols in the plasma membrane and, in turn, forms pores leading to an increase in membrane permeability without affecting the paracellular permeability. It can be applied to determine the resistance of the plasma membrane (please see Materials and Methods section). In this study, nystatin was dissolved in DMSO to obtain a final concentration of 360 μg/mL (stock solution).

P. Ouabain

Ouabain is a cardiac glycoside derived from the seeds of *Strophanthus gratus.* It specifically inhibits Na^+/K^+-ATPase by binding to the extracellular surface of the α subunit of the pump. In this study, ouabain was dissolved in normal bathing solution to obtain a final concentration of 10 mmol/L (stock solution).

Q. Myristoylated PKI (14–22) amide

PKI (14–22), a 14–22 fragment of an endogenous thermostable protein kinase inhibitor, is a pseudosubstrate peptide inhibitor of cAMP-dependent protein kinase or PKA. It targets the substrate-binding site of the PKA catalytic domain. Modification of PKI (14–22) by N-terminal myristoylation (covalent attachment of a myristoyl group to the N-terminal amino acid of a nascent peptide) yields a membrane-permeable form of PKI (14–22). In this study, myristoylated PKI (14–22) was dissolved in distilled water to obtain a final concentration of 0.8 mmol/L (stock solution).

R. PTH (1–34)

PTH (1–34) is the N-terminal active 1–34 fragment of parathyroid hormone. This polypeptide regulates Ca^{2+} transporters in the kidney, bone and intestine in response to the plasma Ca^{2+} levels. In this study, PTH (1–34) was dissolved in distilled water to obtain a final concentration of 20 μmol/L (stock solution).

S. PTH (13–34)

PTH (13–34) is a truncated 13–34 fragment of parathyroid hormone. Since it lacks a functional sequence of the N-terminal amino acids, it is an inactive form of PTH and can be used as a negative control for PTH study. In this study, PTH (13–34) was dissolved in distilled water to obtain a final concentration of 20 μmol/L (stock solution).

T. Wortmannin

Wortmannin, a furanosteroid metabolite of the fungus *Penicillium funiculosum*, is a potent inhibitor of PI3K. It irreversibly inhibits PI3K by forming a covalent bond with a lysine residue in the ATP-binding site of the PI3K catalytic domain. It is more potent but less specific than LY-294002. In this study, wortmannin was dissolved in DMSO to obtain a final concentration of 66.67 mmol/L (stock solution).

APPENDIX C
PREPARATION OF CULTURE MEDIUM

A. Basal DMEM

Basal DMEM was prepared by dissolving 13.5 g powdered DMEM and 3.7 g $NaHCO_3$ in H_2O. The solution was mixed thoroughly using a magnetic stirrer. The pH of the solution was adjusted to 7.4 by 1 M $NaHCO_3$ or 1 M HCl. Thereafter, the volume of the solution was adjusted to 1 L in a volumetric flask. Finally, the solution was filtered through a 0.2-μm-pore membrane (Corning, Corning, NY, USA) and dispensed into a sterile container. The basal DMEM can be stored at 4 °C up to 6 months.

B. Complete DMEM

Complete DMEM was prepared in a class II biosafety cabinet. Basal DMEM was supplemented with 15% heat-inactivated FBS (heat-inactivation at 56 °C for 30 min), 1% NEAA, 1% L-glutamine, and 100 U/mL penicillin-streptomycin. The solution was mixed thoroughly by pipetting. The complete DMEM was stored at 4 °C up to 2 weeks.

APPENDIX D
CACO-2 STORAGE AND THAWING

A. Freezing medium

Freezing medium was 5% v/v DMSO in heat-inactivated FBS. The medium was freshly prepared in a class II biosafety cabinet.

B. Caco-2 storage

After trypsinization, cell suspension was transferred into a sterile 15-mL centrifuge tube and centrifuged at 1500 × g for 5 min. The medium was then discarded and the cells were resuspended in ice-cold freezing medium. Cell suspension was aliquoted into a cryotube (Corning) and slow-stepwise frozen by placing in StrataCooler (Stratagene, La Jolla, CA, USA) and kept at –80 °C overnight. Finally, the frozen cell-containing cryotube was stored in liquid nitrogen.

C. Caco-2 thawing

A cryotube containing frozen Caco-2 cells was gradually heated to 37 °C in a water bath. The cells were later resuspended in complete DMEM.

APPENDIX E
^{3}H-MANNITOL MEASUREMENT

A. Principle

Radioactive ^{3}H-mannitol is measured by detecting radiation of tritium ($^{3}_{1}$H) in its molecule. $^{3}_{1}$H is an isotope of hydrogen containing 1 proton and 2 neutrons. It decays into helium-3 ($^{3}_{2}He^{+}$) by β-decay with a half-life of approximately 12.33 years. This reaction releases 18.6 keV of energy as the following equation.

$$^{3}_{1}H \longrightarrow {}^{3}_{2}He^{+} + \beta^{-} + 18.6\ keV$$

In order to determine the $^{3}_{1}$H radioactivity, a sample is first dissolved in scintillation cocktail which is composed of a solvent and scintillators, i.e., phosphors. The emitted β^{-} particles from the sample are transferred to the scintillators by the solvent. As a consequence, the excited scintillator molecules dissipate the energy by emitting photon of light. The first scintillator which takes up the β^{-} particles and produces light is called primary scintillator. A wavelength of the light generated by the primary scintillator is too short and, therefore, cannot be detected by most photodetectors. This energy is thus absorbed by the secondary scintillator (wavelength shifter) which reemits new photons at a longer wavelength. This light can be detected by a photodetector of a liquid scintillation counter. The radioactivity is shown as counts per minute (cpm).

B. Liquid scintillation cocktail preparation

Liquid scintillation cocktail was prepared by dissolving 5 g 2,5-biphenyloxazole (a primary scintillator which emits light at 360 nm), and 0.3 g 1,4-bis(5-phenyloxazole-2-yl)benzene (a secondary scintillator which emits light at 420 nm) in 300 mL toluene. After mixing by a magnetic stirrer, 200 mL toluene and 500 mL Triton X-100 were added into the solution. Then, the solution was further stirred overnight. Liquid scintillation cocktail was stored at room temperature and kept away from light.

BIOGRAPHY

NAME	Mr. Suparerk Laohapitakworn
DATE OF BIRTH	January 1, 1986
PLACE OF BIRTH	Ubonratchathanee, Thailand
INSTITUTIONS ATTENDED	Mahidol University, 2004–2007 Bachelor of Science (Medical Science) Mahidol University, 2007–2010 Doctor of Philosophy (Molecular Medicine)
SCHOLARSHIP	Medical Scholars Program (MSP), Mahidol University, Thailand
HOME ADDRESS	138/122 Payatai Road, Payatai, Ratchatewee, Bangkok 10400 Thailand Tel. +66–8–9721–4824 E-mail: s_laohapitakworn@hotmail.com
OFFICE ADDRESS	Consortium for Calcium and Bone Research Faculty of Science, Mahidol University Rama VI Road, Bangkok 10400 Thailand
AWARDS	Outstanding Poster Presentation Award at the 39th Annual Scientific Meeting of the Physiological Society of Thailand on May 5–8, 2010 at Amari Orchid Pattaya, Pattaya, Chonburi, Thailand

AWARDS (CONTINUED)

Outstanding Poster Presentation Award
at the Graduate Research Exposition 2010 (Grad Expo 2010)
on October 27, 2010
at the Faculty of Science, Mahidol University, Bangkok, Thailand

PUBLICATION

Laohapitakworn S, Thongbunchoo J, Nakkrasae L, Krishnamra N, Charoenphandhu N. Parathyroid hormone (PTH) rapidly enhances CFTR-mediated HCO_3^- secretion in intestinal epithelium-like Caco-2 monolayer: a novel ion regulatory action of PTH. Am J Physiol Cell Physiol 2011. (Accepted, in press)